DLVO Theory

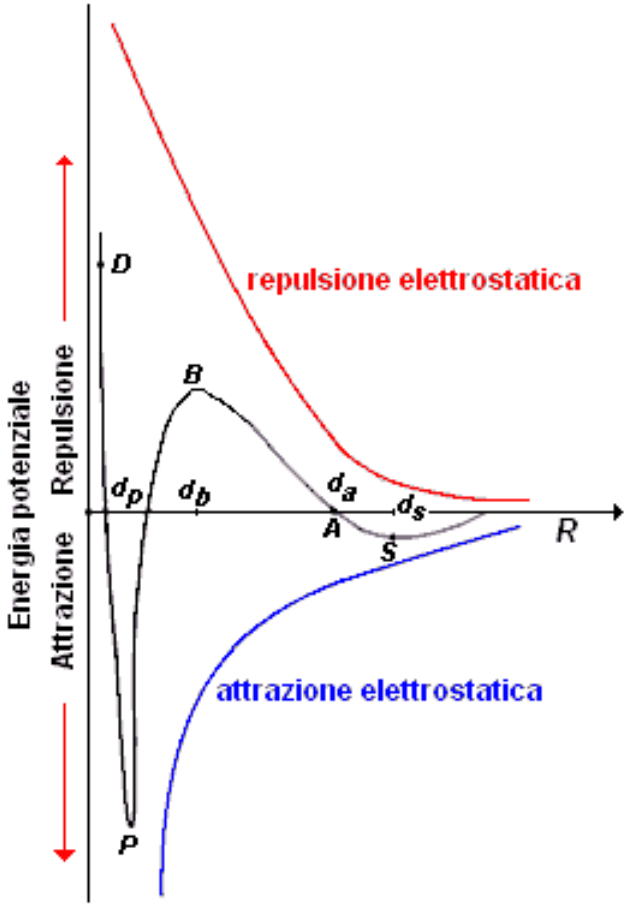
Energia potenziale
Repulsione
Attrazione
D
B
A
S
P
R
repulsione elettrostatica
attrazione elettrostatica

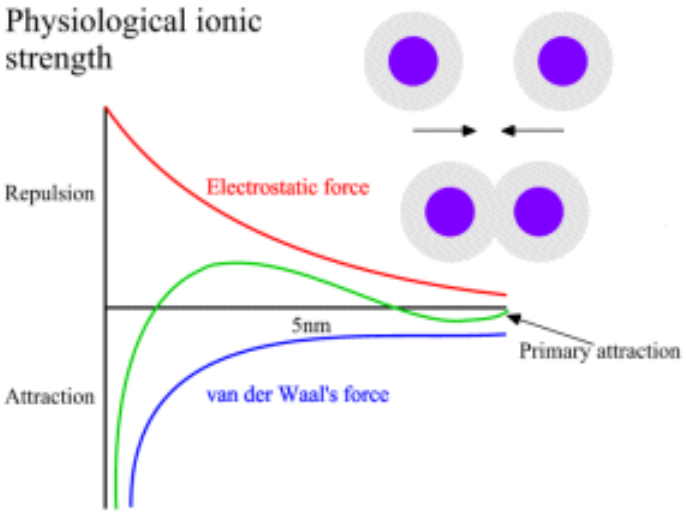
Physiological ionic strength
Repulsion
Attraction
Electrostatic force
van der Waal's force
5nm
Primary attraction

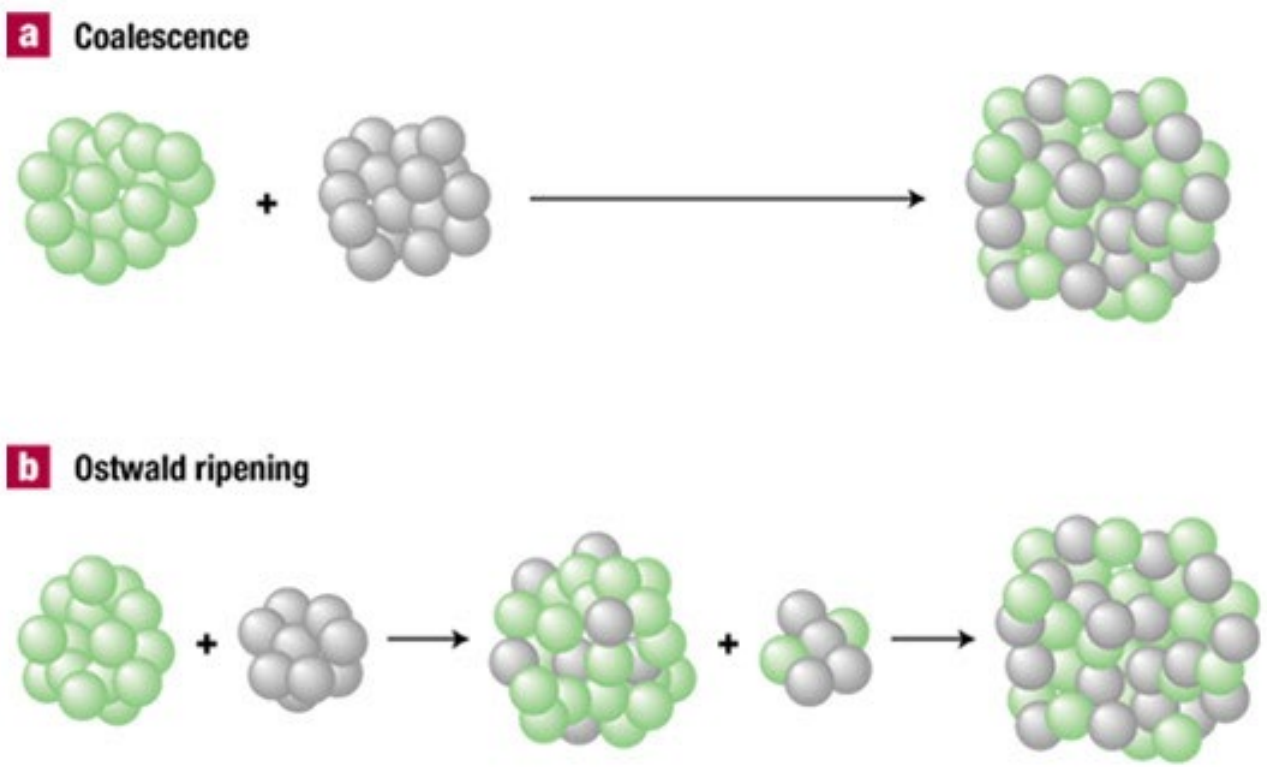

Two main mechanisms are shown here: **a**, coalescence sintering, and **b**, Ostwald ripening sintering. Coalescence sintering occurs when two clusters touch or collide and merge to form one bigger cluster. In contrast, Ostwald ripening sintering occurs by evaporation of atoms from one cluster, which then transfer to another. This is a dynamic process — both clusters exchange atoms, but the rate of loss from the smaller cluster is higher, because of the lower average coordination of atoms at the surface and their relative ease of removal. Thus big clusters get bigger at the expense of smaller clusters, which shrink and eventually disappear. The latter process is the usual form of sintering for metal clusters on a supported surface that are well spaced apart, although coalescence can occur for a high density of clusters. In general, the presence of the surface results in SMORS (surface-mediated Ostwald ripening sintering) in which material is transferred from one cluster to another by diffusion across the surface, and not through the gas phase.

Scheme 1. Modular Design of Hydrophilic Ligands with Terminal Functional Groups Used in This Study

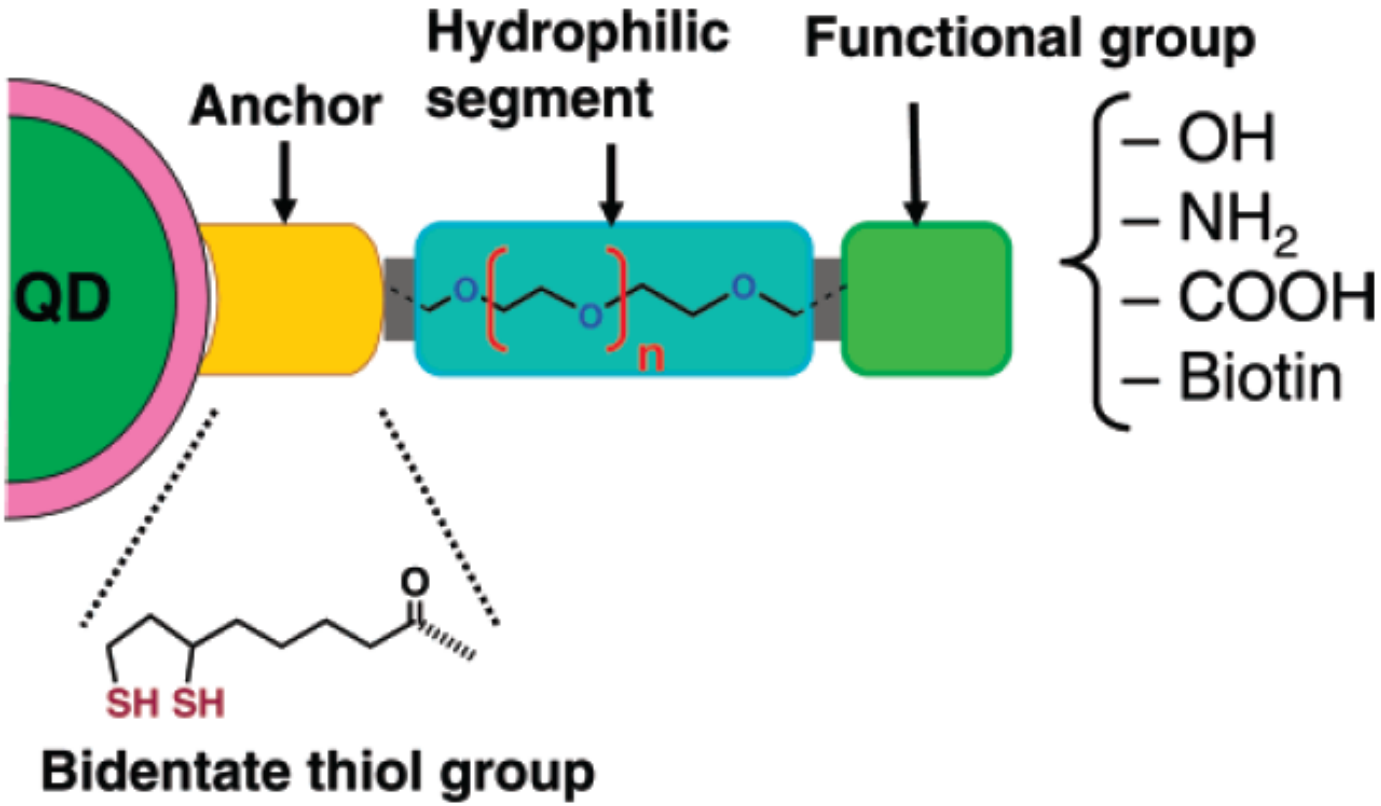

Nanomaterials for Biodiagnostic

- Nucleic Acid
  - Genetic information for identification
  - Diseases, bacterium, virus, pathogen
  - PCR with molecular fluorophore, State of the Art
  - Expansive, Non-portable, Non-multiplexing
- Proteins
  - Cancers and diseases, unusual high concentration of marker
  - ELISA (~pM) with molecular fluorophore
  - No PCR version

Colorimetric Detection of DNA

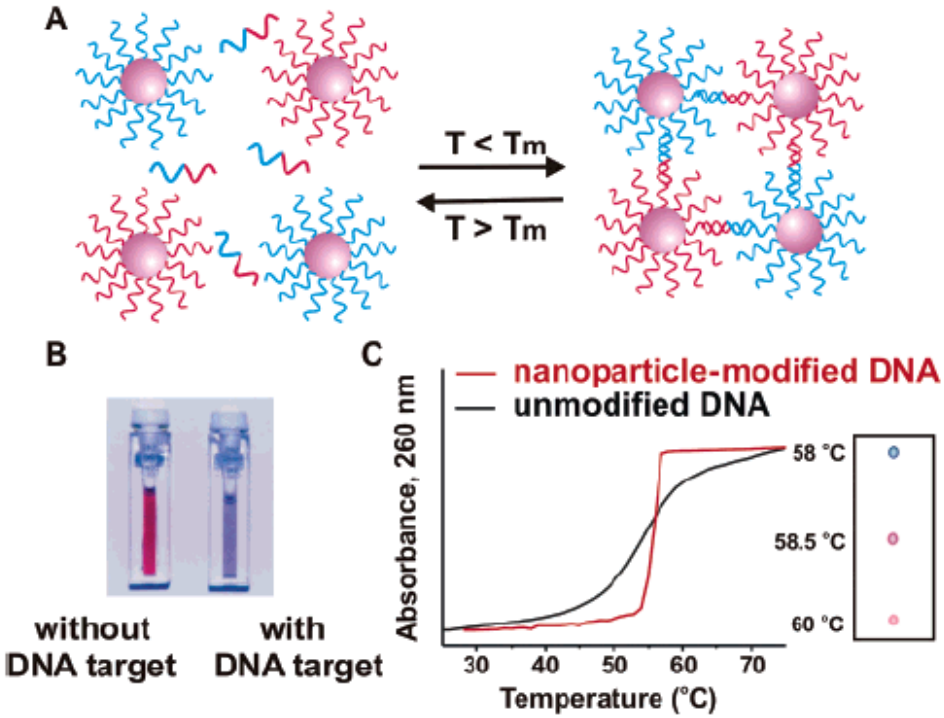

Figure 2. In the presence of complementary target DNA, oligonucleotide-functionalized gold nanoparticles will aggregate (A), resulting in a change of solution color from red to blue (B). The aggregation process can be monitored using UV−vis spectroscopy or simply by spotting the solution on a silica support (C). (Reprinted with permission from *Science* (http://www.aaas.org), ref 29. Copyright 1997 American Association for the Advancement of Science.)

A DNA-based method for rationally assembling nanoparticles into macroscopic materials

Chad A. Mirkin, Robert L. Letsinger, Robert C. Mucic & James J. Storhoff

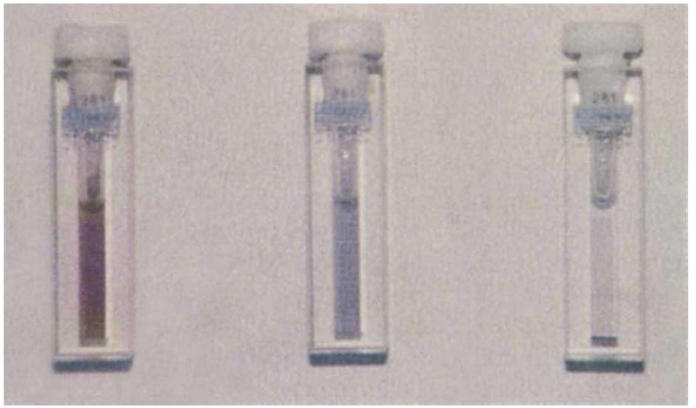

FIG. 2 Cuvettes with the Au colloids and the four DNA strands responsible for the assembly process. Left cuvette, at 80 °C with DNA-modified colloids in the unhybridized state; centre, after cooling to room temperature but before the precipitate settles; and right, after the polymeric precipitate settles to the bottom of the cuvette. Heating either of these cool solutions results in the reformation of the DNA-modified colloids in the unhybridized state (shown in the left cuvette).

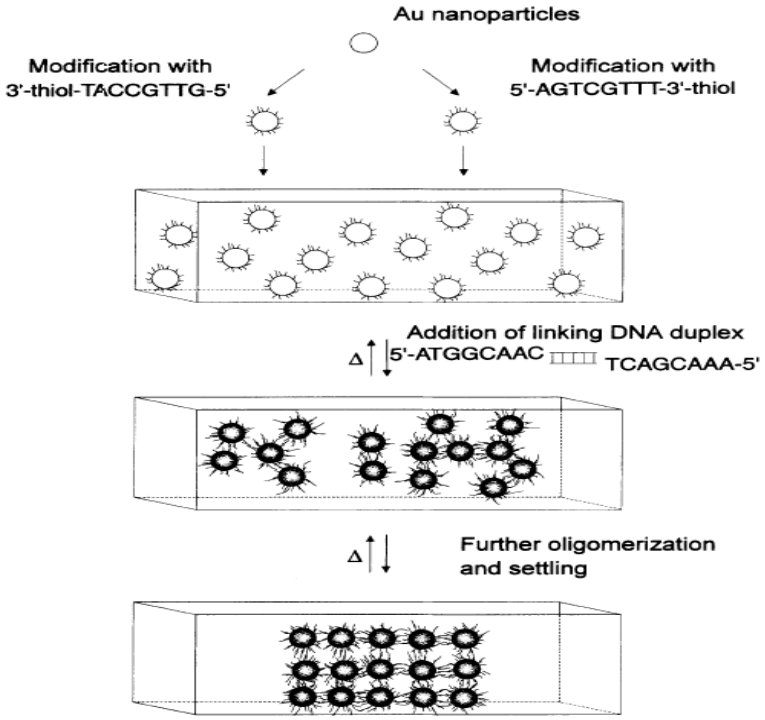

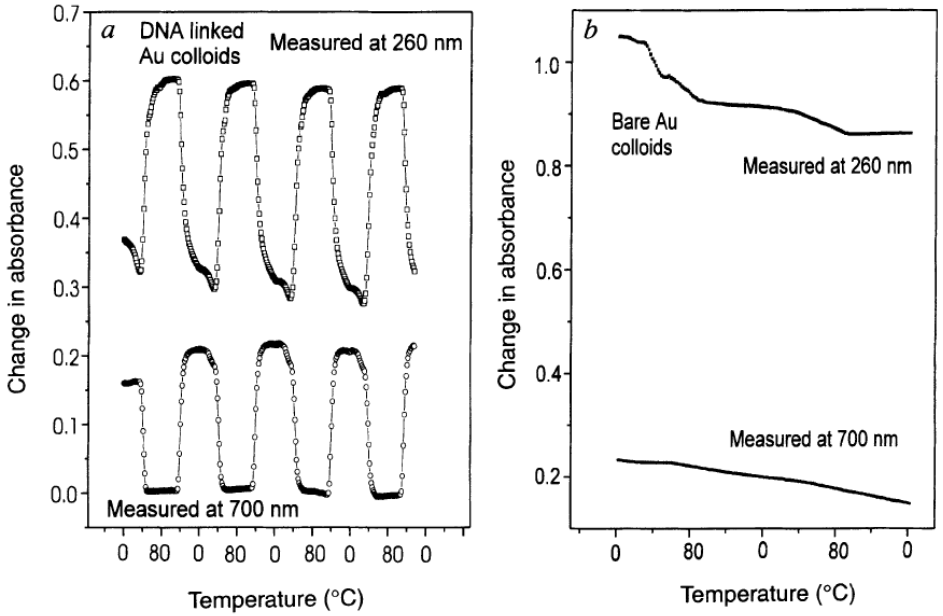

Nature, 1996, 382, 607

Selective Colorimetric Detection of Polynucleotides Based on the Distance-Dependent Optical Properties of Gold Nanoparticles

Robert Elghanian, James J. Storhoff, Robert C. Mucic,
Robert L. Letsinger,* Chad A. Mirkin*

SCIENCE • VOL. 277 • 22 AUGUST 1997

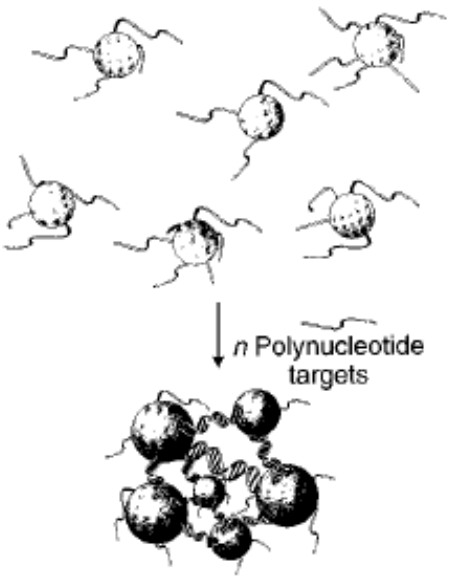

Fig. 1. Schematic representation of the concept for generating aggregates signaling hybridization of nanoparticle-oligonucleotide conjugates with oligonucleotide target molecules. The nanoparticles and the oligonucleotide interconnects are not drawn to scale, and the number of oligomers per particle is believed to be much larger than depicted.

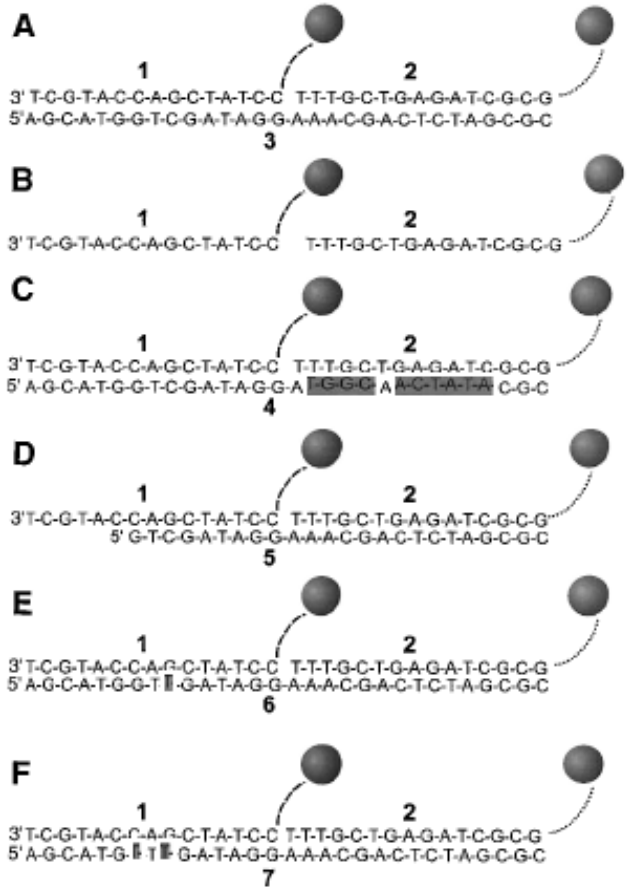

Fig. 2. Mercaptoalkyloligonucleotide-modified 13-nm Au particles and polynucleotide targets used for examining the selectivity of the nanoparticle-based colorimetric polynucleotide detection system. (**A**) Complementary target; (**B**) probes without the target; (**C**) a half-complementary target; (**D**) a 6-bp deletion; (**E**) a 1-bp mismatch; and (**F**) a 2-bp mismatch. For the sake of clarity, only two particles are shown; in reality a polymeric aggregate with many particles is formed. Dashed lines represent flexible spacer portions of the mercaptoalkyloligonucleotide strands bound to the nanoparticles; note that these spacers, because of their noncomplementary nature, do not participate in hybridization. The full sequences for the two probes, **1** and **2**, which bind to targets **3** through **7**, are

1-5′SH-$(CH_2)_6$- [CTA-ATC-CGC-ACA-G]
spacer

[CC-TAT-CGA-CCA-TGC-T]
probe

2-5′SH-$(CH_2)_6$-[ATG-GCA-ACT-ATA-C]
spacer

[GC-GCT-AGA-GTC-GTT-T]
probe

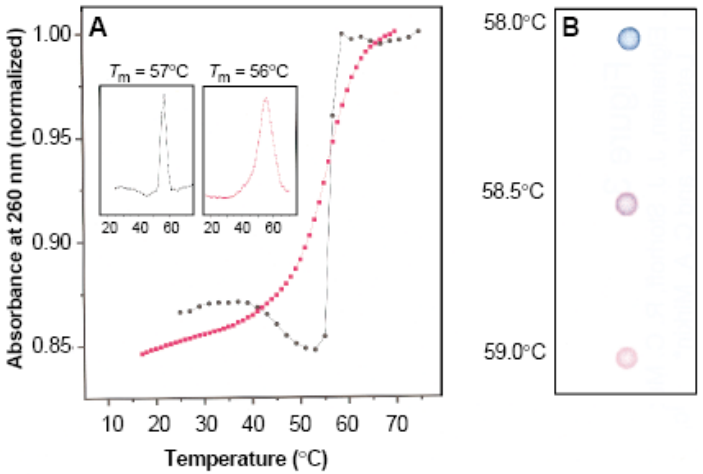

Fig. 3. (**A**) Comparison of the thermal dissociation curves for complexes of mercaptoalkyloligonucleotide-modified Au nanoparticles (black circles) and mercaptoalkyloligonucleotides without Au nanoparticles (red squares) with the complementary target, **3**, in hybridization buffer (0.1 M NaCl, 10 mM phosphate buffer, pH 7.0). For the first set (black circles), a mixture of 150 μl of each colloid conjugate and 3 μl of the target oligonucleotide in hybridization buffer (0.1 M NaCl, 10 mM phosphate, pH 7.0) was frozen at the temperature of dry ice, kept for 5 min, thawed over a period of 15 min, and diluted to 1.0 ml with buffer (final target concentration, 0.02 μM). The absorbance was measured at 1-min intervals with a temperature increase of 1°C per minute. The increase in absorption at 260 nm (A_{260}) was ~0.3 absorption units (AU). In the absence of the oligonucleotide targets, the absorbance of the nanoparticles did not increase with increasing temperature. For the second set, the mercaptoalkyloligonucleotides and complementary target (each 0.33 μM) were equilibrated at room temperature in 1 ml of buffer, and the changes in absorbance with temperature were monitored as before. The increase in A_{260} was 0.08 AU. (**Insets**) Derivative curves for each set (*15*). (**B**) Spot test showing T_c (thermal transition associated with the color change) for the Au nanoparticle probes hybridized with complementary target. A solution prepared from 150 μl of each probe and 3 μl of the target (0.06 μM final target concentration) was frozen for 5 min, allowed to thaw for 10 min, transferred to a 1-ml cuvette, and warmed at 58°C for 5 min in the thermally regulated cuvette chamber of the spectrophotometer. Samples (3 μl) were transferred to a C_{18} reverse phase plate with an Eppendorf pipette as the temperature of the solution was increased incrementally 0.5°C at 5-min intervals.

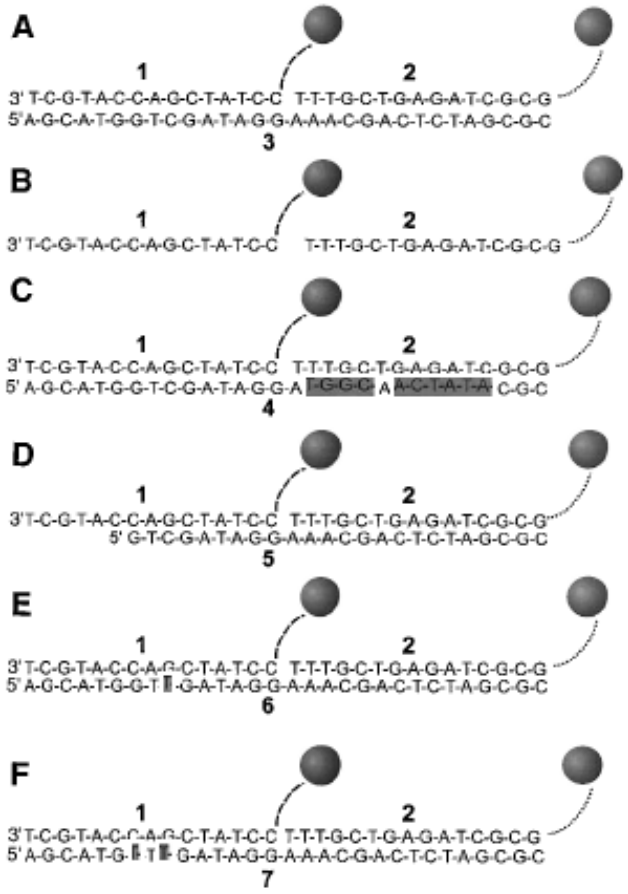

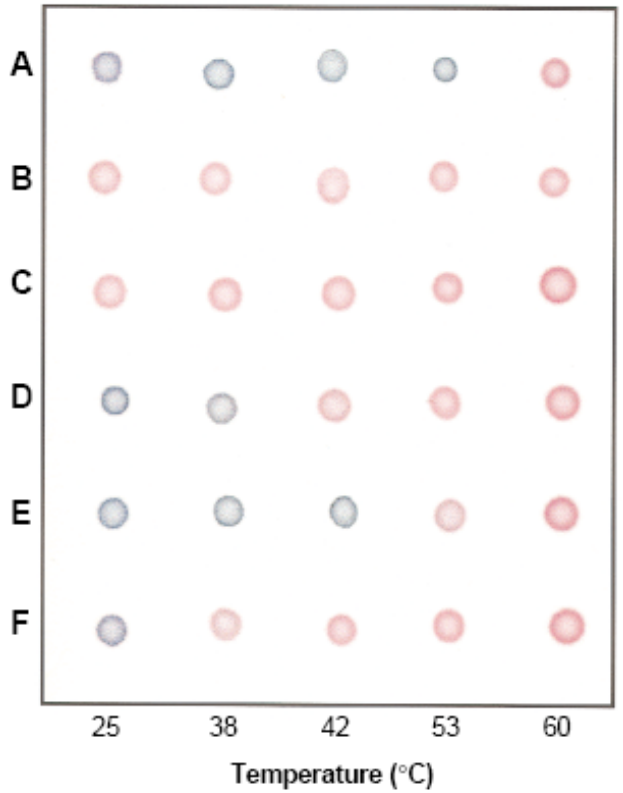

Fig. 4. Selective polynucleotide detection for the target probes shown in Fig. 2: (**A**) complementary target; (**B**) no target; (**C**) complementary to one probe; (**D**) a 6-bp deletion; (**E**) a 1-bp mismatch; and (**F**) a 2-bp mismatch. Nanoparticle aggregates were prepared in a 600-μl thin-walled Eppendorf tube by addition of 1 μl of a 6.6 μM oligonucleotide target to a mixture containing 50 μl of each probe (0.06 μM final target concentration). The mixture was frozen (5 min) in a bath of dry ice and isopropyl alcohol and allowed to warm to room temperature. Samples were then transferred to a temperature-controlled water bath, and 3-μl aliquots were removed at the indicated temperatures and spotted on a C_{18} reverse phase plate.

J. Am. Chem. Soc. **2000,** *122,* 9071−9077

Colloidal Au-Enhanced Surface Plasmon Resonance for Ultrasensitive Detection of DNA Hybridization

Lin He, Michael D. Musick, Sheila R. Nicewarner, Frank G. Salinas, Stephen J. Benkovic, Michael J. Natan, and Christine D. Keating*

Scheme 1. SPR Surface Assembly

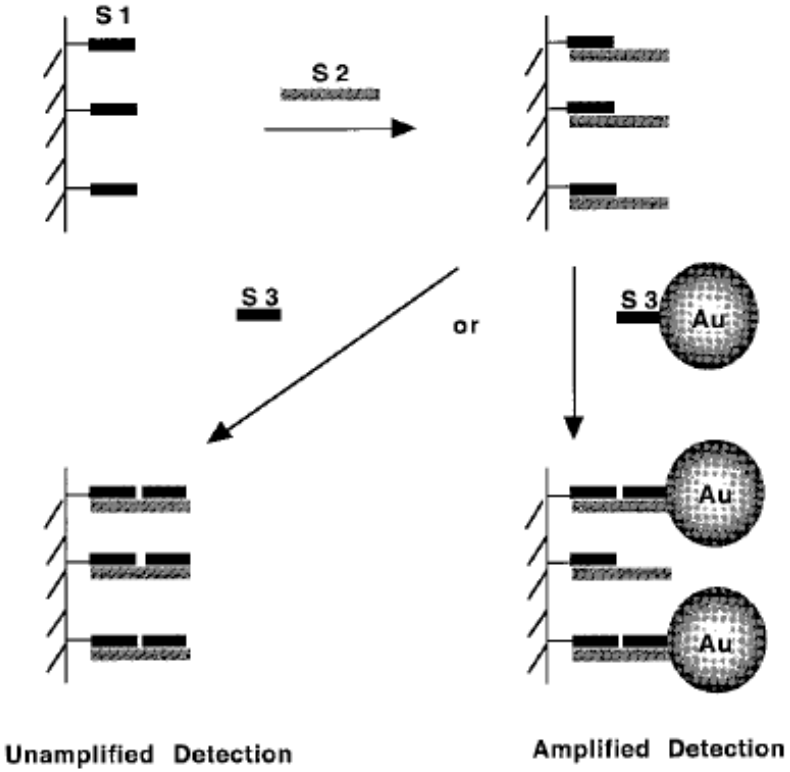

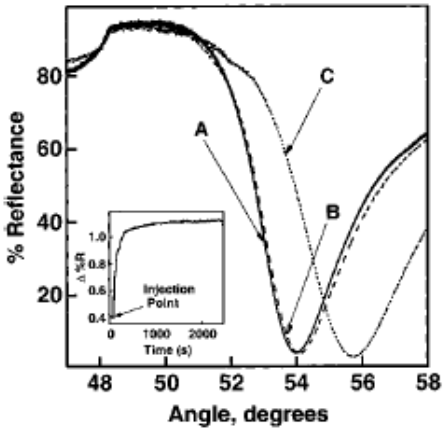

Figure 1. SPR curves of surfaces prepared in sequential steps as illustrated in Scheme 1: a MHA-coated Au film modified with a 12-mer oligonucleotide S1(A), after hybridization with its complementary 24-mer target S2 (B), and followed by introduction of S3:Au conjugate (C) to the surface. Inset: surface plasmon reflectance changes at 53.2° for the oligonucleotide-coated Au film measured during a 60-min exposure to S3:Au conjugates.

Scheme 2. SPR Surface Assembly in the Digestion Experiment

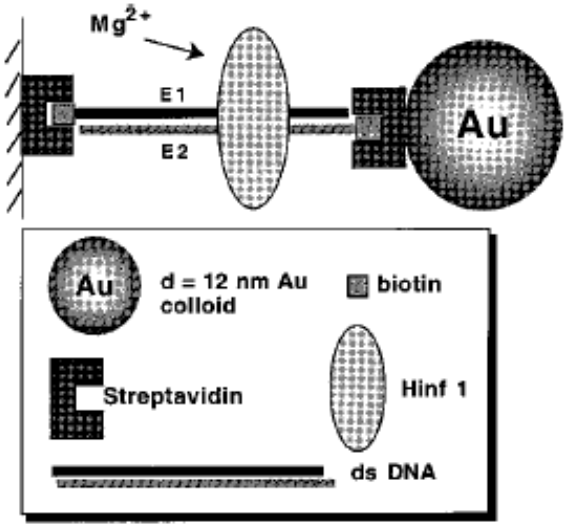

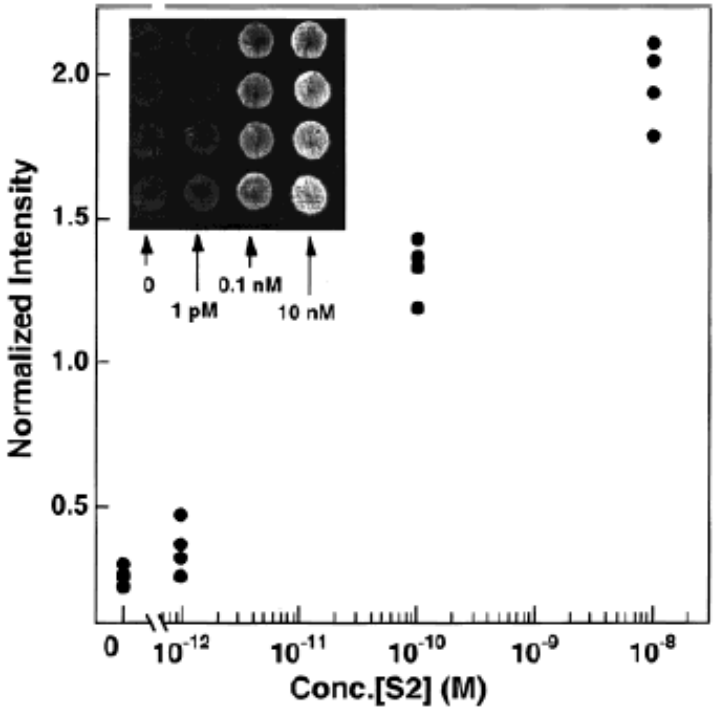

Figure 5. Plot of normalized intensity of SPR reflectance as a function of logarithmic concentration of the analyte 24-mer oligo (S2). Each spot represents one data point at the corresponding concentration. CCD parameters: exposure time = 0.3 s, 16 bit resolution, spot size = 4.5 mm in diameter. Inset: a 2-D SPR image of a Au surface derivatized with 20 μL of buffer blank, 1 pM, 0.1 nM, and 10 nM S2 oligos (from left to right, respectively).

Self-Assembled Nanoparticle Probes for Recognition and Detection of Biomolecules

Dustin J. Maxwell, Jason R. Taylor, and Shuming Nie*,†

9606 ■ J. AM. CHEM. SOC. 2002, *124*, 9606−9612

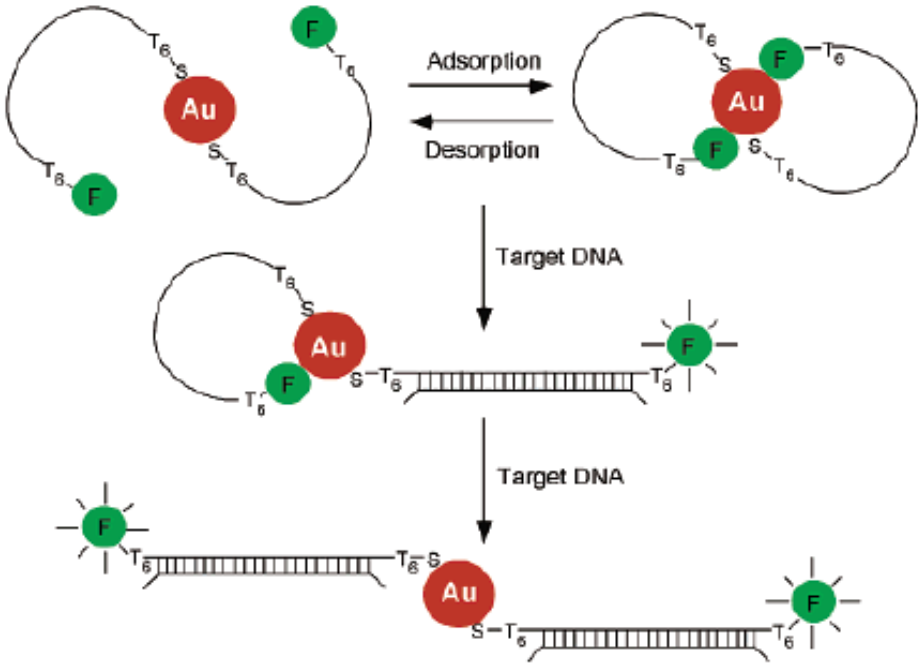

Figure 1. Nanoparticle-based probes and their operating principles. Two oligonucleotide molecules (oligos) are shown to self-assemble into a constrained conformation on each gold particle (2.5 nm diameter). A T_6 spacer (six thymines) is inserted at both the 3′- and 5′-ends to reduce steric hindrance. Single-stranded DNA is represented by a single line and double-stranded DNA by a cross-linked double line. In the assembled (closed) state, the fluorophore is quenched by the nanoparticle. Upon target binding, the constrained conformation opens, the fluorophore leaves the surface because of the structural rigidity of the hybridized DNA (double-stranded), and fluorescence is restored. In the open state, the fluorophore is separated from the particle surface by about 10 nm. See text for detailed explanation. Au, gold particle; F, fluorophore; S, sulfur atom.

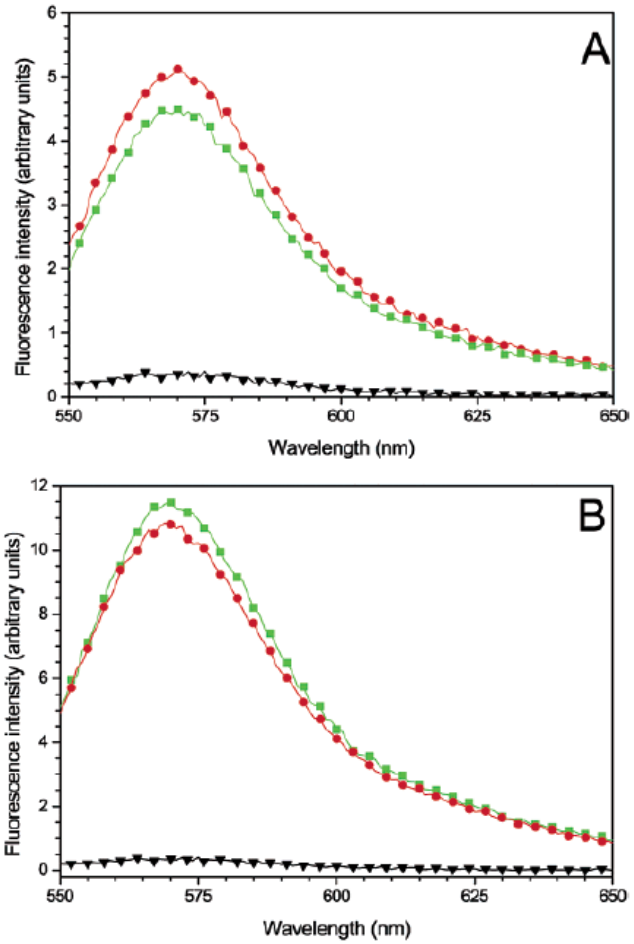

Figure 5. Fluorescence responses and the lack of sequence recognition abilities observed for nonthiolated nanoparticle probes. (A) Fluorescence spectra of nonthiolated probes generated by a complementary target (red curve), a noncomplementary target (green curve), and no target (black curve). These probes are considered nonfunctional because they do not recognize specific DNA sequences. (B) Fluorescence signals obtained from the supernatant solution when the probes were treated with a complementary target (red curve) or a noncomplementary target (green curve). The result revealed that the oligos were released into solution by nonspecific adsorption of the target on the particle surface. With a thiol group, this release was not observed (little or no signal in solution, black curve in B). The nonfunctional probes were prepared in the same way as the functional probes, except that the 3′-end thiol group was deleted. The intensity differences for the red and green curves were within experimental errors and had no particular significance.

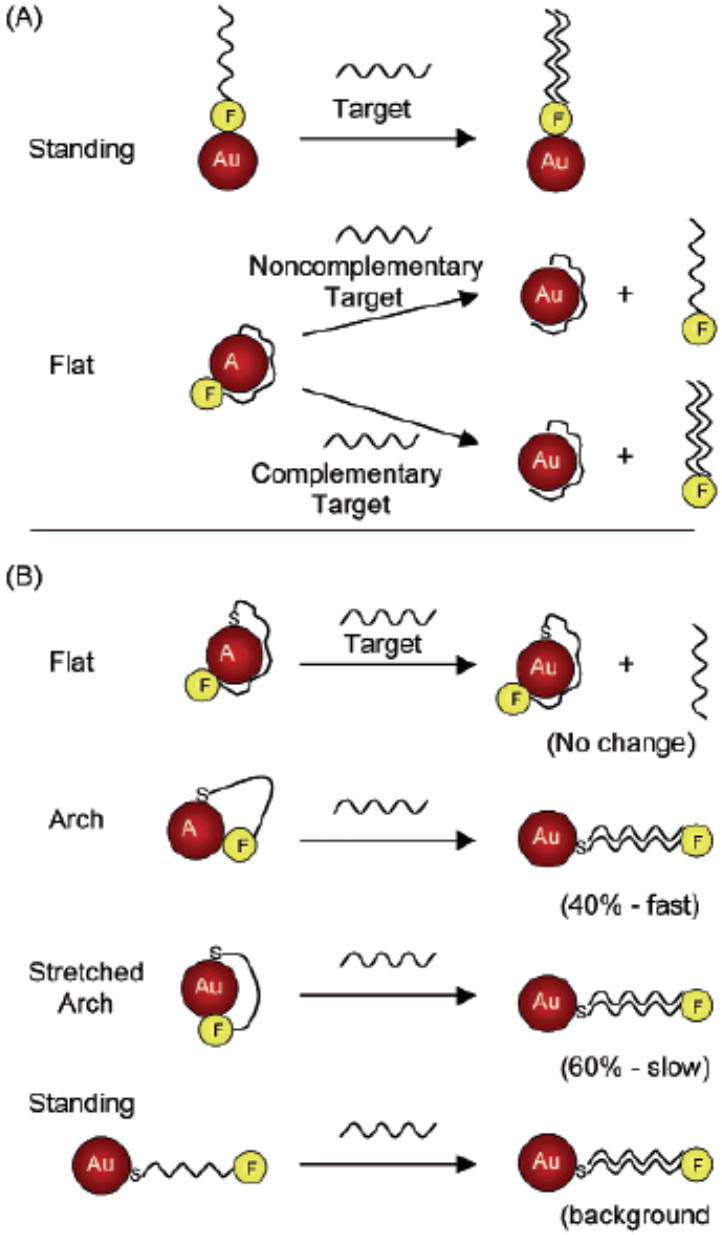

Figure 6. Schematic illustration of possible configurations for (a) nonthiolated and (b) thiolated oligonucleotides adsorbed on colloidal gold nanocrystals. Detailed discussion in text.

Scanometric DNA Array Detection with Nanoparticle Probes

SCIENCE VOL 289 8 SEPTEMBER 2000

T. Andrew Taton,[1,2] Chad A. Mirkin,[1,2]* Robert L. Letsinger[1]*

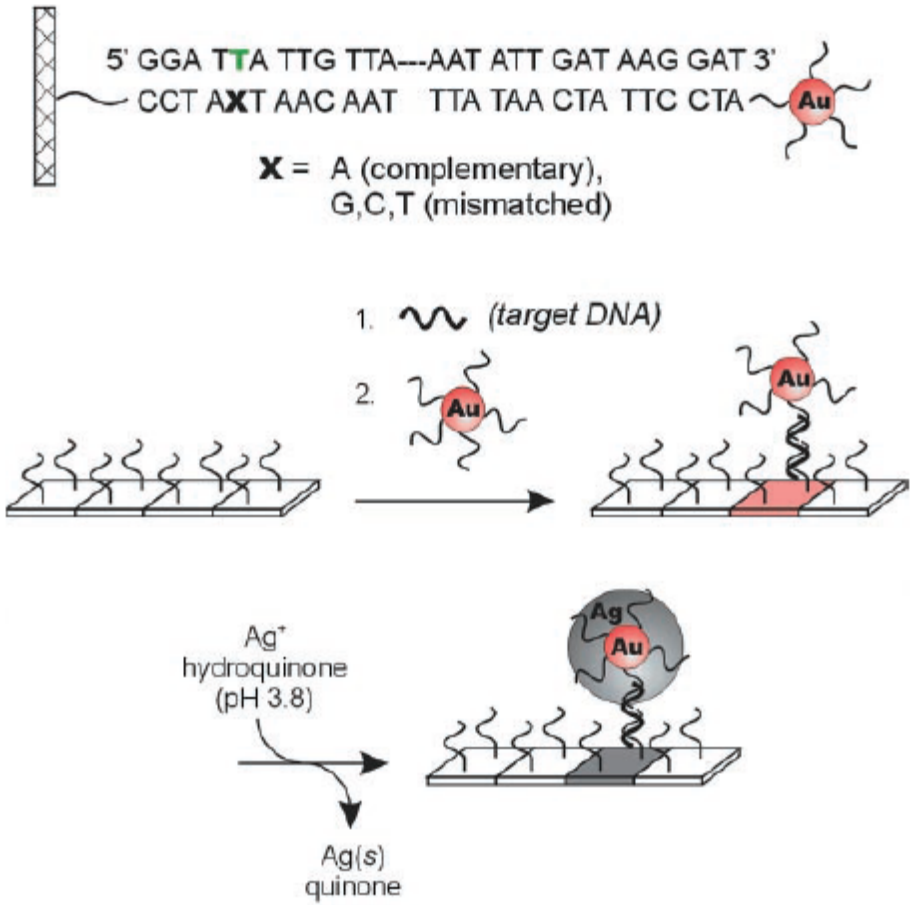

50 fM => 0.2 fM

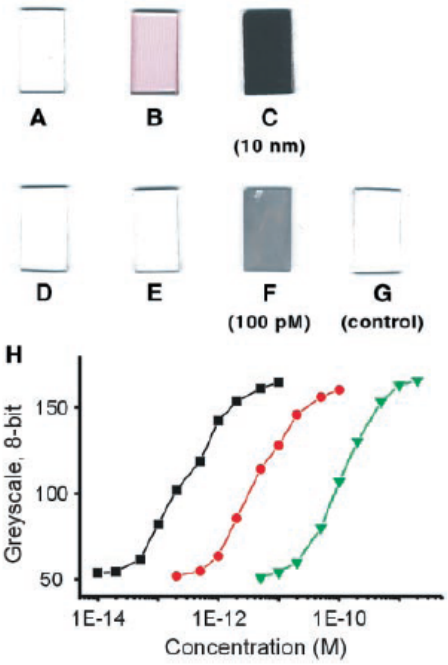

Fig. 1. Images of 7 mm by 13 mm, oligonucleotide-functionalized, float glass slides, obtained with a flatbed scanner. (**A**) Slide before hybridization of target and nanoparticle probe. (**B**) A slide identical to (A) after hybridization with oligonucleotide target (10 nM) and then nanoparticle probes (5 nM in particles). The pink color derives from the Au nanoparticle probes. (**C**) A slide identical to (B) after exposure to silver amplification solution for 5 min. (**D**) Slide before hybridization of target and nanoparticle probe. (**E**) A slide identical to (D) after hybridization with target (100 pM) and then nanoparticle probe (5 nM). The extinction of the submonolayer of nanoparticles is too low to be observed visually or with a flatbed scanner. (**F**) A slide identical to (E) after exposure to silver amplification solution for 5 min. Slide (F) is lighter than slide (C), indicating a lower concentration of target. (**G**) A control slide exposed to 5 nM nanoparticle probe and then exposed to silver amplification solution for 5 min. No darkening of the slide is observed. (**H**) Graph of 8-bit gray scale values as a function of target concentration. The gray scale values were taken from flatbed scanner images of oligonucleotide-functionalized glass surfaces that had been exposed to varying concentrations of oligonucleotide target, labeled with 5 nM oligonucleotide probe and immersed in silver amplification solution. For any given amplification time, the grayscale range is limited by surface saturation at high grayscale values and the sensitivity of the scanner at low values. Therefore, the dynamic range of this system can be adjusted by means of hybridization and amplification conditions (that is, lower target concentrations require longer amplification periods). Squares: 18-base capture-target overlap (*5*), 8× PBS hybridization buffer [1.2 M NaCl and 10 mM NaH_2PO_4/Na_2HPO_4 buffer (pH 7)], 15 min amplification time. Circles: 12-base capture-target overlap, 8× PBS hybridization buffer, 10 min amplification time. Triangles: 12-base capture-target overlap, 2× PBS hybridization buffer [0.3 M NaCl, 10 mM NaH_2PO_4/Na_2HPO_4 buffer (pH 7)], 5 min amplification time. The lowest target concentration that can be effectively distinguished from the background baseline is 50 fM.

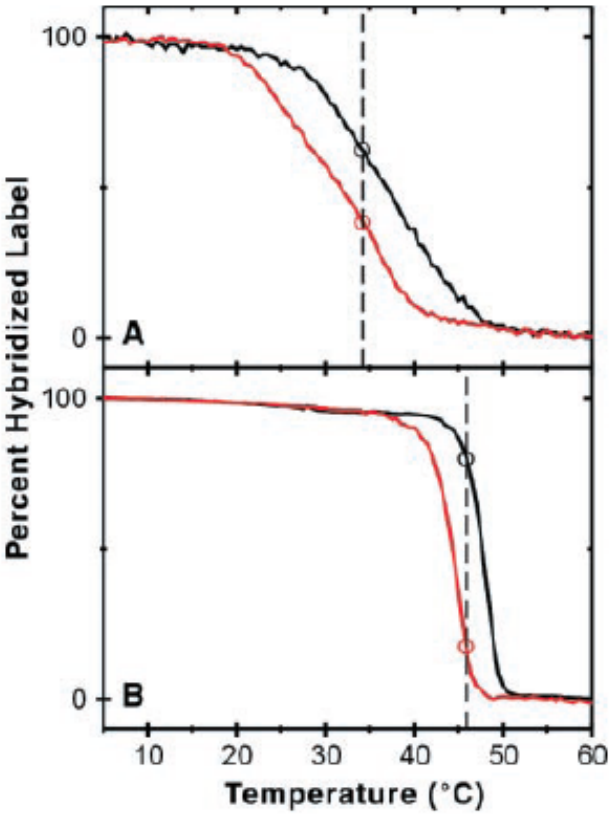

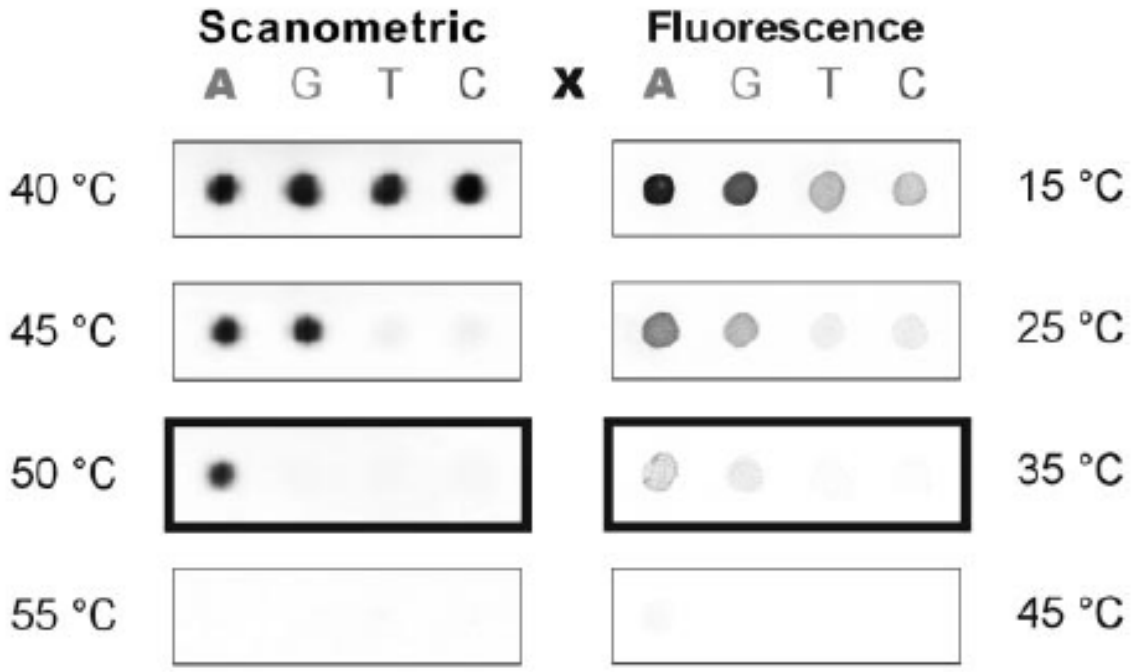

Fig. 3. (**Left**) Nanoparticle-labeled arrays developed at different stringency temperatures. Model oligonucleotide arrays (with the capture sequences shown in Scheme 1) were treated with oligonucleotide target and nanoparticle probes, followed by a 2-min buffer wash at the temperatures shown and subsequent silver amplification (*13*). Images were obtained with an Epson Expression 636 (600 dots per inch) flatbed scanner (Epson America, Long Beach, California). The darkened border indicates the array that showed optimum selectivity for the perfectly complementary target; at this temperature, the ratio of background-subtracted, 8-bit gray scale values for elements A:G:T:C, obtained from histogram averages in Adobe Photoshop (Adobe Systems, San Jose, California), is 96:9:7:6. (**Right**) Fluorophore-labeled arrays washed at different stringency temperatures. Model oligonucleotide arrays identical to those shown at left were treated with oligonucleotide target and Cy3-labeled oligonucleotide probes, followed by a 2-min buffer wash at the temperatures shown. Images were obtained with a ScanArray Confocal Microarray Scanner (GSI Lumonics, Billerica, Massachusetts). The darkened border indicates the array that showed the highest selectivity for the perfectly complementary target, as calculated by the QuantArray Analysis software package (GSI Lumonics); at this temperature, the intensity ratio (in percent, with the intensity of the X = A element at 15°C set to 100%) for elements A:G:T:C is 18:7:1:1.

Nanoparticles with Raman Spectroscopic Fingerprints for DNA and RNA Detection

YunWei Charles Cao, Rongchao Jin, Chad A. Mirkin*

30 AUGUST 2002 VOL 297 SCIENCE

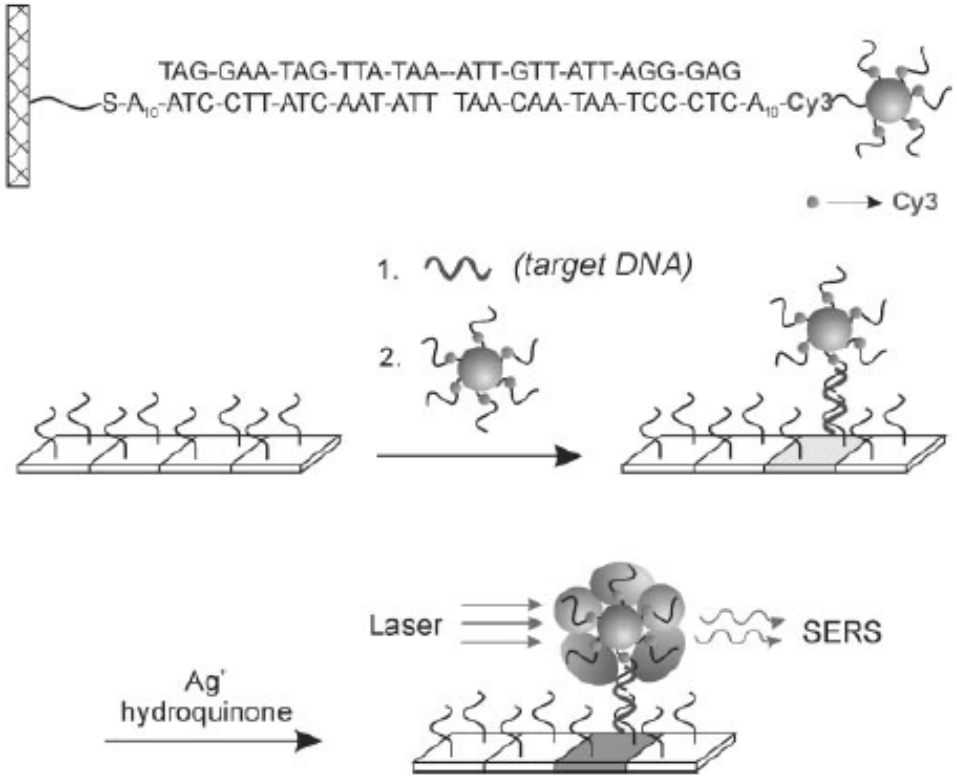

1 fM

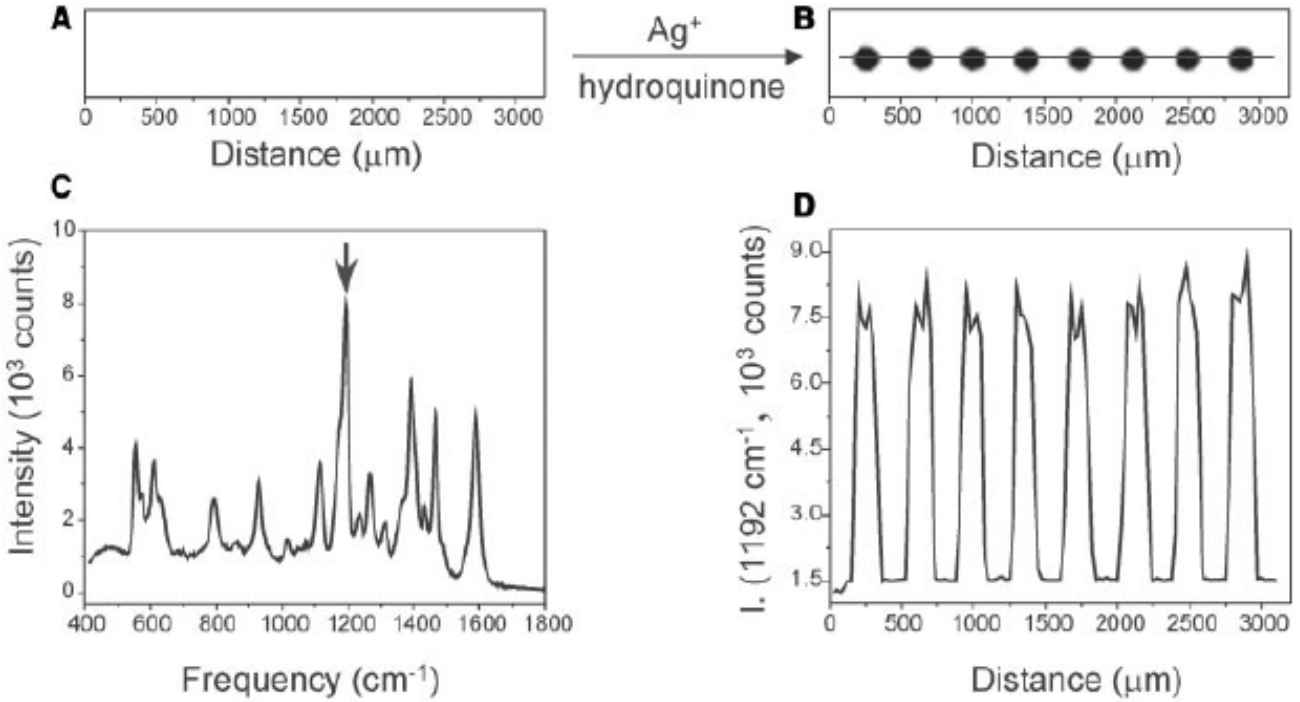

Fig. 1. Flatbed scanner images of microarrays hybridized with nanoparticles (**A**) before and (**B**) after Ag enhancing. (**C**) A typical Raman spectrum acquired from one of the Ag spots. (**D**) A profile of Raman intensity at 1192 cm^{-1} as a function of position on the chip; the laser beam from the Raman instrument is moved over the chip from left to right as defined by the line in (B).

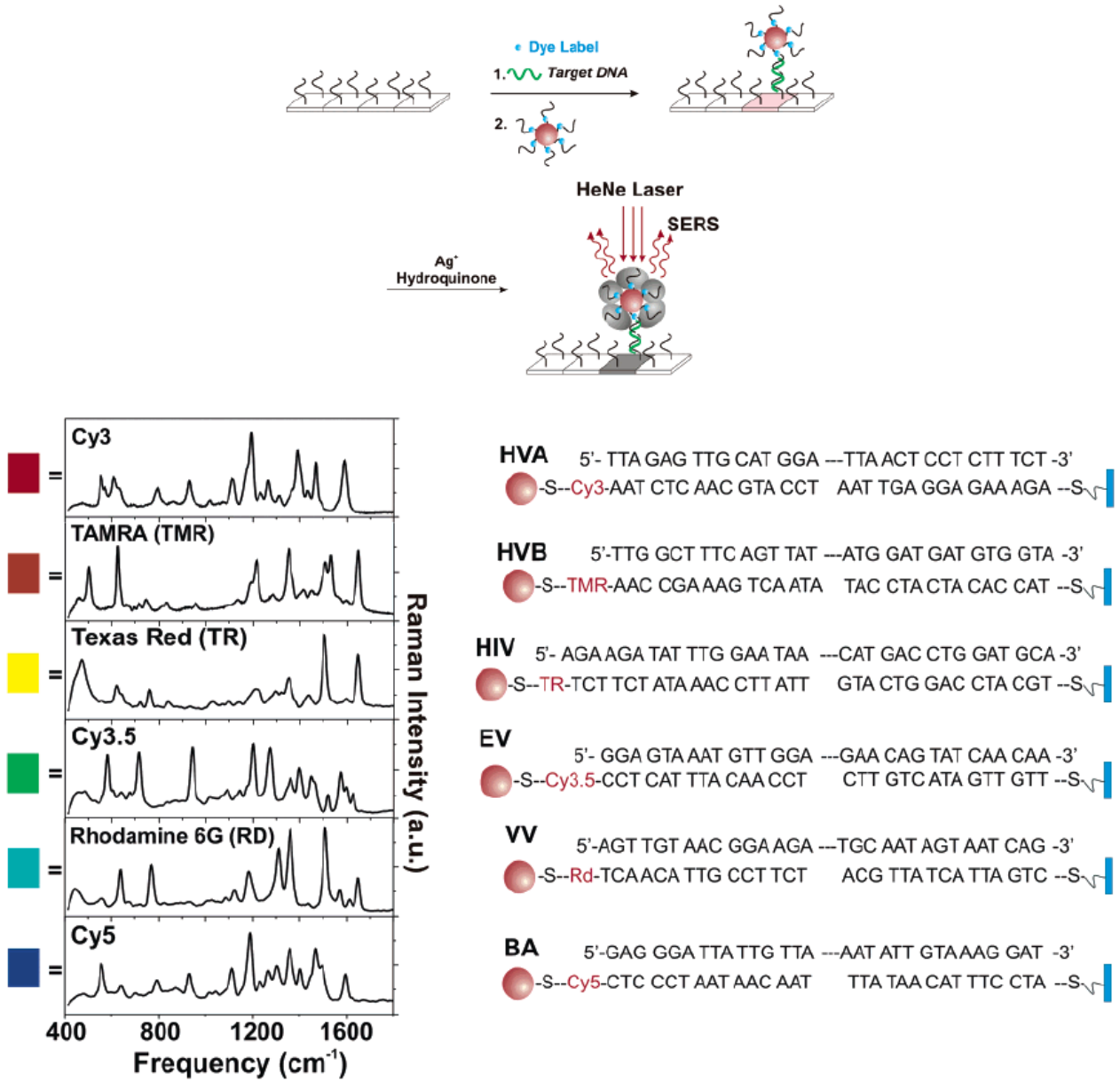

Figure 5. If Raman dyes (blue spheres) are attached to the labeling probe in the scanometric assay, the targets can be encoded and detected via the Raman signal of their labels. (Reprinted with permission from *Science* (http://www.aaas.org), ref 68. Copyright 2002 American Association for the Advancement of Science.)

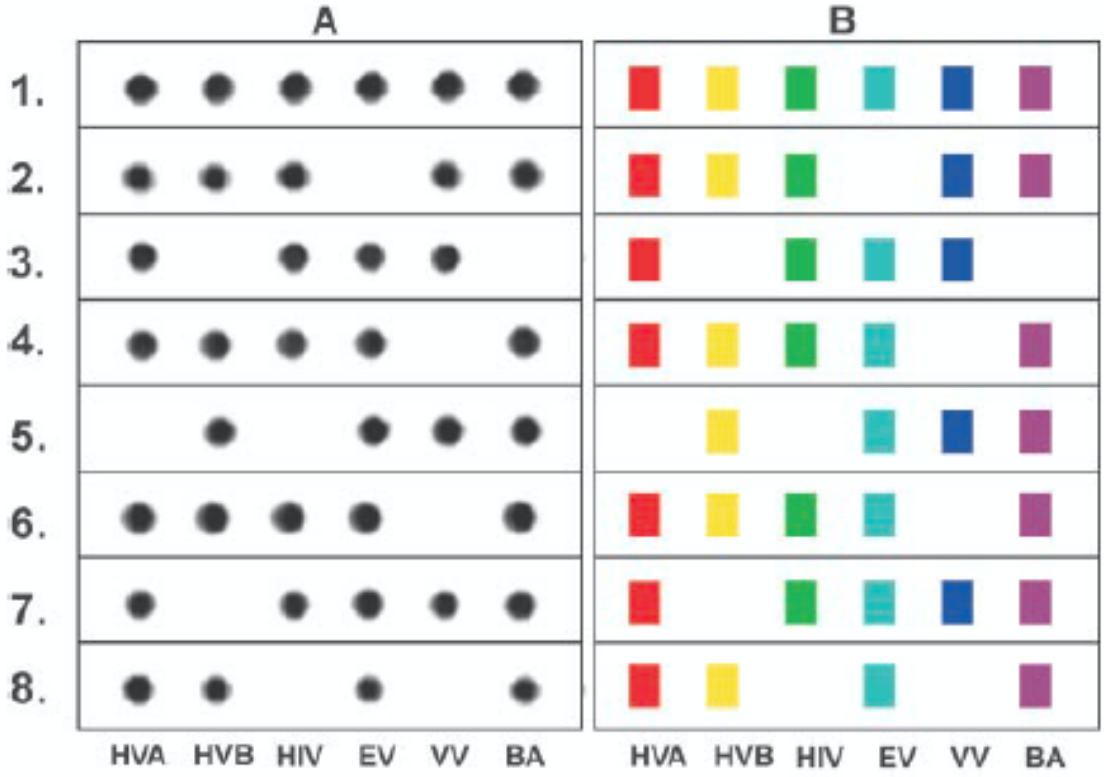

Fig. 3. (**A**) Flatbed scanner images of Ag-enhanced microarrays and (**B**) corresponding Raman spectra. The colored boxes correlate with the color-coded Raman spectra in Fig. 2. No false-positives or false-negatives were observed.

Bio-Bar-Code-Based DNA Detection with PCR-like Sensitivity

Jwa-Min Nam, Savka I. Stoeva, and Chad A. Mirkin*

J. AM. CHEM. SOC. 2004, *126*, 5932−5933

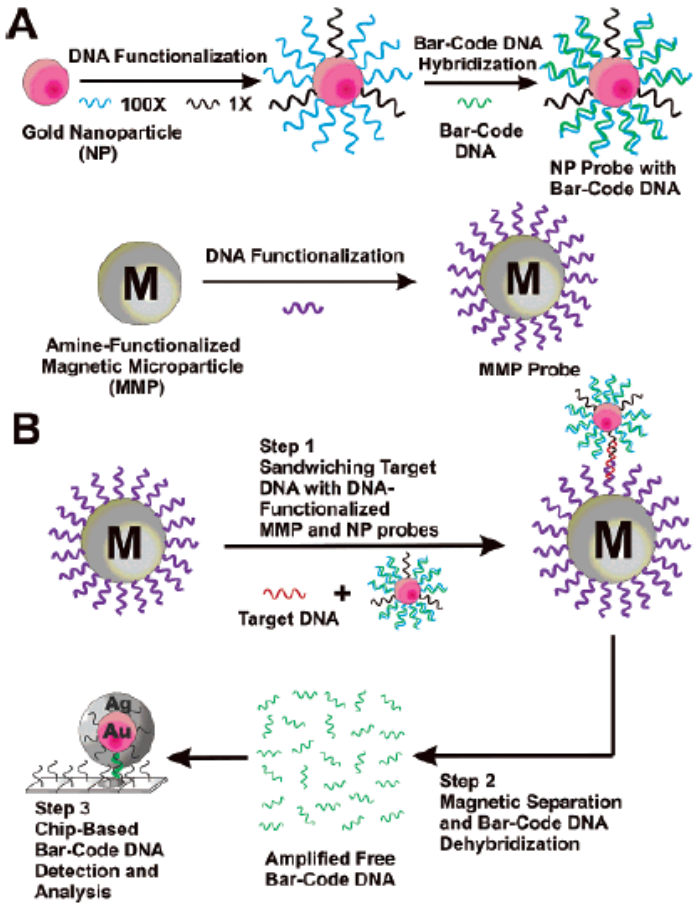

Figure 1. The DNA-BCA assay. (A) Nanoparticle and magnetic microparticle probe preparation. (B) Nanoparticle-based PCR-less DNA amplification scheme.

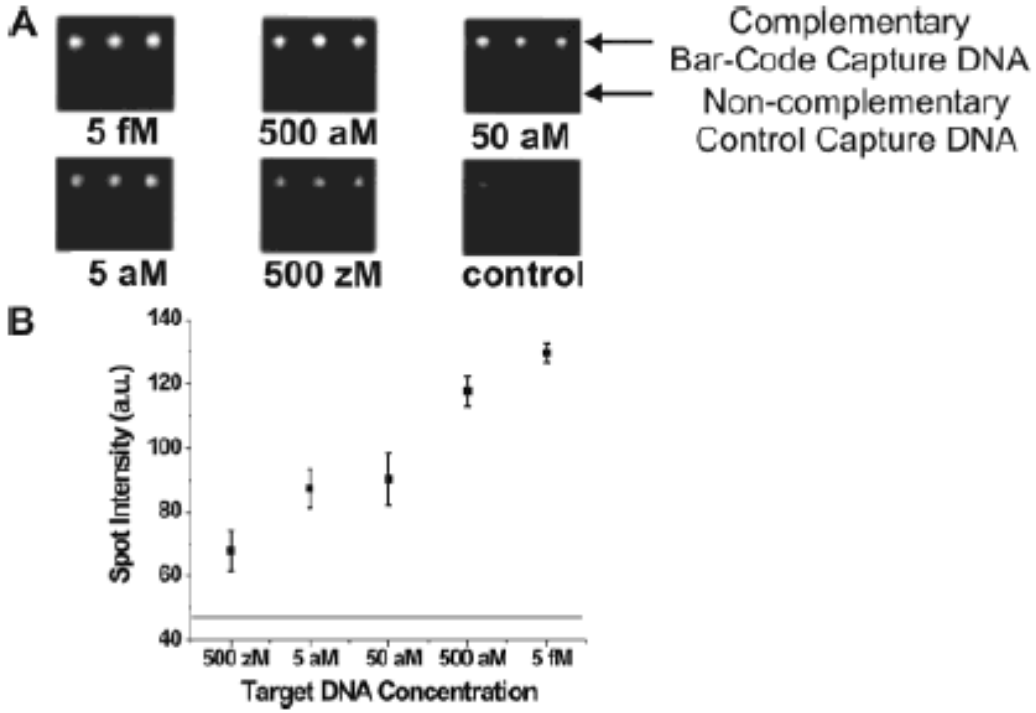

Figure 2. Amplified anthrax bar-code DNA detection with the Verigene ID system. (A) Anthrax bar-code DNA detection with 30 nm NP probes. (B) Quantitative data of spot intensities with 30 nm NP probes (Adobe Photoshop, Adobe Systems, Inc., San Jose, CA). The horizontal line represents control signal intensity (47 ± 2).

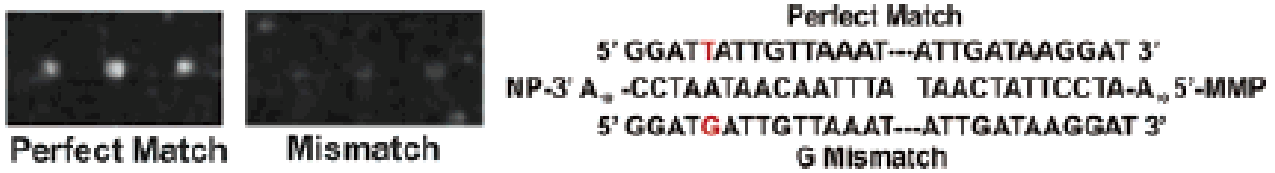

Figure 3. Single base mismatch experiment.

Nanoparticle-Based Bio–Bar Codes for the Ultrasensitive Detection of Proteins

26 SEPTEMBER 2003 VOL 301 SCIENCE

Jwa-Min Nam,* C. Shad Thaxton,* Chad A. Mirkin†

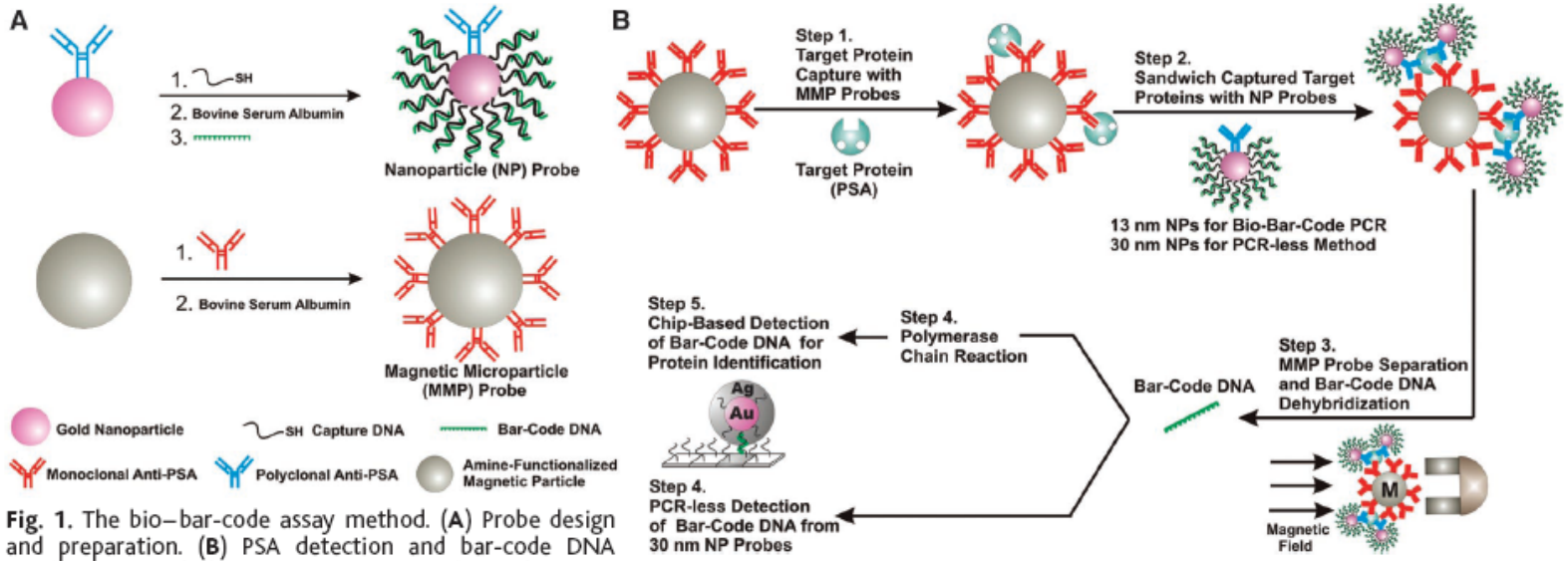

Fig. 1. The bio–bar-code assay method. (**A**) Probe design and preparation. (**B**) PSA detection and bar-code DNA amplification and identification. In a typical PSA-detection experiment, an aqueous dispersion of MMP probes functionalized with mAbs to PSA (50 μl of 3 mg/ml magnetic probe solution) was mixed with an aqueous solution of free PSA (10 μl of PSA) and stirred at 37°C for 30 min (Step 1). A 1.5-ml tube containing the assay solution was placed in a BioMag microcentrifuge tube separator (Polysciences, Incorporated, Warrington, PA) at room temperature. After 15 s, the MMP-PSA hybrids were concentrated on the wall of the tube. The supernatant (solution of unbound PSA molecules) was removed, and the MMPs were resuspended in 50 μl of 0.1 M phosphate-buffered saline (PBS) (repeated twice). The NP probes (for 13-nm NP probes, 50 μl at 1 nM; for 30-nm NP probes, 50 μl at 200 pM), functionalized with polyclonal Abs to PSA and hybridized bar-code DNA strands, were then added to the assay solution. The NPs reacted with the PSA immobilized on the MMPs and provided DNA strands for signal amplification and protein identification (Step 2). This solution was vigorously stirred at 37°C for 30 min. The MMPs were then washed with 0.1 M PBS with the magnetic separator to isolate the magnetic particles. This step was repeated four times, each time for 1 min, to remove everything but the MMPs (along with the PSA-bound NP probes). After the final wash step, the MMP probes were resuspended in NANOpure water (50 μl) for 2 min to dehybridize bar-code DNA strands from the nanoparticle probe surface. Dehybridized bar-code DNA was then easily separated and collected from the probes with the use of the magnetic separator (Step 3). For bar-code DNA amplification (Step 4), isolated bar-code DNA was added to a PCR reaction mixture (20-μl final volume) containing the appropriate primers, and the solution was then thermally cycled (*20*). The bar-code DNA amplicon was stained with ethidium bromide and mixed with gel-loading dye (*20*). Gel electrophoresis or scanometric DNA detection (*24*) was then performed to determine whether amplification had taken place. Primer amplification was ruled out with appropriate control experiments (*20*). Notice that the number of bound NP probes for each PSA is unknown and will depend upon target protein concentration.

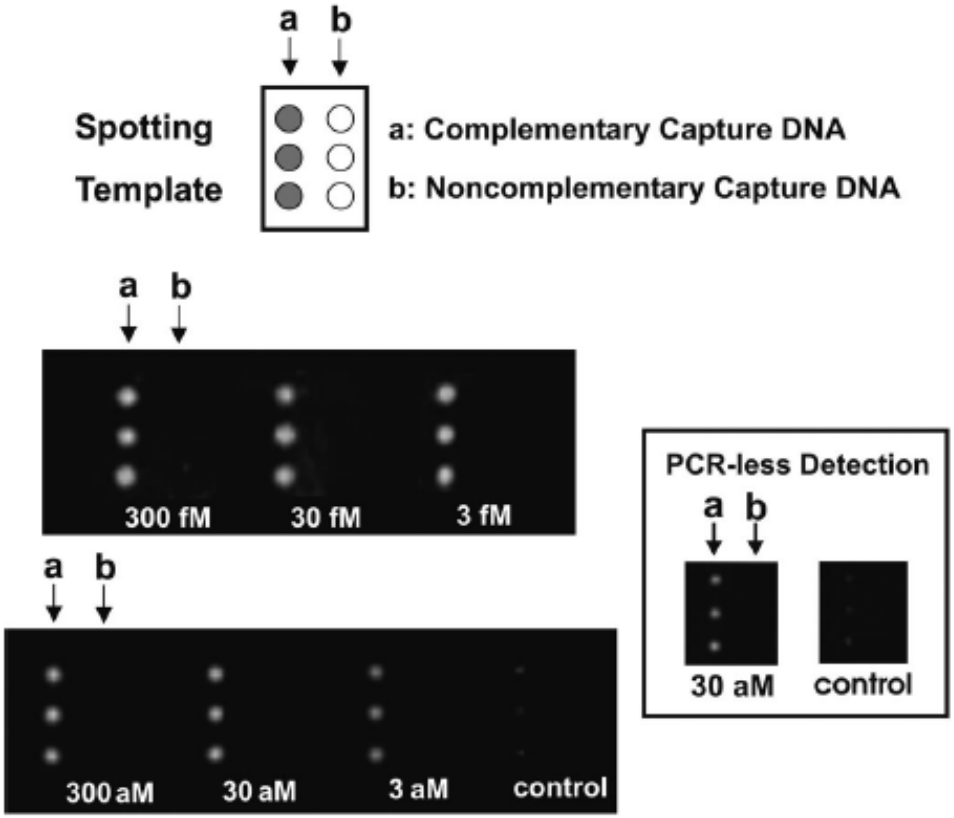

Fig. 2. Scanometric detection of PSA-specific bar-code DNA. PSA concentration (sample volume of 10 μl) was varied from 300 fM to 3 aM and a negative control sample where no PSA was added (control) is shown. For all seven samples, 2 μl of antidinitrophenyl (10 pM) and 2 μl of β-galactosidase (10 pM) were added as background proteins. Also shown is PCR-less detection of PSA (30 aM and control) with 30 nm NP probes (inset). Chips were imaged with the Verigene ID system (*20*).

Table 1. Detection Limits of Nucleic Acid Assays[a]

	assay	ss DNA	PCR products	genomic DNA
nanostructure-based methods	colorimetric[29] (cross-linked Au nanoparticles)	~10 nM		
	colorimetric[36] (non-cross-linked Au nanoparticles)	60 nM		
	magnetic relaxation[97] (iron oxide nanoparticles)	20 pM		
	electrochemical[96] (nanoparticles)	270 pM		
	scanometric[35,66,67] (Au nanoparticles with Ag amplification)	50 fM	100 aM[b]	200 fM
	Raman spectroscopy[68] (Au nanoparticles with Ag amplification)	~1 fM		
	electrical[93] (Au nanoparticles with Ag amplification)	500 fM		
	electrical[99] (Si nanowire)	10 fM		
	electrical[103] (carbon nanotube)	54 aM		
	resonant light-scattering[61–66] (metal nanoparticles)	170 fM[b]		33 fM
	fluorescence[56] (ZnS and CdSe quantum dots)	2 nM		
	surface plasmon resonance[41] (Au nanoparticles)	10 pM		
	quartz crystal microbalance[94] (Au nanoparticles)	~1 fM		
	laser diffraction[42] (Au nanoparticles)	~50 fM		
	fluorescence[45] (fluorescent nanoparticles)	~1 fM		
	bio-bar-code amplification[71] (Au nanoparticles with Ag amplification)	500 zM		
other non-enzymatic based methods	fluorescence[35] (molecular fluorophores)		~600 fM[b]	
	fluorescence (dendrimer amplification)[134]		2.5 μg	
	electrochemical amplification[136] (electroactive reporter molecules)	100 aM		

[a] Detection limits can vary based on target length and sequence; therefore, it is difficult to compare assays without testing them using identical targets and conditions. [b] Values taken from ref 34.

Table 2. Detection Limits of Protein Assays

	assay	target	protein in saline	protein in serum
nanostructure-based methods	optical[72] (Au nanoshells)	rabbit IgG	0.88 ng/mL (~4.4 pM)[a]	0.88 ng/mL (~4.4 pM)[c]
	optical[74] (Au nanoparticles)	IgE and IgG1	~20 nM	
	magnetic relaxation[98] (iron oxide nanoparticles)	adenovirus (ADV) and herpes simplex virus (HSV)	100 ADV/ 100μL	50 HSV/ 100 μL
	scanometric[79] (Au nanoparticles with Ag amplification)	mouse IgG	200 pM	
	Raman[82] (Au nanoparticles with Raman labels)	prostate-specific antigen		30 fM
	surface plasmon resonance[83,84] (triangular Ag particles on surfaces)	streptavidin(S A) and anti-biotin (AB)	~1 pM SA and ~700 pM AB	
	electrical[110] (single-walled carbon nanotubes)	10E3 antibody to U1A RNA splicing factor	~1 nM	
	electrical[20] (Si nanowires)	streptavidin	10 pM	
	bio-bar-code amplification[75] (Au nanoparticles with Ag amplification)	prostate-specific antigen	30 aM (3 aM)[b]	(30 aM)[b]
molecular fluorophore methods	enzyme-linked immunosorbent assay	various	pM range	pM range
electrochemical methods	electrochemical amplification[137] (oligonucleotide reporter molecules)	IgG	13 fM	
enzyme-based amplification methods	immuno-PCR[76]	bovine serum albumin	2 fM	
	rolling circle amplification[77]	prostate-specific antigen	3 fM	

[a] Reported in ng/mL; authors converted to molar concentration for ease of comparison. [b] These values are the lower limits when PCR is used to amplify the bar-code DNA prior to scanometric detection of bar codes.

Surface Plasmon

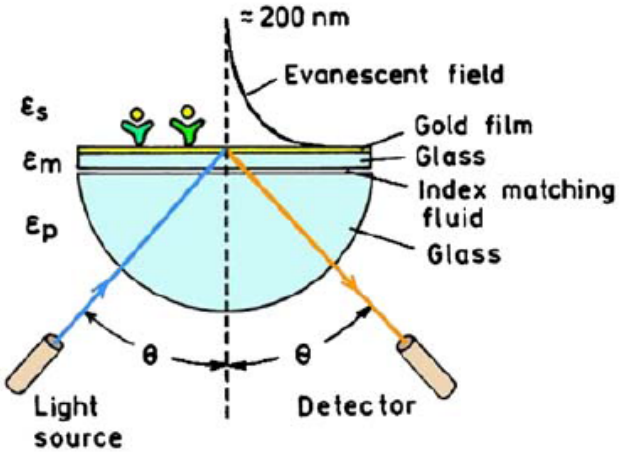

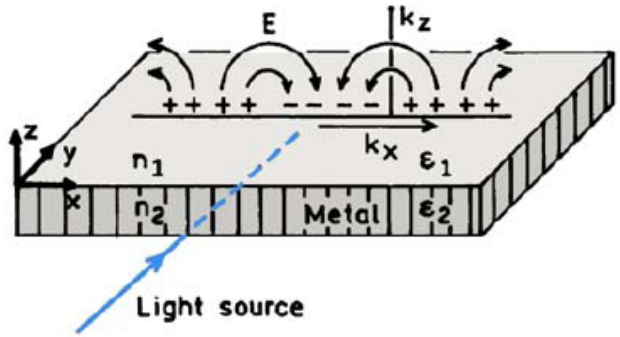

Figure 3. Schematics of an SPR experiment (top) and of the light-induced surface plasmons (bottom).

(b)

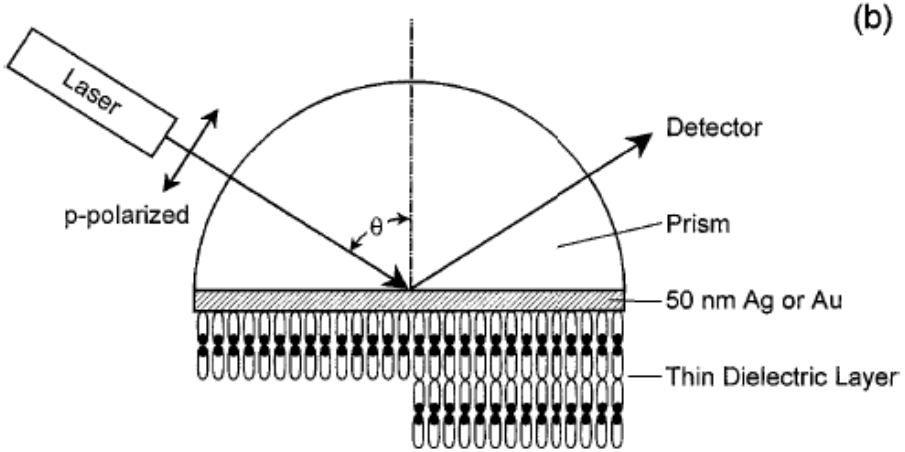

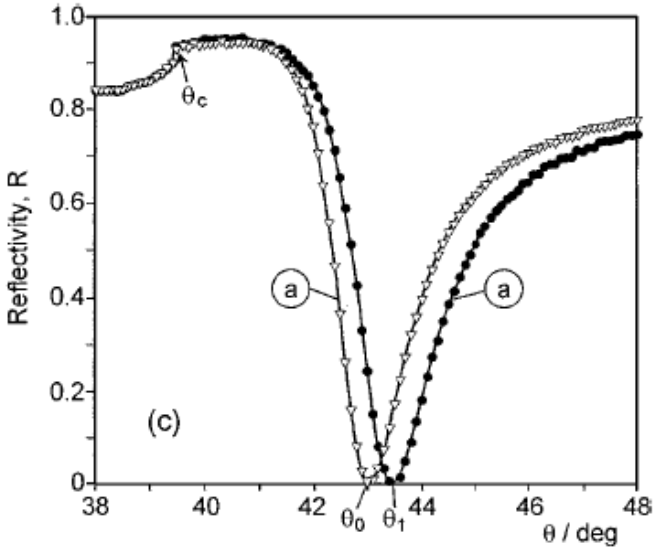

Drift: Drude model

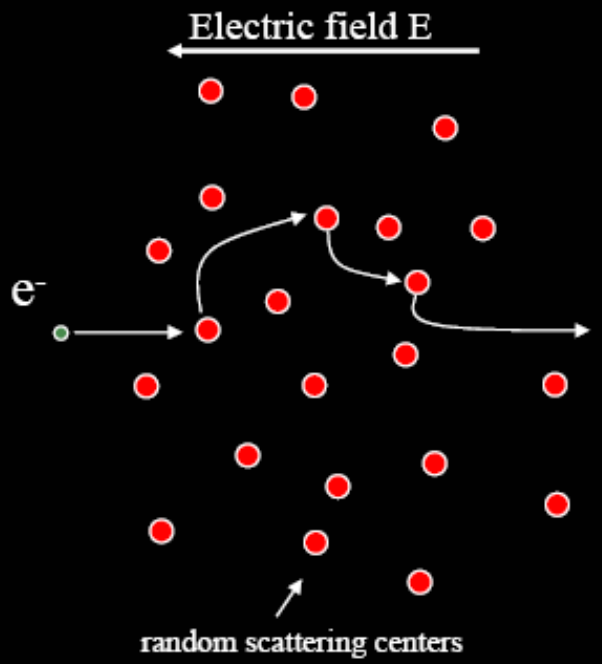

$$F = ma$$

$$eE = m\frac{\partial v}{\partial t}$$

$$v_{avg} = \underbrace{\frac{e\tau}{m}}_{\mu} E$$

$$j = nev_{avg} = \underbrace{\frac{ne^2\tau}{m}}_{\sigma} E$$

$$m\frac{\partial}{\partial t}\langle\vec{v}\rangle = q\vec{E} - \gamma\langle\vec{v}\rangle$$

$$\sigma(\omega) = \frac{\sigma_0}{1 + i\omega\tau}$$

AC Dielectric Response

$$\varepsilon_m = 1 - \frac{\omega_p^2}{\omega^2}$$

Plasma frequency

polarizability of a small metal sphere with dielectric function $\varepsilon(\lambda)$

$$\alpha = R^3 \frac{\varepsilon - 1}{\varepsilon + 2}\,.$$

$$\varepsilon = \varepsilon_\mathrm{b} + 1 - \frac{\omega_\mathrm{P}^2}{\omega^2 + \mathrm{i}\omega\gamma}\,,$$

$$\alpha = \frac{R^3(\varepsilon_\mathrm{b}\omega^2 - \omega_\mathrm{P}^2) + i\omega\gamma\varepsilon_\mathrm{b}}{[(\varepsilon_\mathrm{b} + 3)\omega^2 - \omega_\mathrm{P}^2] + i\omega\gamma(\varepsilon_\mathrm{b} + 3)}\,.$$

$\omega_\mathrm{R} = \frac{\omega_\mathrm{P}}{\sqrt{\varepsilon_\mathrm{b}+3}}$ $\qquad\qquad$ $\gamma(\varepsilon_\mathrm{b} + 3)$.

Biomolecular Binding in Real Time

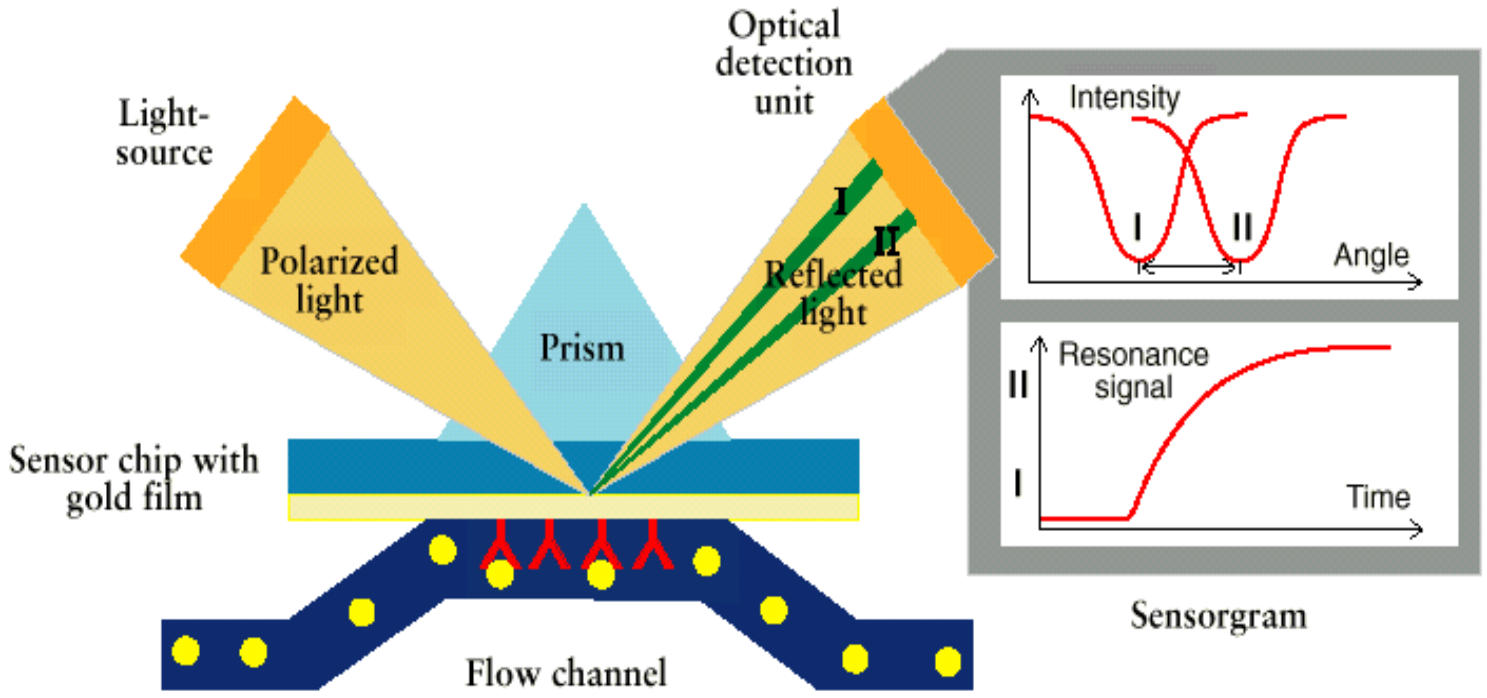

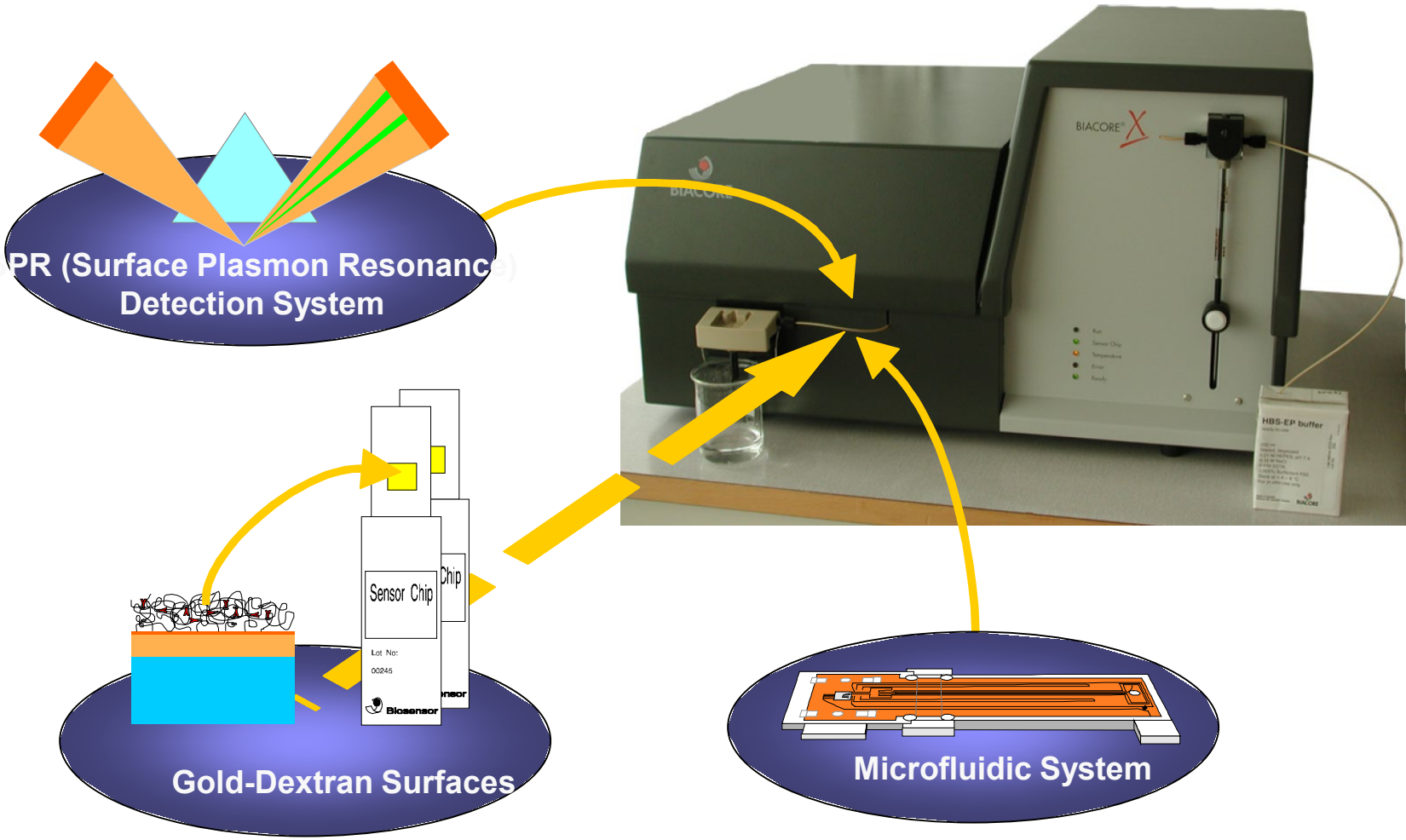
SPR (Surface Plasmon Resonance)
Detection System
BIACORE X
HBS-EP buffer
Sensor Chip
Lot No:
00245
Biosensor
Gold-Dextran Surfaces
Microfluidic System

SPR Imaging Apparatus

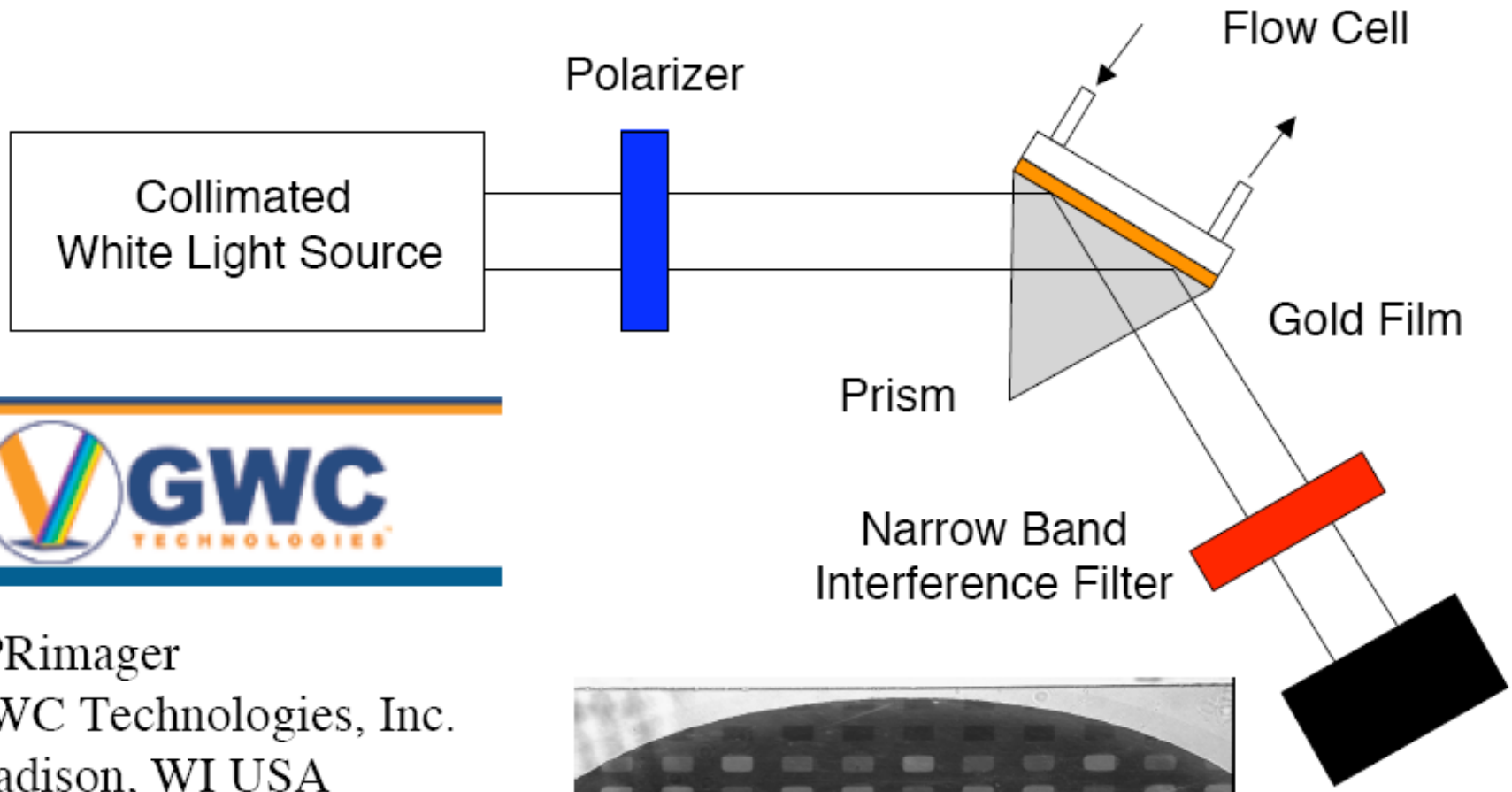

SPRimager
GWC Technologies, Inc.
Madison, WI USA

www.gwctechnologies.com

Raw Image

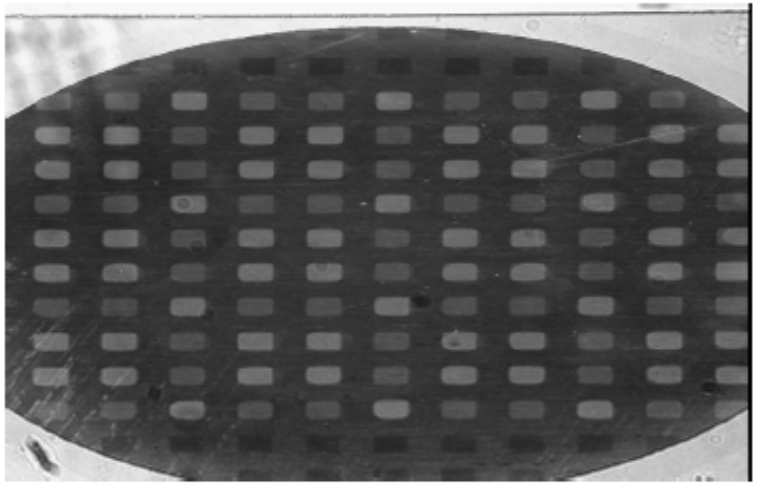

UCIrvin
University of California, Ir

Localized Plasmon

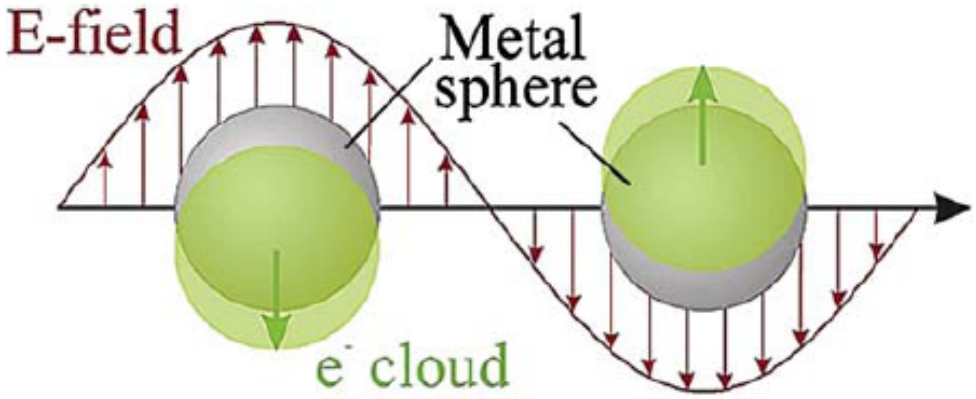

Figure 6. Schematic of plasmon oscillation for a sphere. From [39].

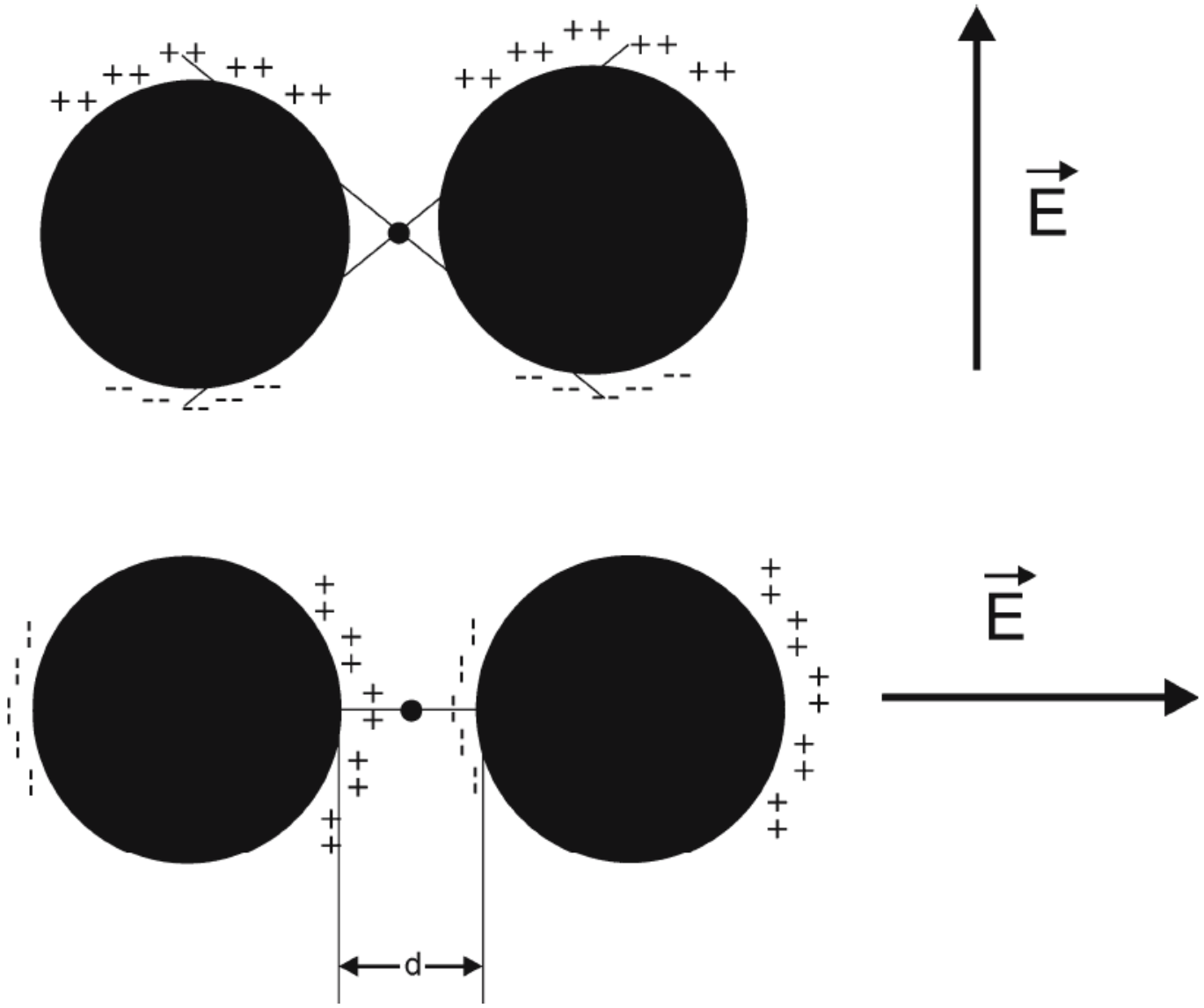
E
E
d

field enhancement

$E_s = gE_0$, where E_0 is the magnitude of the incident field

$$E_R \propto \alpha_R E_s \propto \alpha_R g E_0$$

$$E_{SERS} \propto \alpha_R g g' E_0$$

$$I_{SERS} \propto |\alpha_R|^2 |gg'|^2 I_0$$

$$g \cong g'$$

$$|E_L|^4 = |g|^4.$$

Probing Single Molecules and Single Nanoparticles by Surface-Enhanced Raman Scattering

SCIENCE • VOL. 275 • 21 FEBRUARY 1997

Shuming Nie* and Steven R. Emory

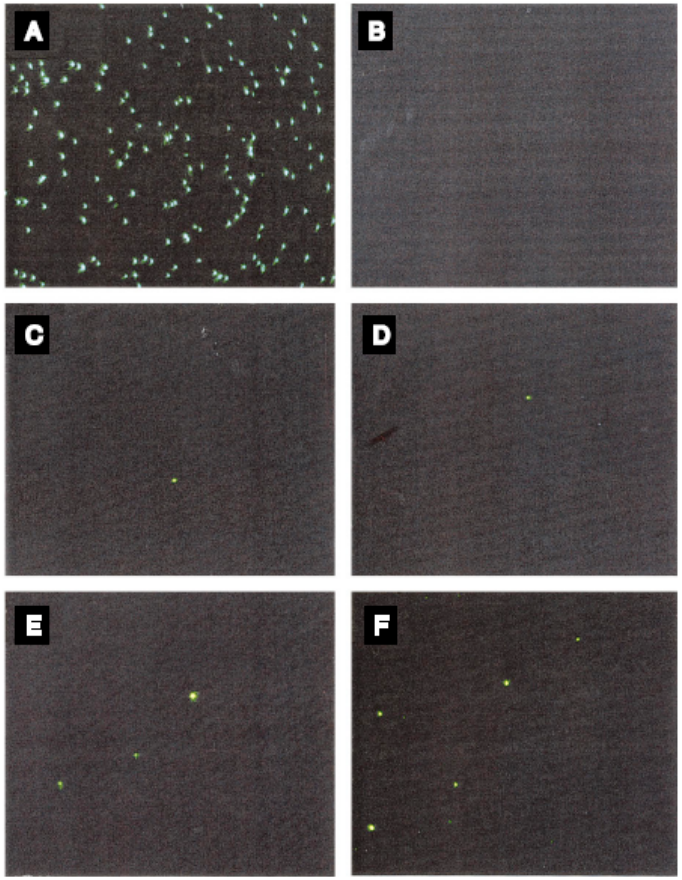

Fig. 1. Single Ag nanoparticles imaged with evanescent-wave excitation. Total internal reflection of the laser beam at the glass-liquid interface was used to reduce the laser scattering background. The instrument setup for evanescent-wave microscopy was adapted from Funatsu *et al.* (*11*). The images were directly recorded on color photographic film (ASA-1600) with a 30-s exposure by a Nikon 35-mm camera attached to the microscope. (**A**) Unfiltered photograph showing scattered laser light from all particles immobilized on a polylysine-coated surface. (**B**) Filtered photographs taken from a blank Ag colloid sample (incubated with 1 mM NaCl and no R6G analyte molecules). (**C**) and (**D**) Filtered photographs taken from a Ag colloid sample incubated with 2×10^{-11} M R6G. These images were selected to show at least one Raman scattering particle. Different areas of the cover slip were rapidly screened, and most fields of view did not contain visible particles. (**E**) Filtered photograph taken from Ag colloid incubated with 2×10^{-10} M R6G. (**F**) Filtered photograph taken from Ag colloid incubated with 2×10^{-9} M R6G. A high-performance bandpass filter was used to remove the scattered laser light and to pass Stokes-shifted Raman signals from 540 to 580 nm (920 to 2200 cm^{-1}). Continuous-wave excitation at 514.5 nm was provided by an Ar ion laser. The total laser power at the sample was 10 mW. Note the color differences between the scattered laser light in (A) and the red-shifted light in (C) through (F).

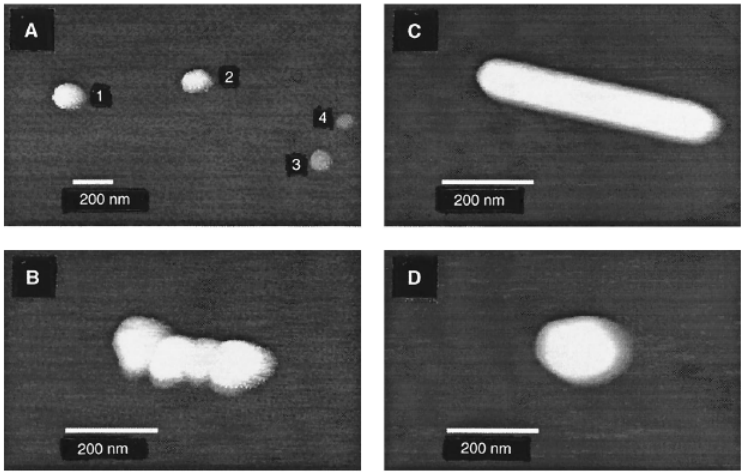

Fig. 2. Tapping-mode AFM images of screened Ag nanoparticles. (**A**) Large area survey image showing four single nanoparticles. Particles 1 and 2 were highly efficient for Raman enhancement, but particles 3 and 4 (smaller in size) were not. (**B**) Close-up image of a hot aggregate containing four linearly arranged particles. (**C**) Close-up image of a rod-shaped hot particle. (**D**) Close-up image of a faceted hot particle.

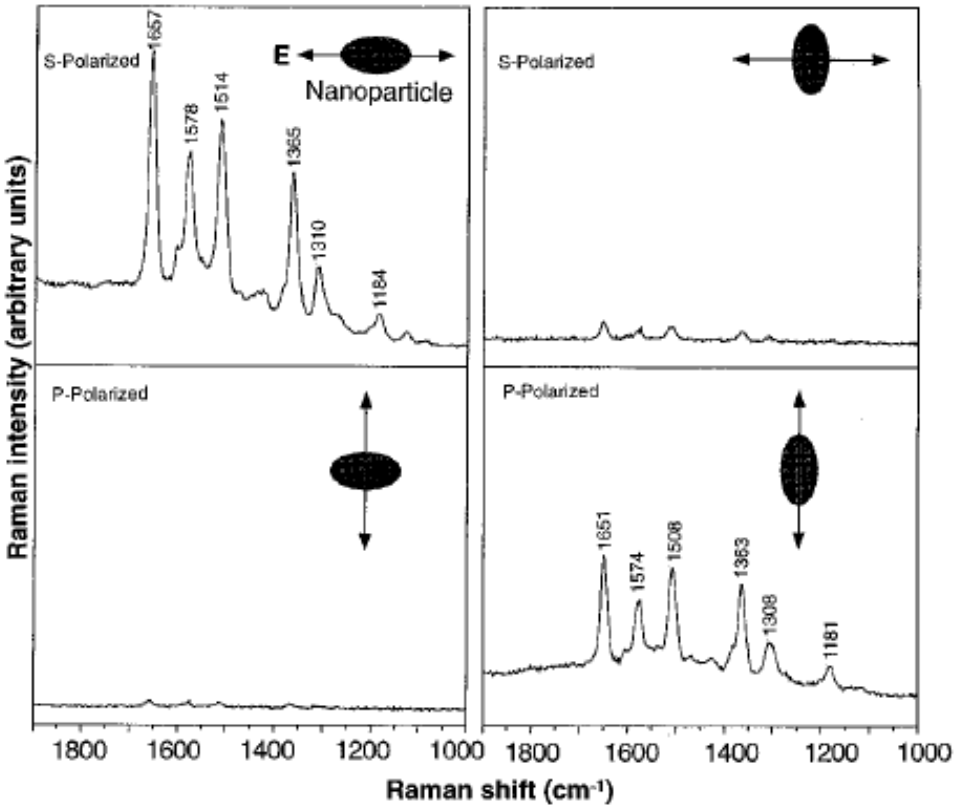

Fig. 3. Surface-enhanced Raman spectra of R6G obtained with a linearly polarized confocal laser beam from two Ag nanoparticles. The R6G concentration was 2×10^{-11} M, corresponding to an average of 0.1 analyte molecule per particle. The direction of laser polarization and the expected particle orientation are shown schematically for each spectrum. Laser wavelength, 514.5 nm; laser power, 250 nW; laser focal radius, ~250 nm; integration time, 30 s. All spectra were plotted on the same intensity scale in arbitrary units of the CCD detector readout signal.

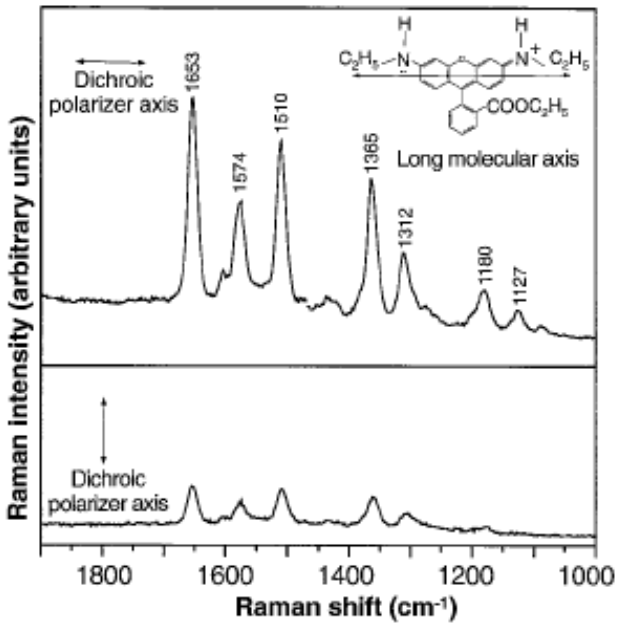

Fig. 4. Emission-polarized surface-enhanced Raman signals of R6G observed from a single Ag nanoparticle with a polarization-scrambled confocal laser beam. A dichroic sheet polarizer was rotated 90° to select Raman scattering signals polarized parallel (upper spectrum) or perpendicular (lower spectrum) to the long molecular axis of R6G. (**Inserts**) Structure of R6G, the electronic transition dipole (along the long axis when excited at 514.5 nm), and the dichroic polarizer orientations. Other conditions as in Fig. 3.

troscopic signatures of adsorbed molecules. For single rhodamine 6G molecules adsorbed on the selected nanoparticles, the intrinsic Raman enhancement factors were on the order of 10^{14} to 10^{15}, much larger than the ensemble-averaged values derived from conventional measurements. This enormous enhancement leads to vibrational Raman signals that are more intense and more stable than single-molecule fluorescence.

Electromagnetic contributions to single-molecule sensitivity in surface-enhanced Raman scattering

PRE 62 4318

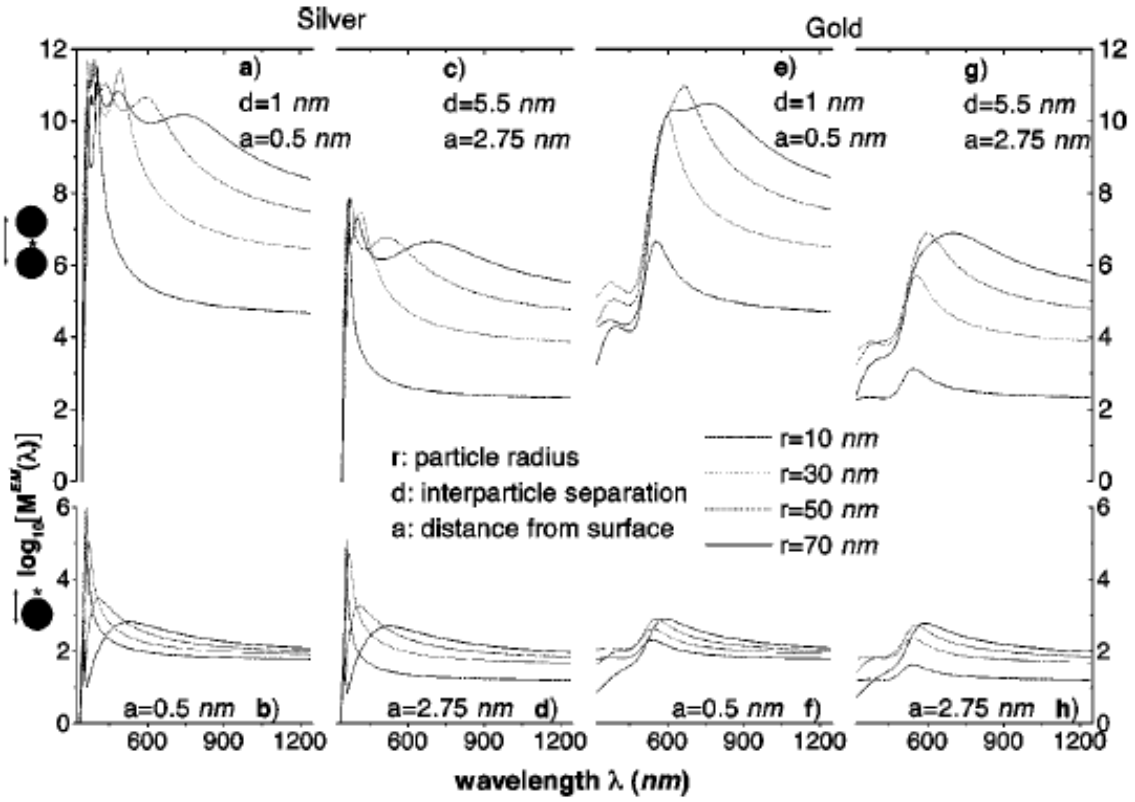

FIG. 3. (Color) EM-enhancement factor M^{EM} at a cross section through six different silver particle configurations. The wavelength of the incident field is $\lambda = 514.5$ nm with vertical polarization. The left-hand column illustrates the EM enhancement for dimer configurations of two spheres (top) and two polygons (bottom) with a separation of 1 nm. The middle column shows the same situation, but with a separation distance of 5.5 nm. The right-hand column shows the case of an isolated single particle. All particles share a common largest dimension of 90 nm. Note that the color scale from dark blue to dark red is logarithmic, covering the interval $10^0 < M^{EM} < 10^8$. Regions with enhancement outside this interval are shown in dark blue and dark red, respectively.

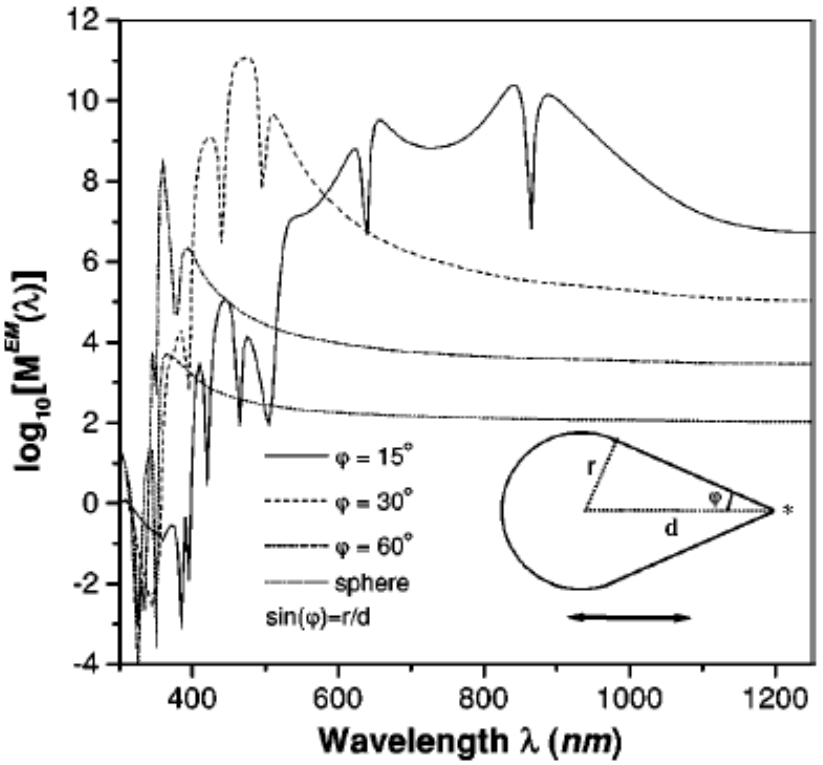

FIG. 5. EM-enhancement factor for a rotationally symmetric silver droplet as a function of the angle defining the opening edge ϕ. The field is polarized parallel to the axis of the droplet and the evaluation position (star) is located 0.5 nm outside the tip. As the droplet becomes sharper the enhancement increases several orders of magnitude.

Nanosphere Arrays with Controlled Sub-10-nm Gaps as Surface-Enhanced Raman Spectroscopy Substrates

J. AM. CHEM. SOC. 2005, *127*, 14992−14993

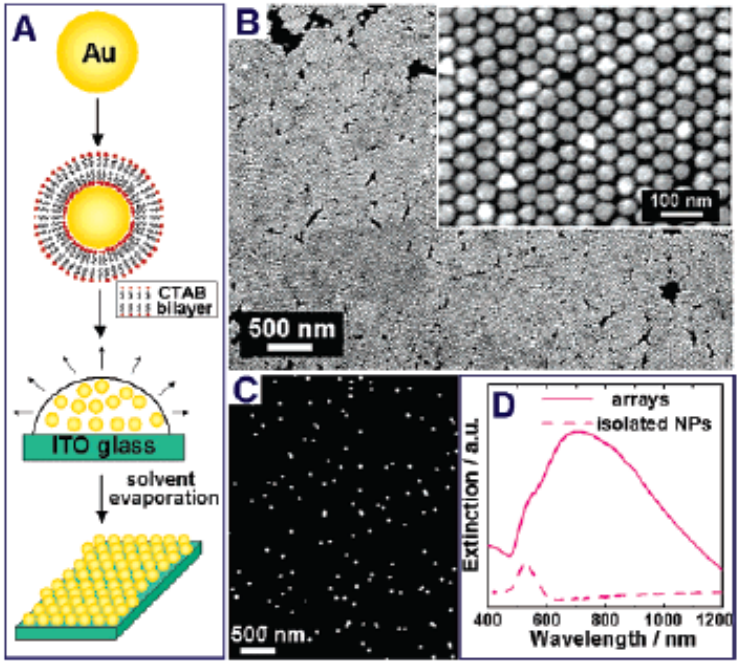

Figure 1. (A) Schematic illustration of the fabrication of sub-10-nm gap Au NP arrays. (B) SEM image of the arrays. (C) SEM image of monolayer of isolated Au NPs on ITO glass. (D) Vis−NIR extinction spectrum of the monolayer of isolated Au NPs and arrays.

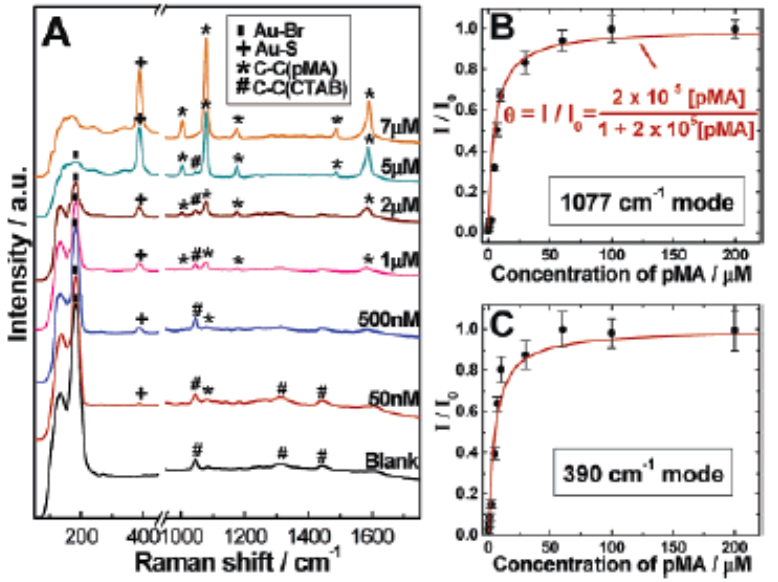

Figure 2. (A) SERS spectra of 5 μL of pMA with different concentrations deposited on the NP arrays. The excitation laser wavelength is 785 nm. Adsorption isotherm of pMA on the NP arrays obtained according to (B) 1077 and (C) 390 cm^{-1} modes in the SERS spectra. I_0 is the peak intensity of a saturated pMA monolayer.

Profiling the Near Field of a Plasmonic Nanoparticle with Raman-Based Molecular Rulers

NANO LETTERS

2006
Vol. 6, No. 10
2338−2343

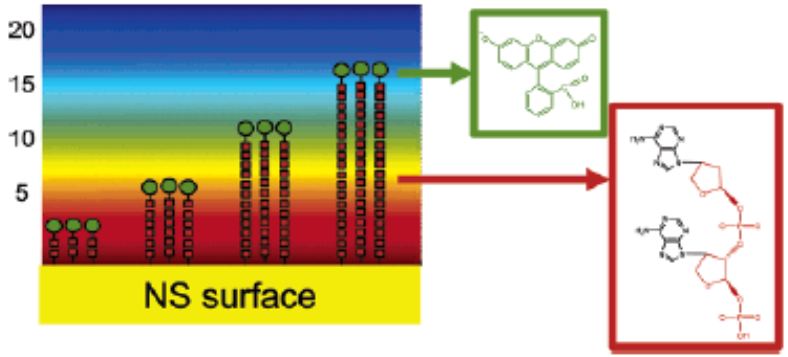

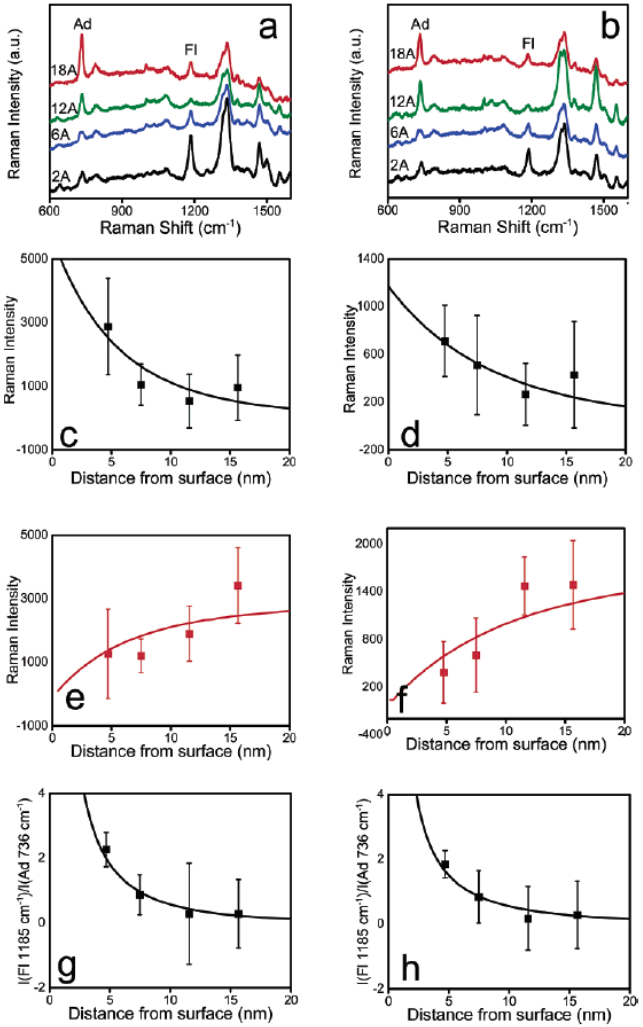

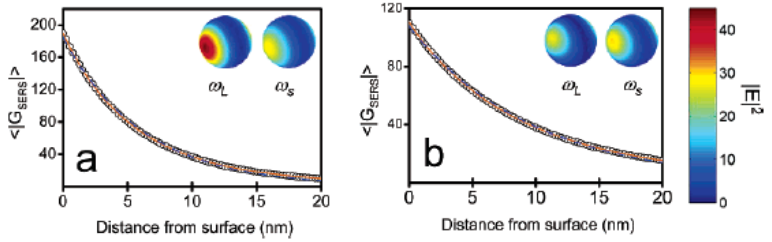

Anal. Chem. 2003, *75*, 6171−6176

Spectroscopic Tags Using Dye-Embedded Nanoparticles and Surface-Enhanced Raman Scattering

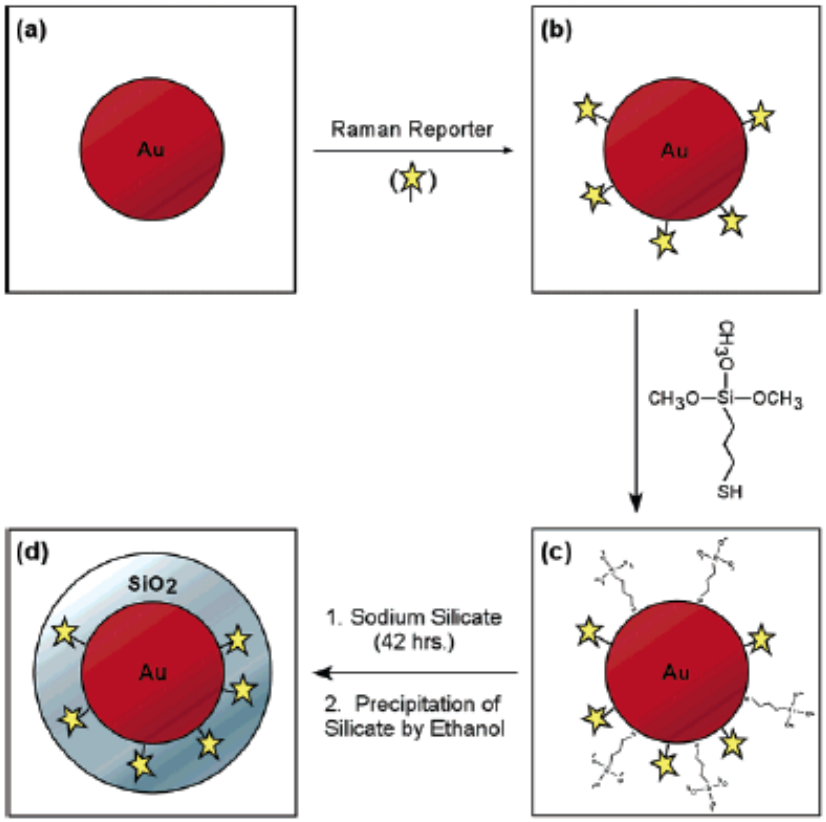

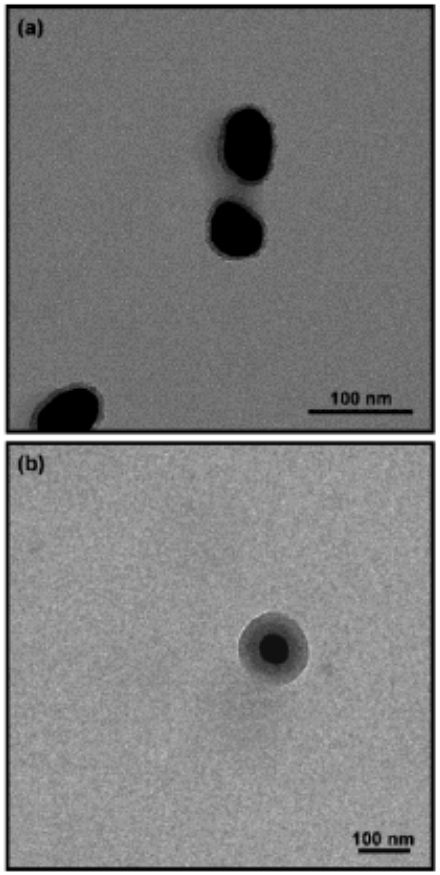

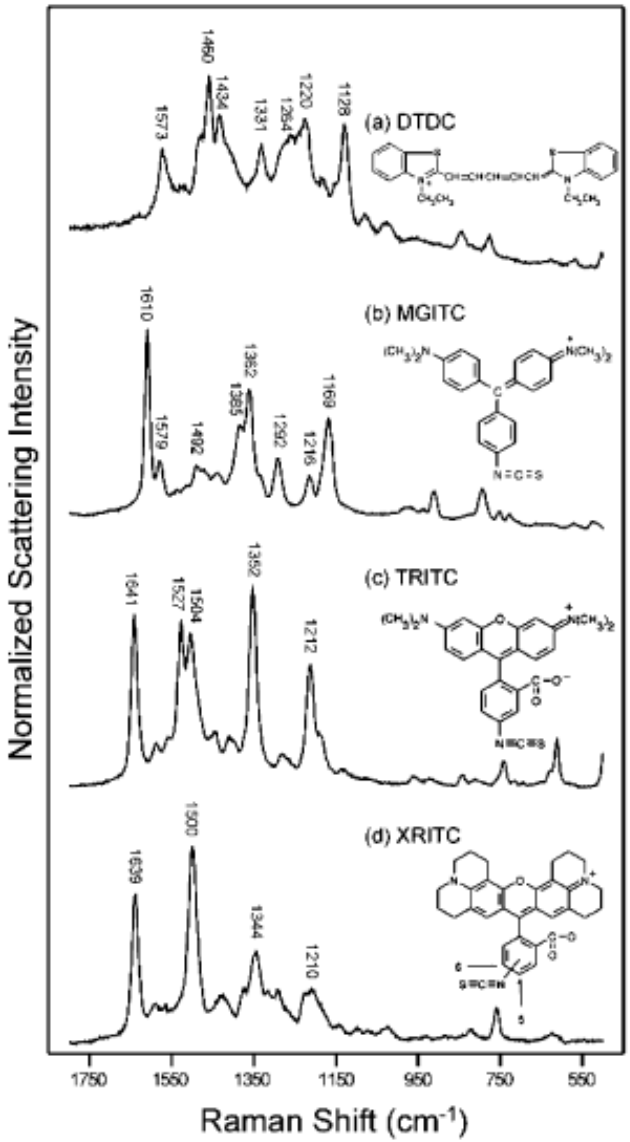

Figure 4. Chemical structures of four Raman reporters and their surface-enhanced resonance Raman spectra: (a) 3,3′-Diethylthiadicarbocyanine iodide (DTDC); (b) malachite green isothiocyanate (MGITC); (c) tetramethylrhodamine-5-isothiocyanate (TRITC); and (e) rhodamine-5-(and-6)-isothiocyanate (XRITC).

Anal. Chem. 2006, *78*, 6967−6973

Nanoparticle Probes with Surface Enhanced Raman Spectroscopic Tags for Cellular Cancer Targeting

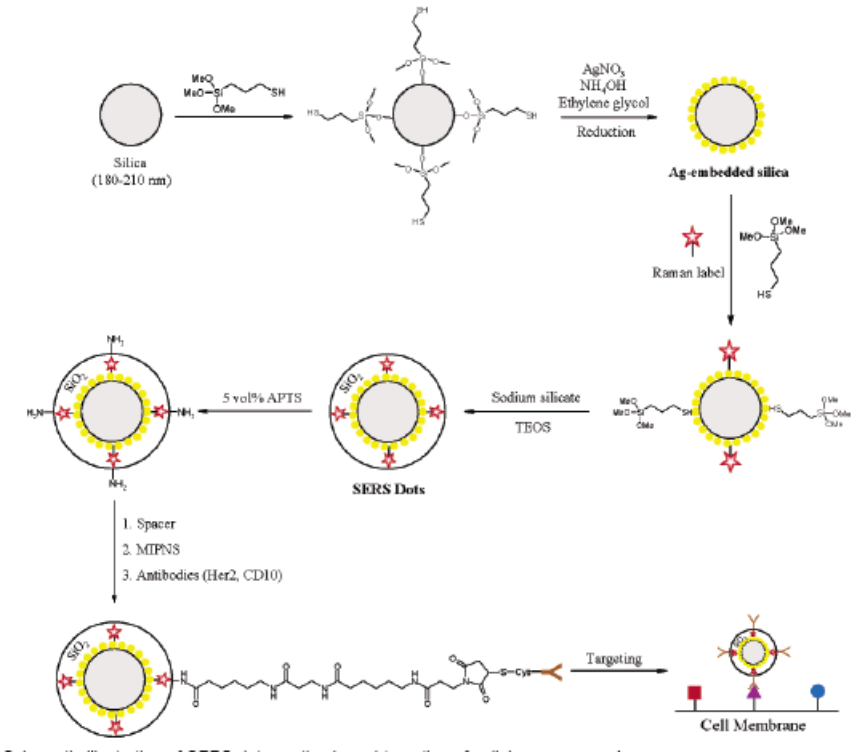

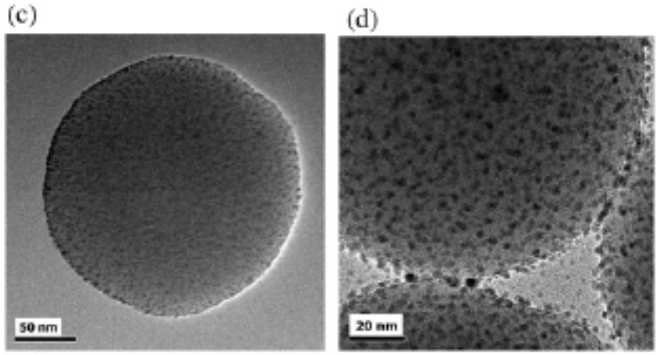

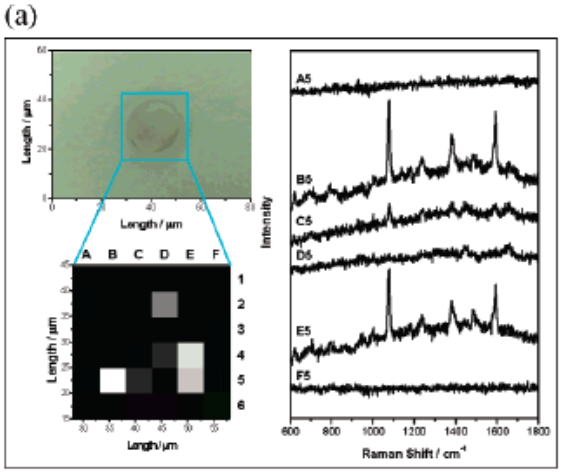

Anal. Chem. 2007, *79*, 916−922

Biological Imaging of HEK293 Cells Expressing PLCγ1 Using Surface-Enhanced Raman Microscopy

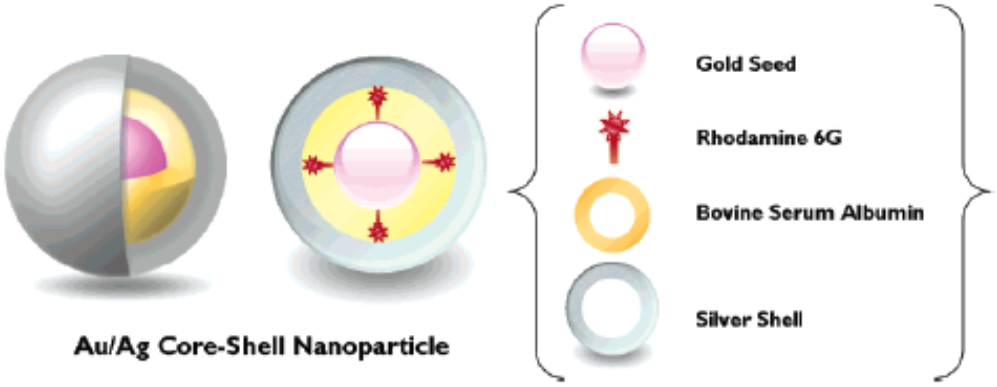

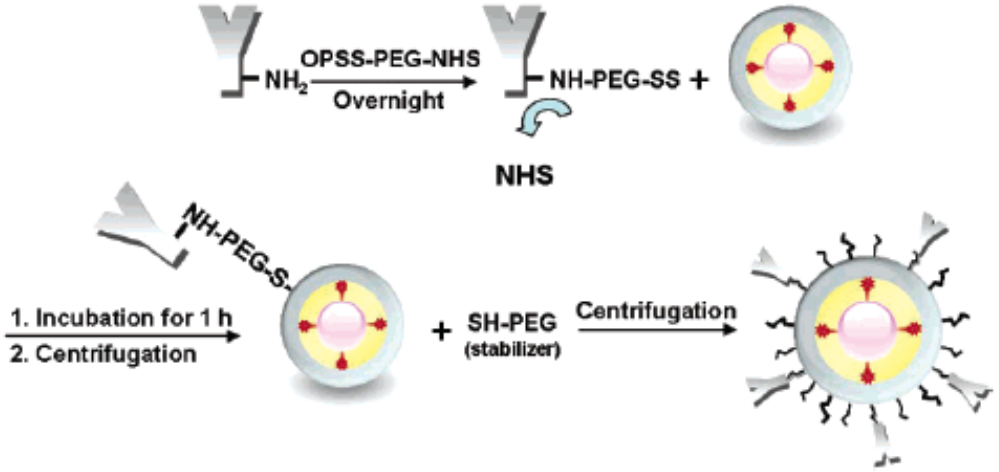

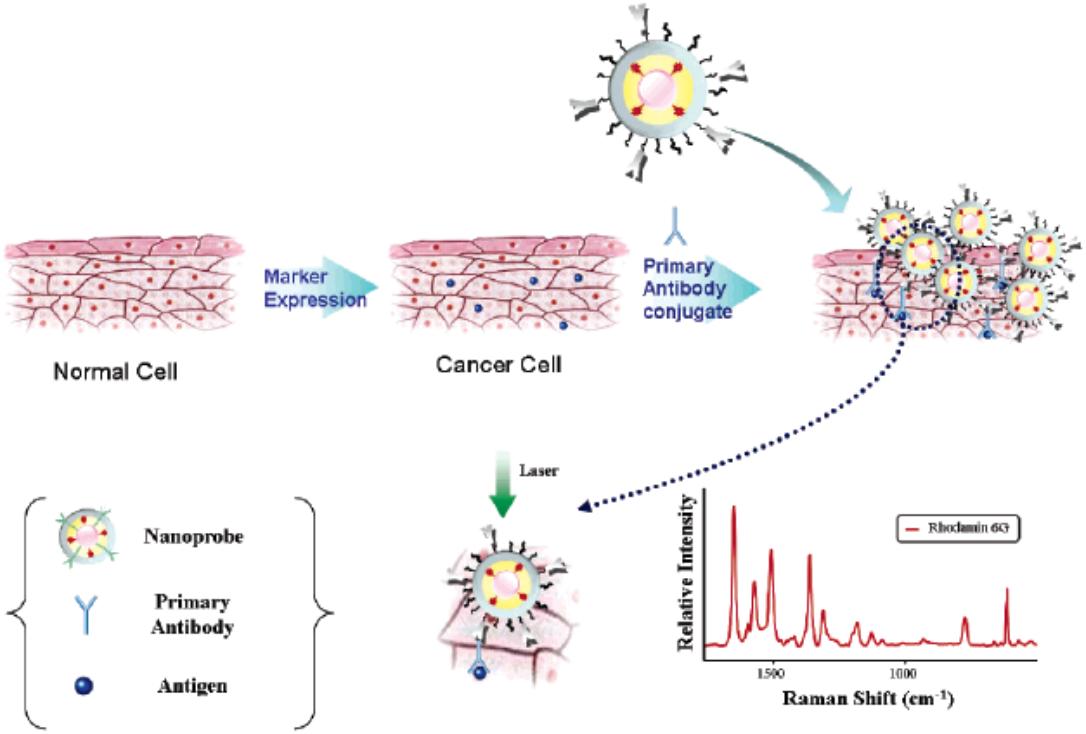

Figure 4. Schematic diagram depicting immobilization of Au/Ag core−shell nanoprobes on PLCγ1-expressing HEK293 cells and their SERS detection.

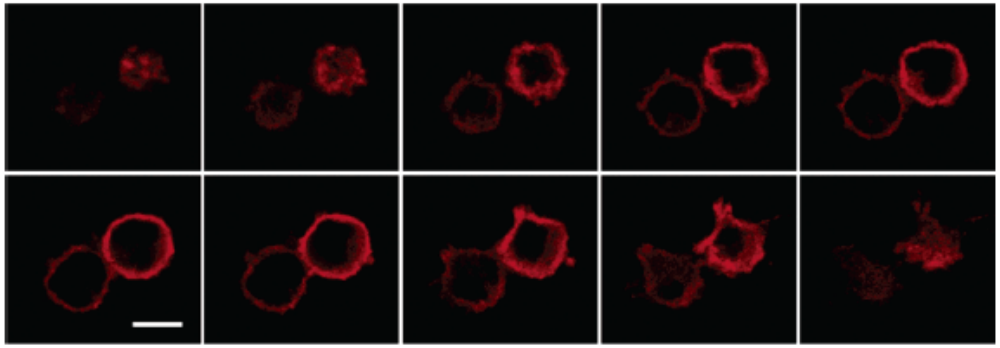

Figure 5. Serial fluorescence optical sections of PLCγ1-expressing HEK293 cells using red QDs. The *z*-axis interval of optical slices is 1.3 μm. Cells were incubated for 30 min in red QDs, after which the free QDs were washed away. These fluorescence images indicate that PLCγ1 markers are only expressed on the surface membranes. Scale bar, 10 μm.

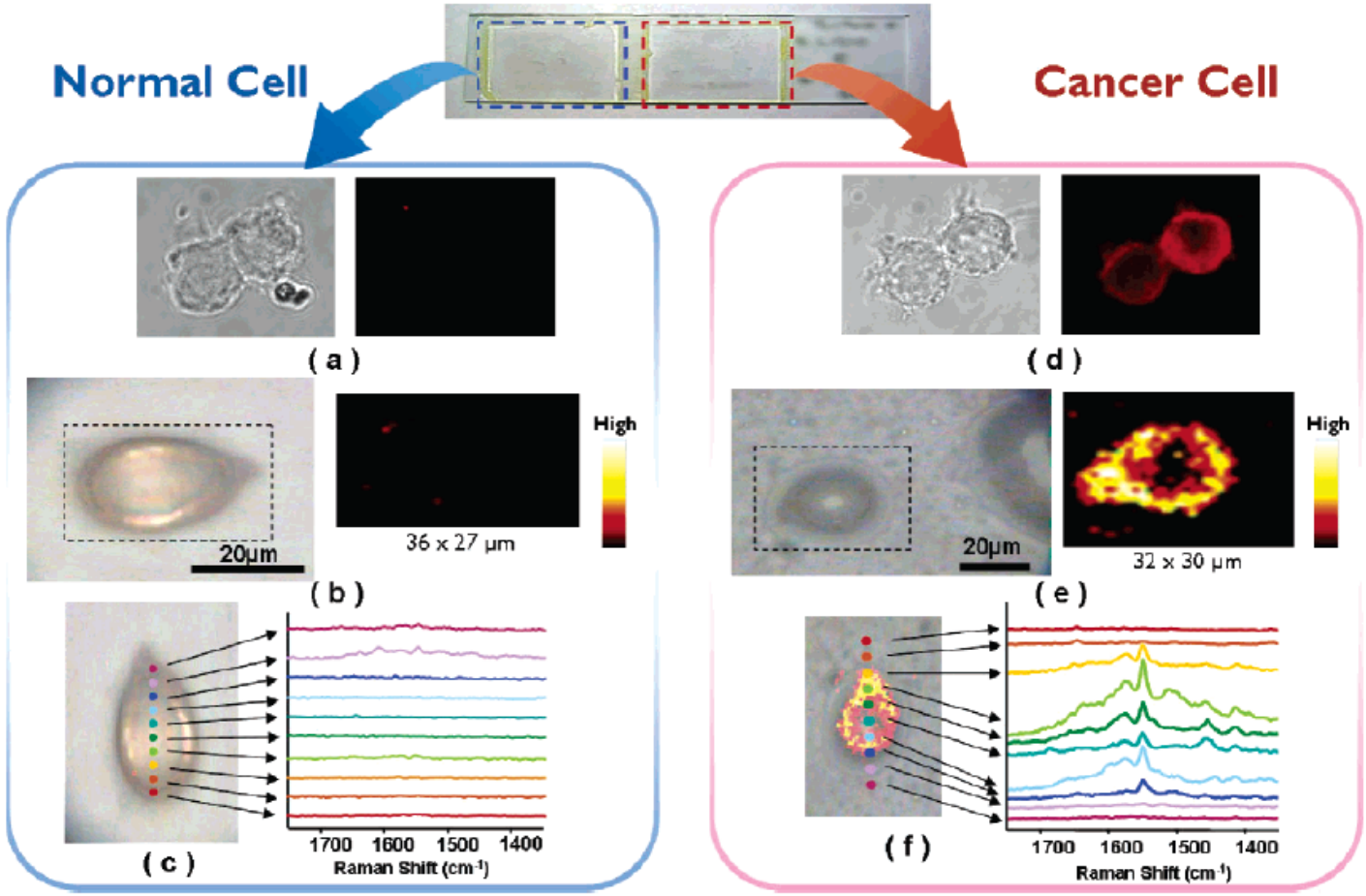

Figure 6. Fluorescence and SERS images of normal HEK293 cells and PLCγ1-expressing HEK293 cells. (a) QD-labeled fluorescence images of normal cells: (left) brightfield image, (right) fluorescence image. (b) SERS images of single normal cell: (left) brightfield image, (right) Raman mapping image of single normal cell based on the 1650-cm^{-1} R6G peak. The cell area was scanned with an interval of 1 μm. Intensities are scaled to the highest value in each area. (c) Overlay image of brightfield and Raman mapping for single normal cell. Colorful spots indicate the laser spots across the middle of the cell along the *y* axis. (d) QD-labeled fluorescence images of cancer cells: (left) brightfield image, (right) fluorescence image. (e) SERS images of single cancer cell: (left) brightfield image, (right) Raman mapping image of single cancer cell based on the 1650-cm^{-1} R6G peak. The cell area was scanned with an interval of 1 μm. Intensities are scaled to the highest value in each area. (f) Overlay image of brightfield and Raman mapping for single cancer cell. Colorful spots indicate the laser spots across the middle of the cell along the *y* axis.

J|A|C|S
COMMUNICATIONS

Published on Web 12/15/2006

Mammalian Cell Surface Imaging with Nitrile-Functionalized Nanoprobes: Biophysical Characterization of Aggregation and Polarization Anisotropy in SERS Imaging

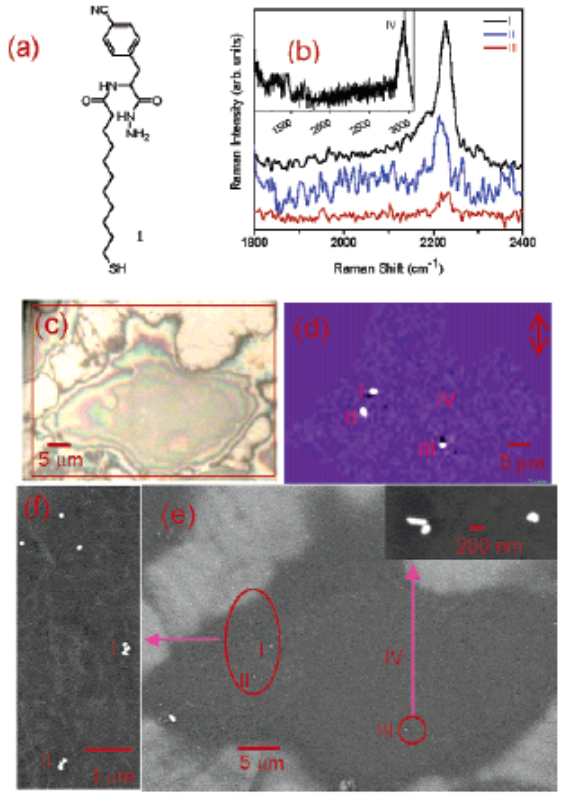

Figure 1. (a) The chemical structure of Raman reporter **1**; (b) Raman spectra of the CN vibration mode extracted from positions I, II, and III of the cell shown in the optical image (c). Inset of (b) is a cellular Raman spectrum taken from spot IV of the same cell. (d) Raman intensity map of the C≡N band of the same cell, and (e) the corresponding SEM image. Inset in (e) showed the NPs in the lower right circle. (f) The group of NPs as shown in the large oval of (e).

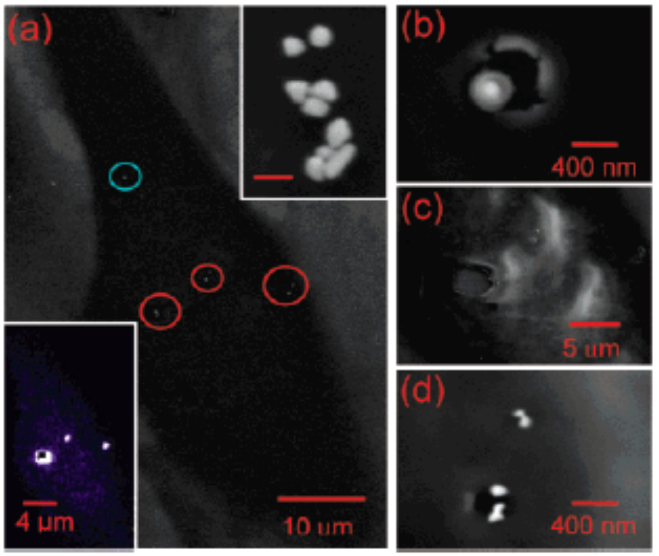

Figure 2. (a) SEM image of a cell. Upper right inset: magnification of a group of aggregated NPs. The scale bar is 200 nm. Lower left inset: the corresponding Raman intensity image of the same cell obtained with a power density of 10^5 W/cm^2. Laser-induced damage to the cell is shown in (b) the monomer (blue circle in a), (c) the aggregates, and (d) a pair of dimers.

Molecular imaging of live cells by Raman microscopy

Almar F Palonpon[1,2], Mikiko Sodeoka[2,3] and Katsumasa Fujita[1,2]

Current Opinion in Chemical Biology 2013, **17**:708–715

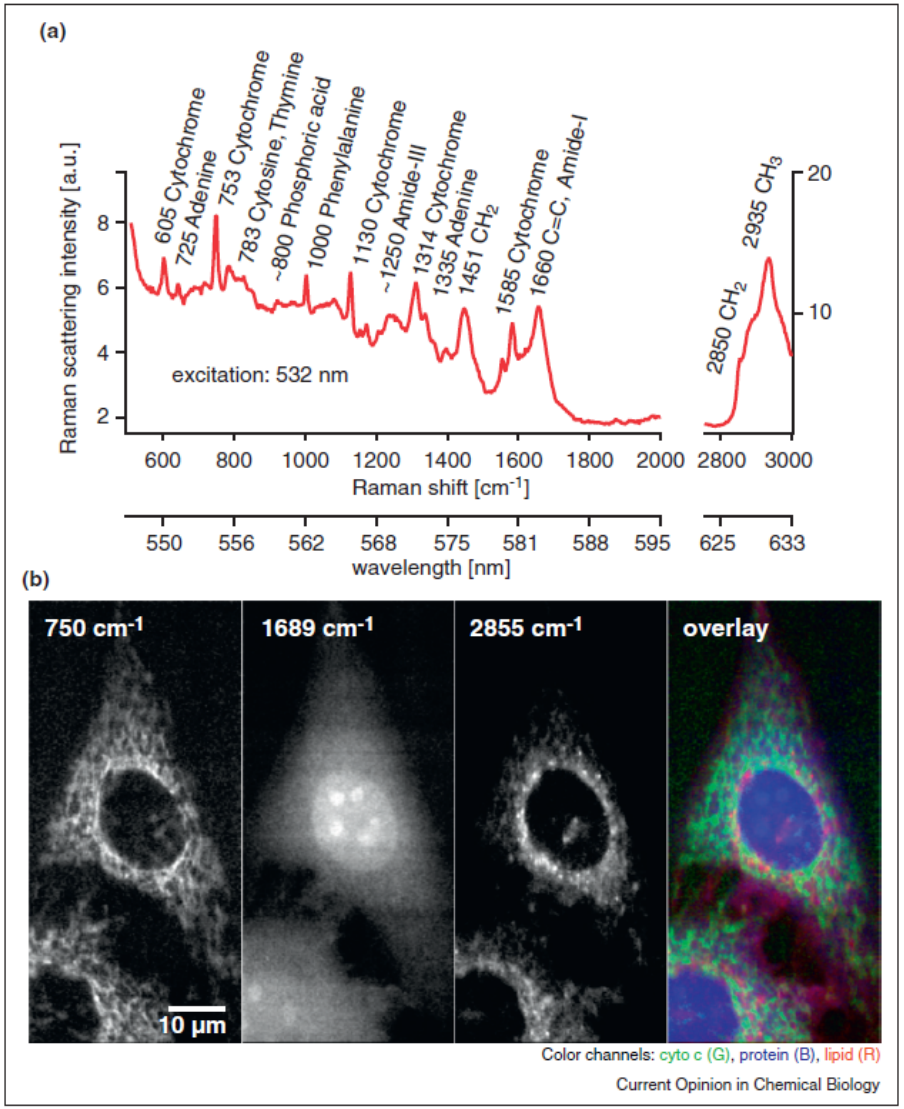

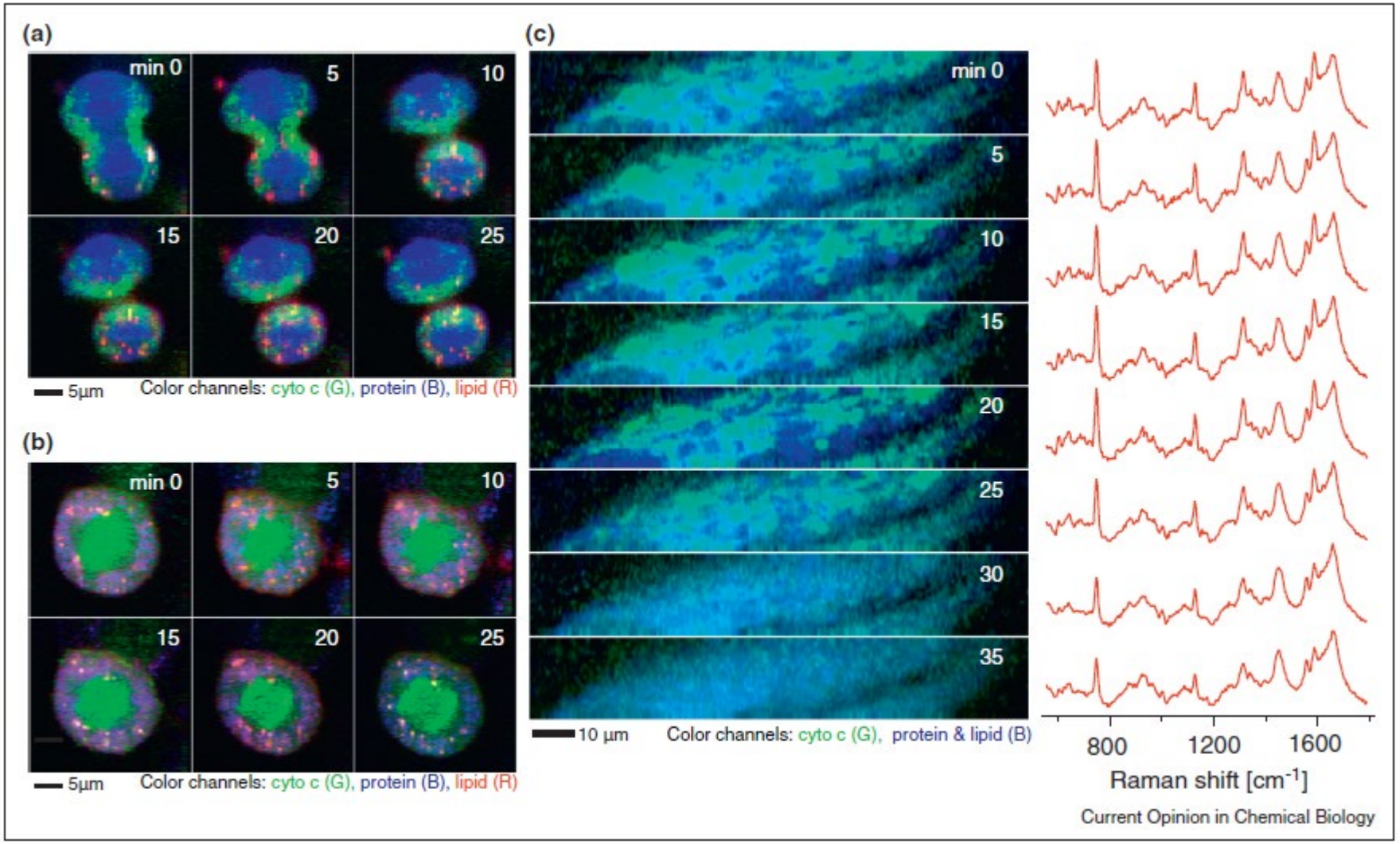
(a)
min 0
5
10
15
20
25
5µm
Color channels: cyto c (G), protein (B), lipid (R)
(b)
min 0
5
10
15
20
25
5µm
Color channels: cyto c (G), protein (B), lipid (R)
(c)
min 0
5
10
15
20
25
30
35
10 µm
Color channels: cyto c (G), protein & lipid (B)
800
1200
1600
Raman shift [cm-1]
Current Opinion in Chemical Biology

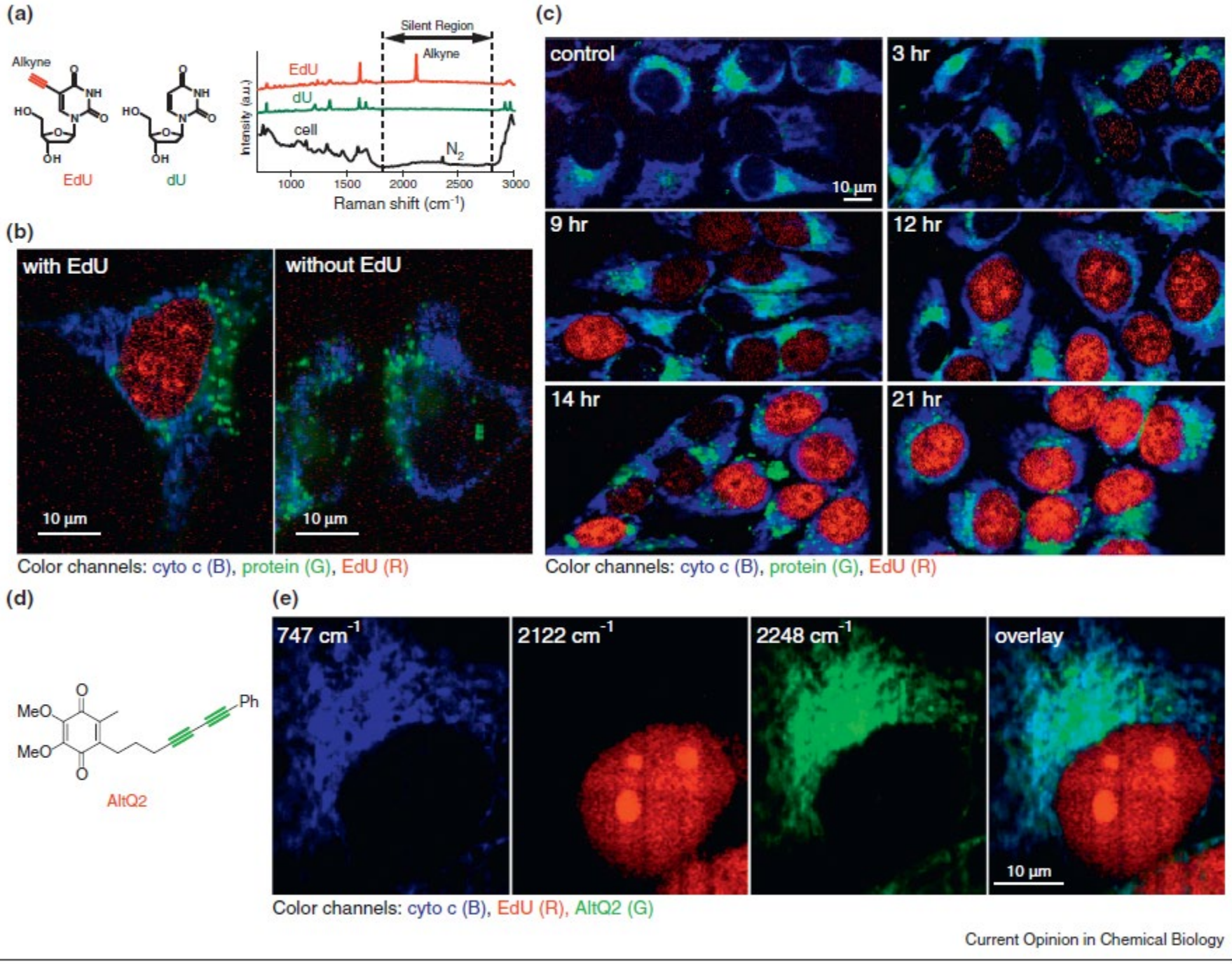
(a)
Alkyne
EdU
dU
Silent Region
Alkyne
EdU
dU
cell
N_2
Intensity (a.u.)
1000
1500
2000
2500
3000
Raman shift (cm^{-1})
(b)
with EdU
without EdU
10 μm
10 μm
Color channels: cyto c (B), protein (G), EdU (R)
(c)
control
3 hr
9 hr
12 hr
14 hr
21 hr
10 μm
Color channels: cyto c (B), protein (G), EdU (R)
(d)
MeO
MeO
Ph
AltQ2
(e)
747 cm^{-1}
2122 cm^{-1}
2248 cm^{-1}
overlay
10 μm
Color channels: cyto c (B), EdU (R), AltQ2 (G)

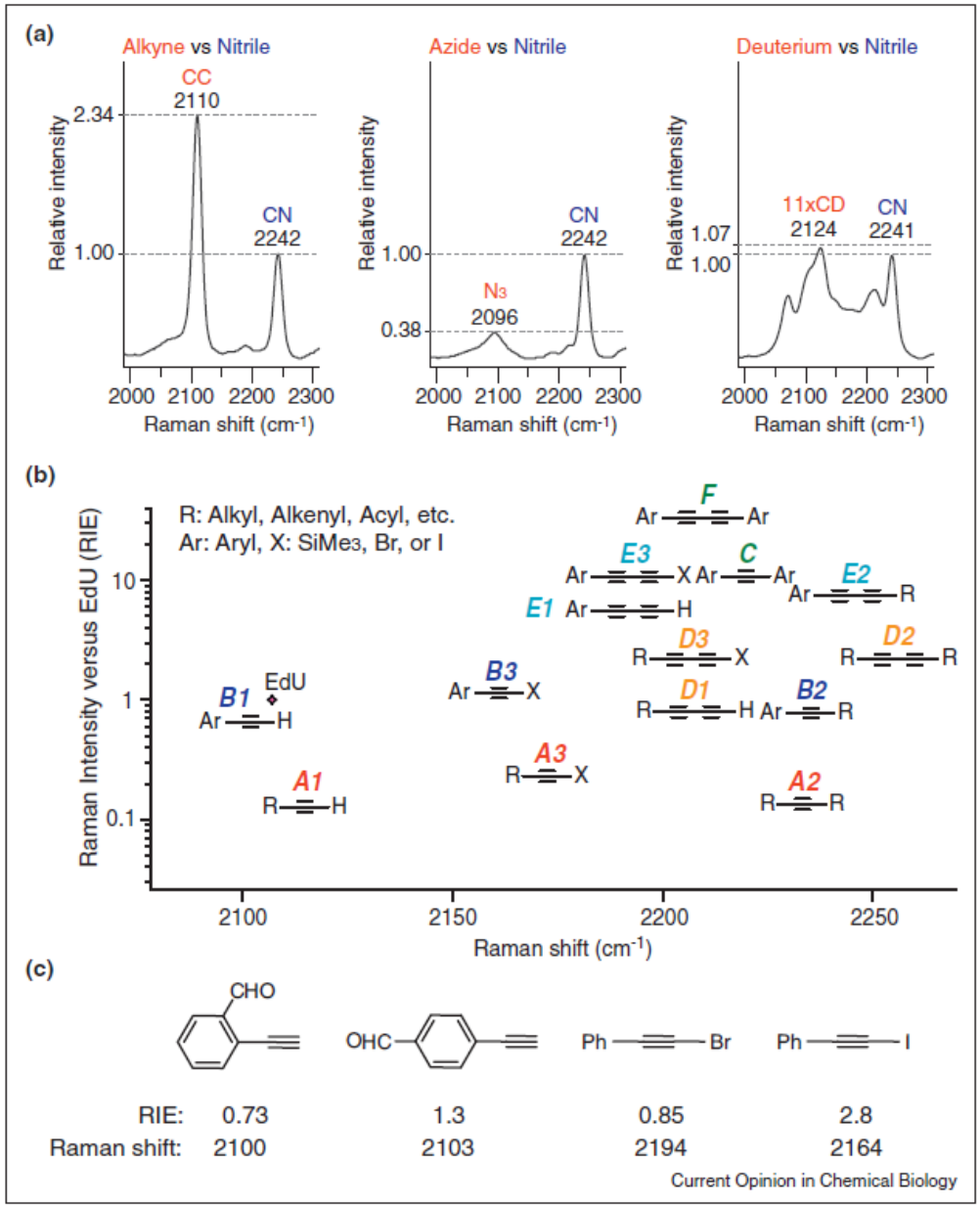
(a)
Alkyne vs Nitrile
CC
2110
2.34
1.00
CN
2242
Relative intensity
2000 2100 2200 2300
Raman shift (cm-1)
Azide vs Nitrile
CN
2242
1.00
N3
2096
0.38
Relative intensity
2000 2100 2200 2300
Raman shift (cm-1)
Deuterium vs Nitrile
11xCD
2124
CN
2241
1.07
1.00
Relative intensity
2000 2100 2200 2300
Raman shift (cm-1)
(b)
R: Alkyl, Alkenyl, Acyl, etc.
Ar: Aryl, X: SiMe3, Br, or I
Raman Intensity versus EdU (RIE)
10
1
0.1
F
Ar Ar
E3
Ar X
C
Ar Ar
E2
Ar R
E1
Ar H
D3
R X
D2
R R
B3
Ar X
D1
R H
B2
Ar R
EdU
B1
Ar H
A3
R X
A1
R H
A2
R R
2100
2150
2200
2250
Raman shift (cm-1)
(c)
CHO
OHC
Ph Br
Ph I
RIE: 0.73 1.3 0.85 2.8
Raman shift: 2100 2103 2194 2164
Current Opinion in Chemical Biology

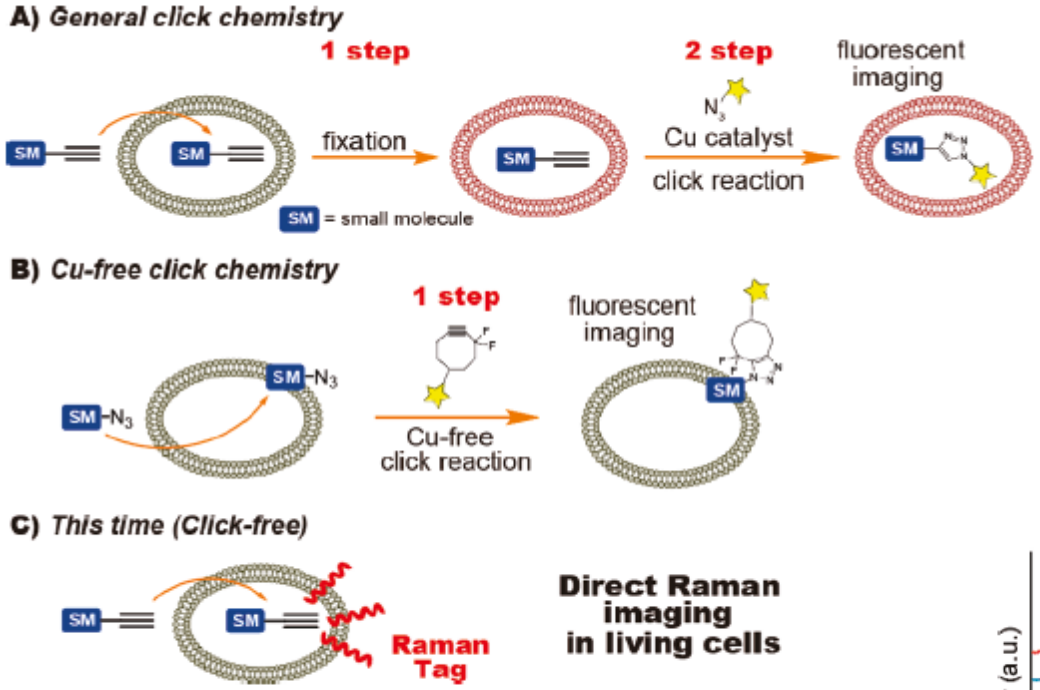

Figure 1. Concept of click-free imaging.

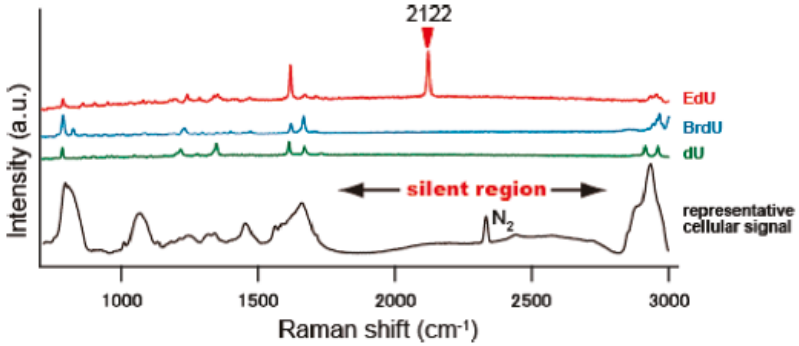

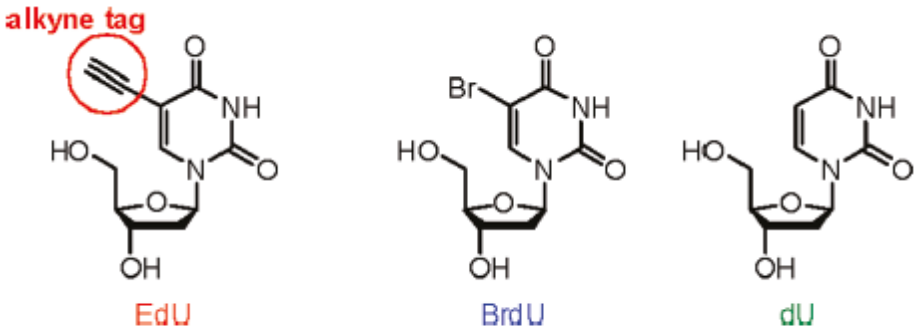

Figure 2. Structures of thymidine analogues.

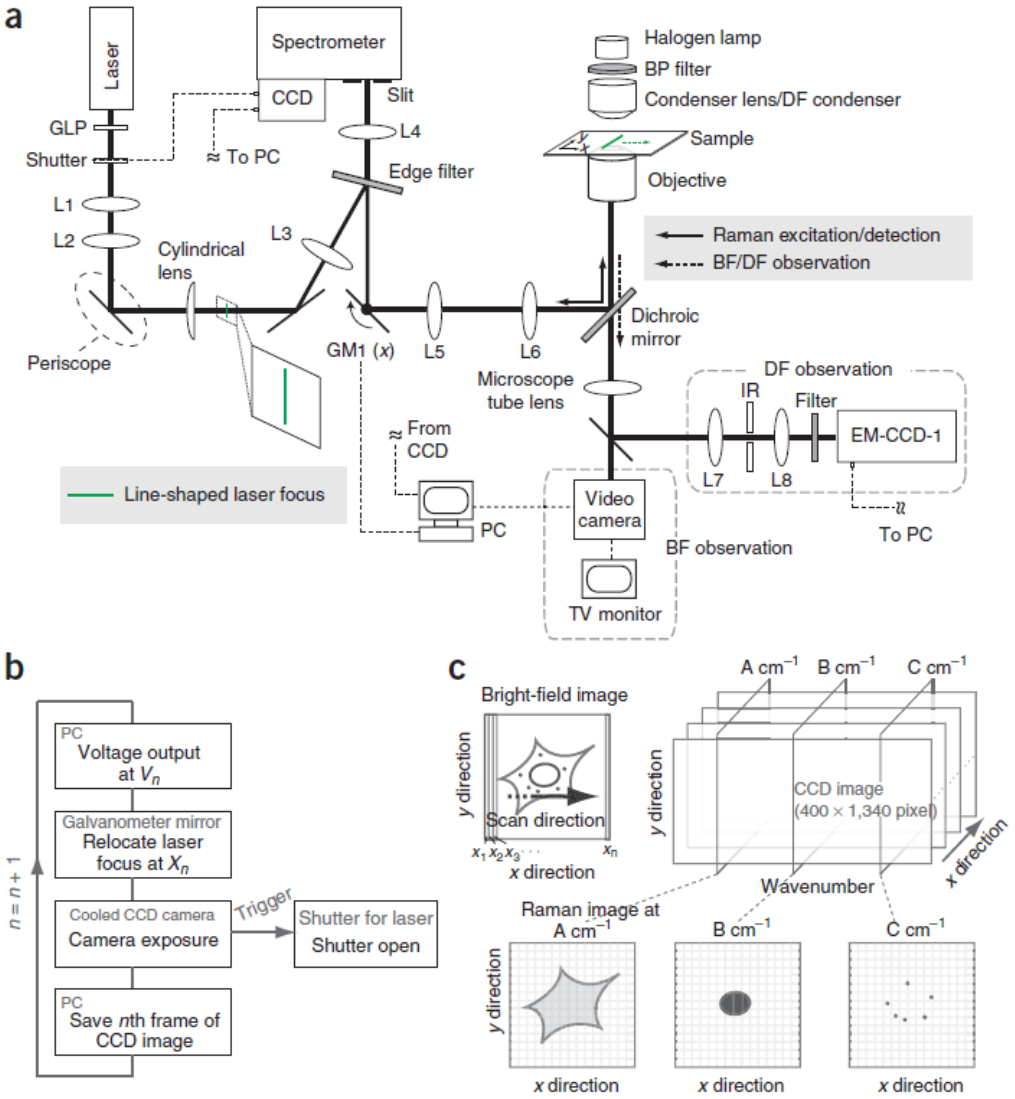
a
Laser
Spectrometer
CCD
Slit
GLP
L4
Shutter
To PC
Edge filter
L1
L2
L3
Cylindrical lens
Periscope
GM1 (x)
L5
L6
Halogen lamp
BP filter
Condenser lens/DF condenser
Sample
Objective
Raman excitation/detection
BF/DF observation
Dichroic mirror
Microscope tube lens
DF observation
IR
Filter
EM-CCD-1
L7
L8
To PC
From CCD
PC
Video camera
BF observation
TV monitor
Line-shaped laser focus
b
PC
Voltage output at V_n
Galvanometer mirror
Relocate laser focus at X_n
Cooled CCD camera
Camera exposure
Trigger
Shutter for laser
Shutter open
PC
Save nth frame of CCD image
n = n + 1
c
Bright-field image
y direction
Scan direction
x direction
A cm^{-1}
B cm^{-1}
C cm^{-1}
CCD image (400 × 1,340 pixel)
Wavenumber
Raman image at A cm^{-1}
B cm^{-1}
C cm^{-1}

Alkynyl sugar analogs for the labeling and visualization of glycoconjugates in cells

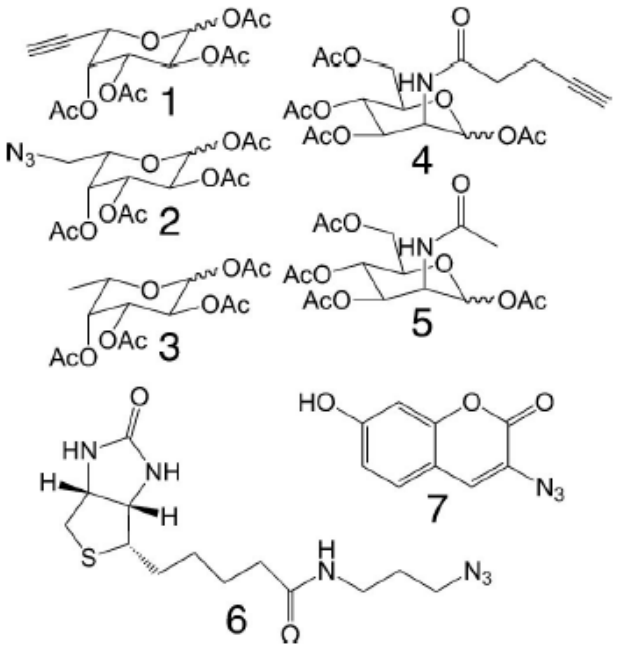

Scheme 1. Modified sugar analogs and probes used in this study.

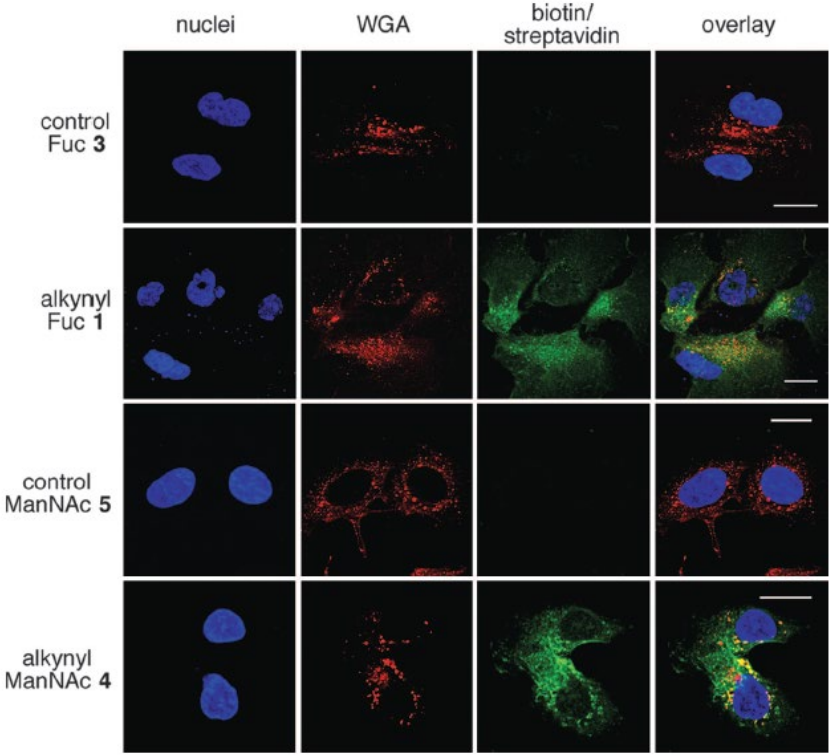

Cell-permeable probe for identification and imaging of sialidases

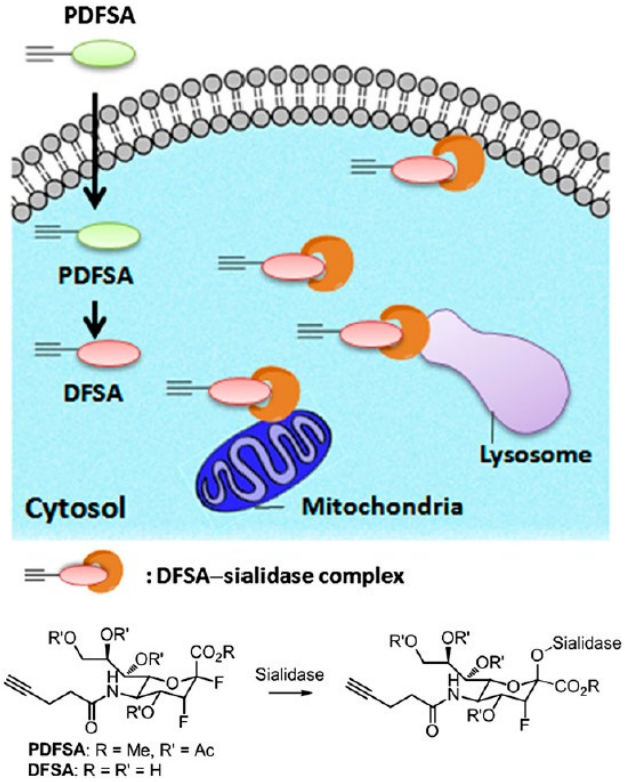

Fig. 1. Identification and imaging of sialidase with activity changes using these activity-based sialidase probes.

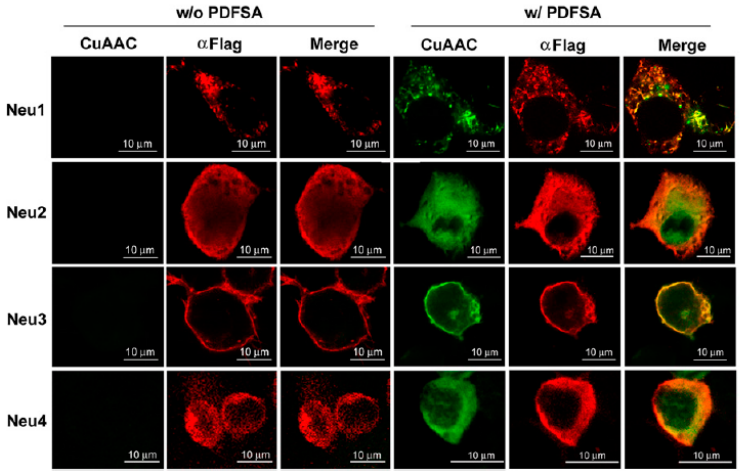

Antibody and Antigen

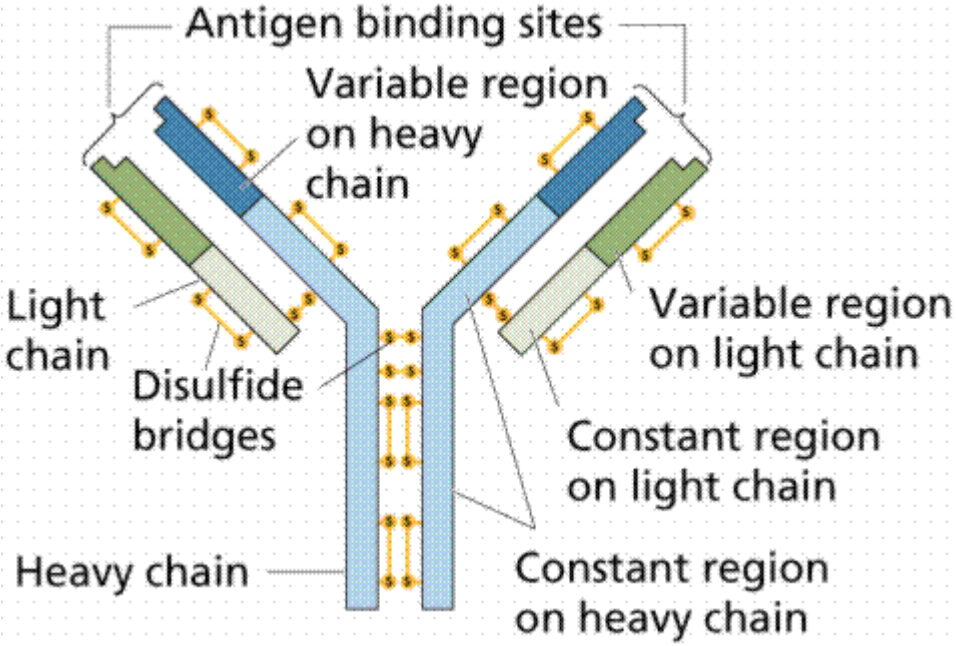

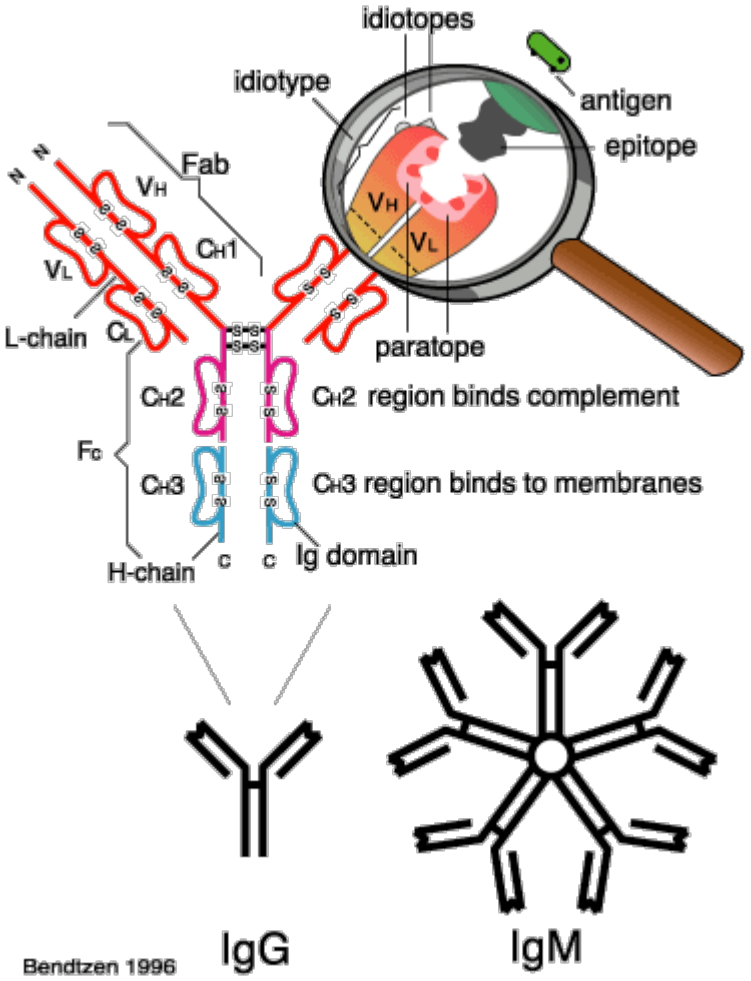

Enzyme-Linked ImmunoSorbent Assay (ELISA)

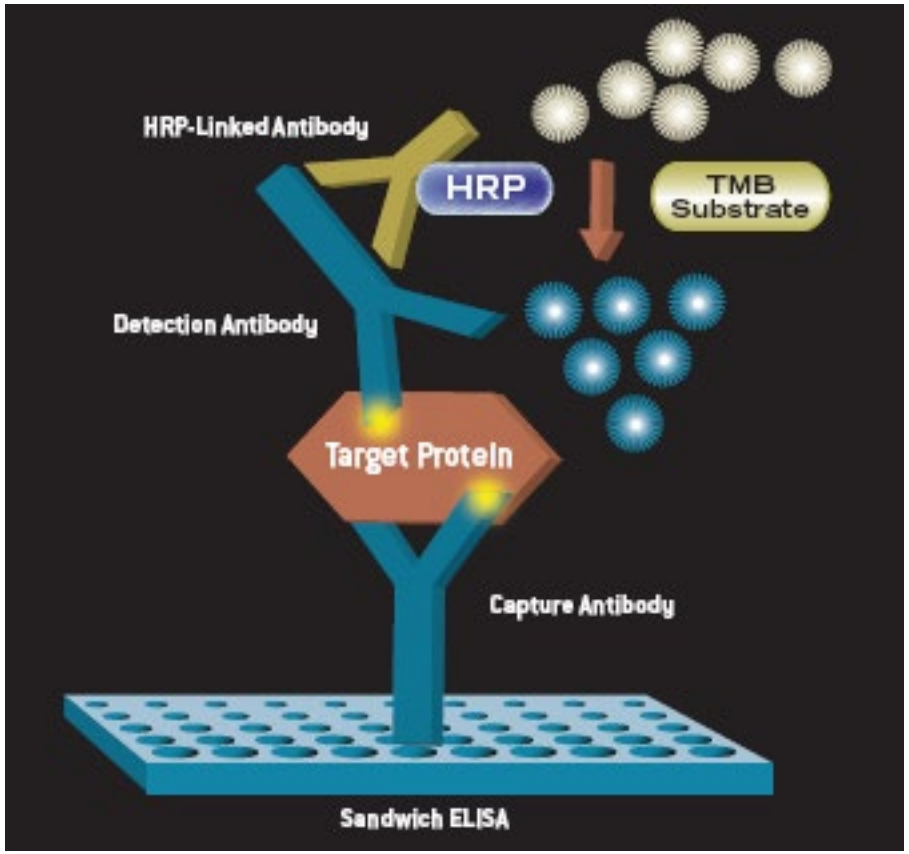

Labeling
BSA/PEG

Microarray

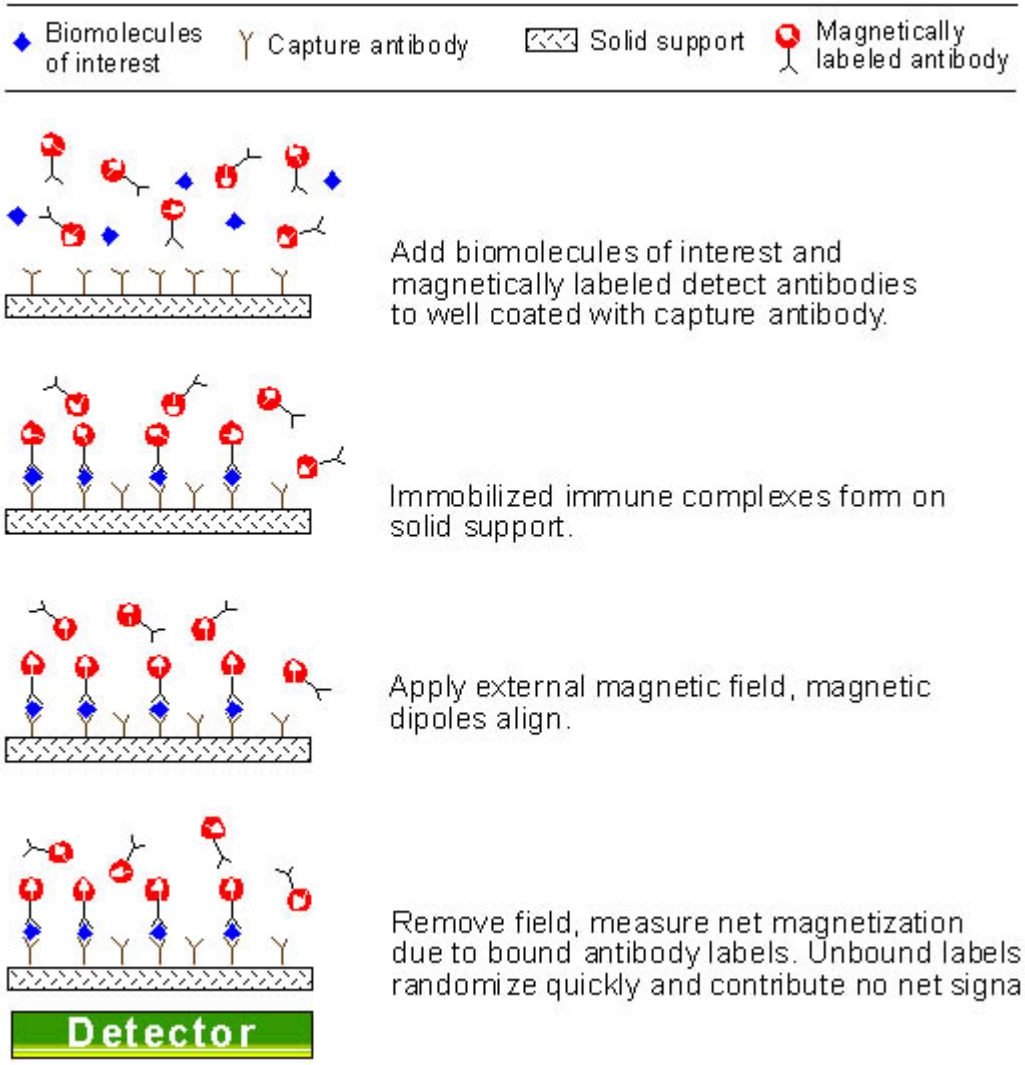
Biomolecules of interest
Capture antibody
Solid support
Magnetically labeled antibody
Add biomolecules of interest and magnetically labeled detect antibodies to well coated with capture antibody.
Immobilized immune complexes form on solid support.
Apply external magnetic field, magnetic dipoles align.
Remove field, measure net magnetization due to bound antibody labels. Unbound labels randomize quickly and contribute no net signal.
Detector

Microarray

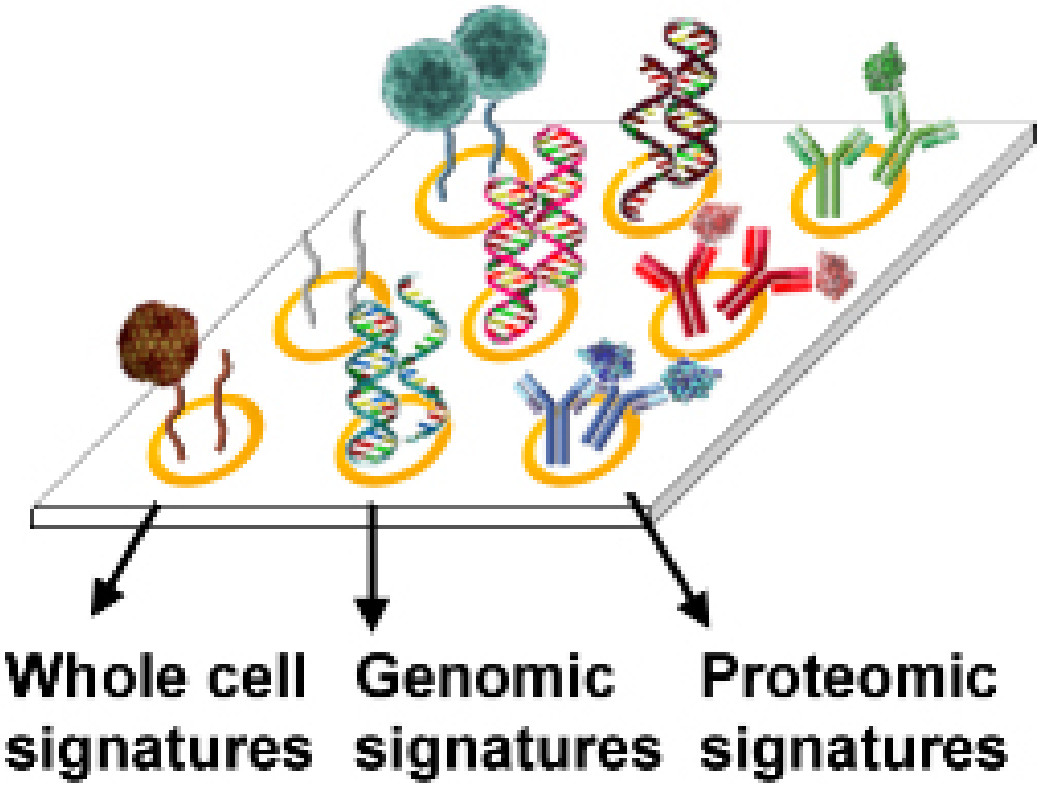
Whole cell signatures
Genomic signatures
Proteomic signatures

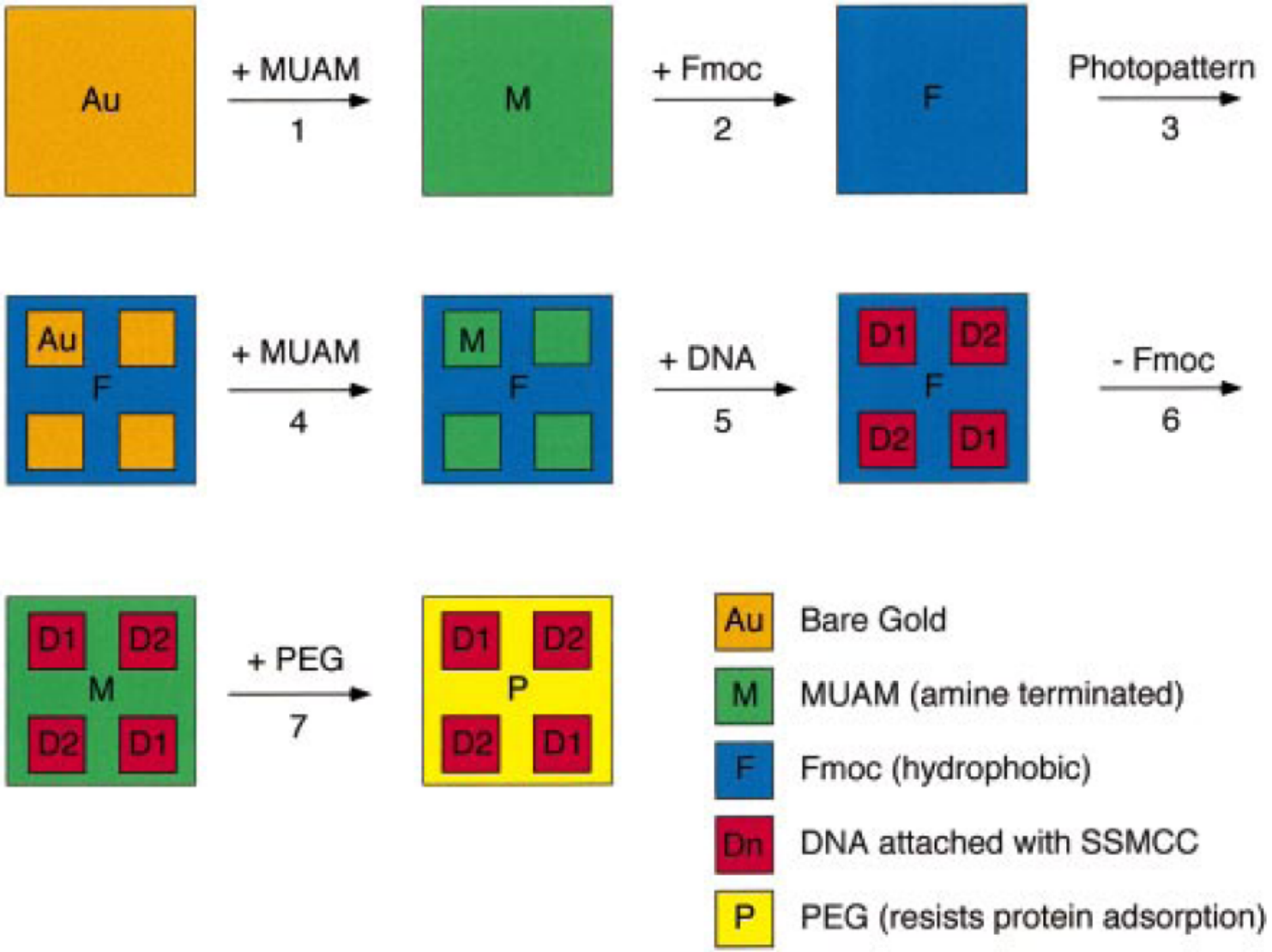

Figure 1. Fabrication scheme for the construction of multi-element DNA arrays. A clean gold surface is reacted with the amine-terminated alkanethiol MUAM, and subsequently reacted with Fmoc-NHS to create a hydrophobic surface. This surface is then exposed to UV radiation through a quartz mask and rinsed with solvent to remove the MUAM+Fmoc from specific areas of the surface, leaving bare gold pads. These bare gold areas on the sample surface are filled in with MUAM, resulting in an array of MUAM pads surrounded by a hydrophobic Fmoc background. Solutions of DNA are then delivered by pipet onto the specific array locations and are covalently bound to the surface via the bifunctional linker SSMCC. In the final two steps, the Fmoc-terminal groups on the array background are removed and replaced by PEG groups which prohibit the nonspecific binding of analyte proteins to the background.

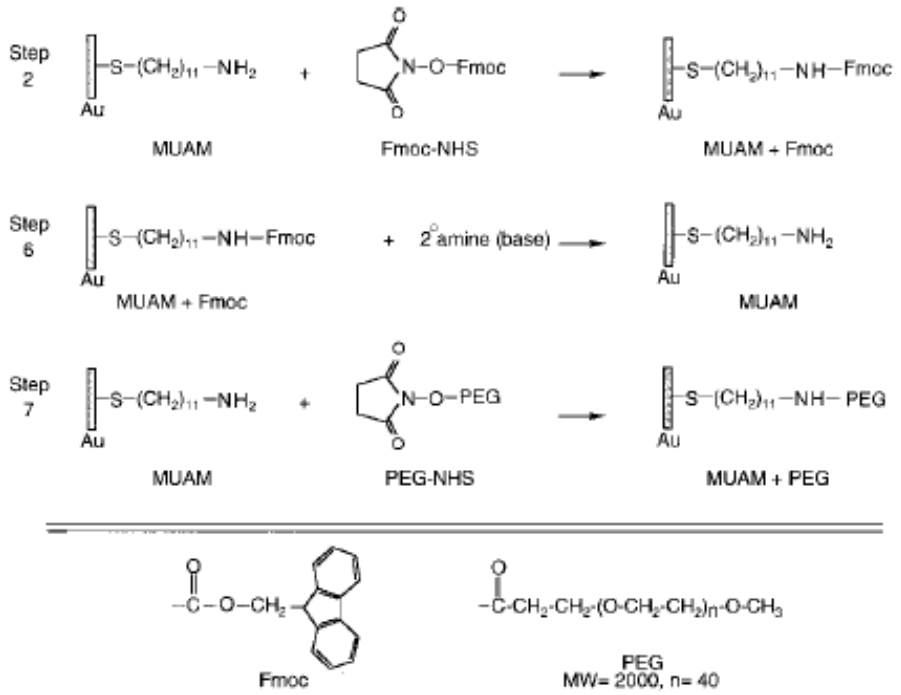

Figure 2. Surface reaction scheme showing the steps involved in the reversible modification of the array background. (Step 2) The starting amine-terminated alkanethiol surface (MUAM) is reacted with the Fmoc-NHS protecting group to form a carbamate linkage thus creating a hydrophobic Fmoc-terminated surface. (Step 6) After DNA immobilization (see Figure 3), the hydrophobic Fmoc group is removed from the surface with a basic secondary amine, resulting in the return of the original MUAM surface. (Step 7) In the final array fabrication step, the deprotected MUAM is reacted with PEG-NHS to form an amide bond that covalently attaches PEG to the array surface.

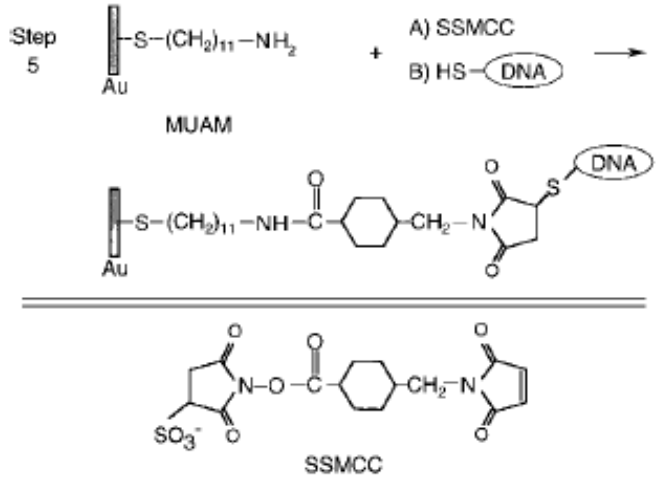

Figure 3. Surface reaction scheme showing the immobilization of thiol-terminated DNA to the array surface. In Step 5 of the DNA array fabrication, the heterobifunctional linker SSMCC is used to attach 5′-thiol modified oligonucleotide sequences to reactive pads of MUAM. This linker contains an NHSS ester functionality (reactive toward amines) and a maleimide functionality (reactive toward thiols). The surface is first exposed to a solution of the linker, whereby the NHSS ester end of the molecule reacts with the MUAM surface. Excess linker is rinsed away and the array surface is then spotted with 5′-thiol-modified DNA that reacts with the maleimide groups forming a covalent bond to the surface monolayer.

Glass Surface Modification

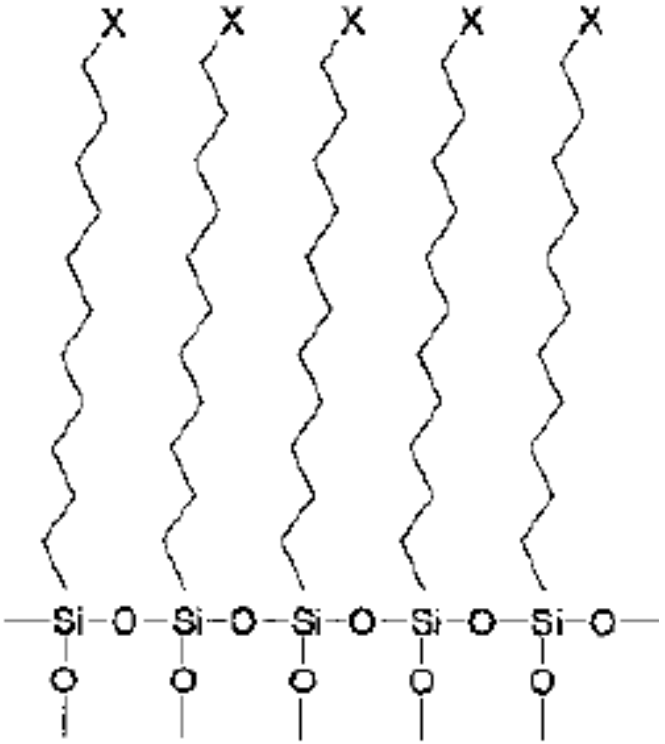

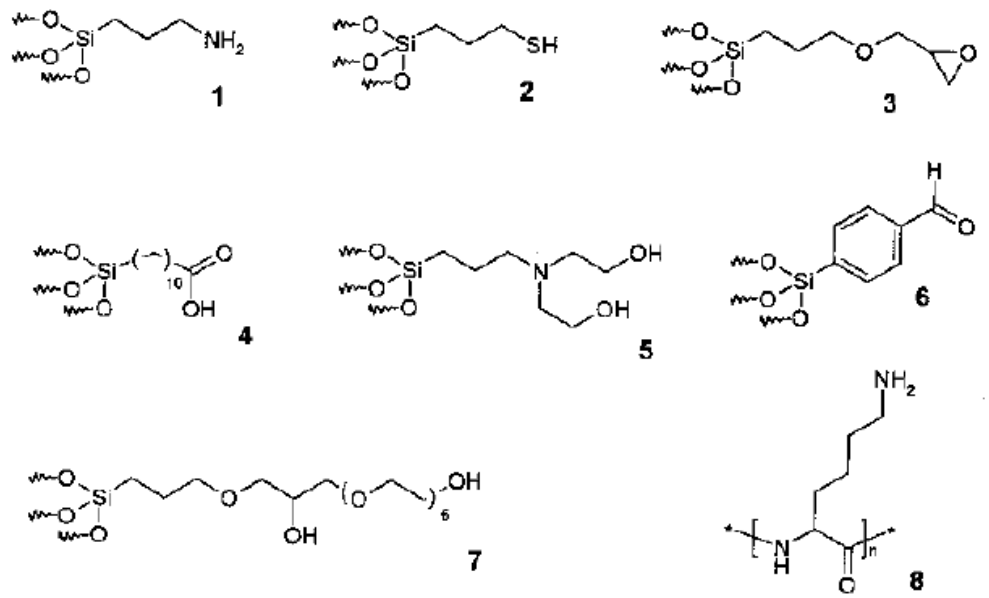

Scheme 2.2 Reagents for derivatization of glass surfaces. 1 APTES = aminopropyltriethoxysilane; **2** MPTS = 3-mercaptopropyltrimethoxysilane; **3** GPTS = glycidoxypropyltrimethoxysilane; **4** TETU = triethoxysilane undecanoic acid; **5** HE-APTS = bis(hydroxyethyl)aminopropyltriethoxysilane); **6** 4-trimethoxysilylbenzaldehyde; **7** GPTS/HEG = glycidoxypropyltrimethoxysilane-hexaethylene glycol; **8** poly(lysine).

Scheme 2.1 2D schematic description of a polysiloxane monolayer on a glass surface (X = terminal functional

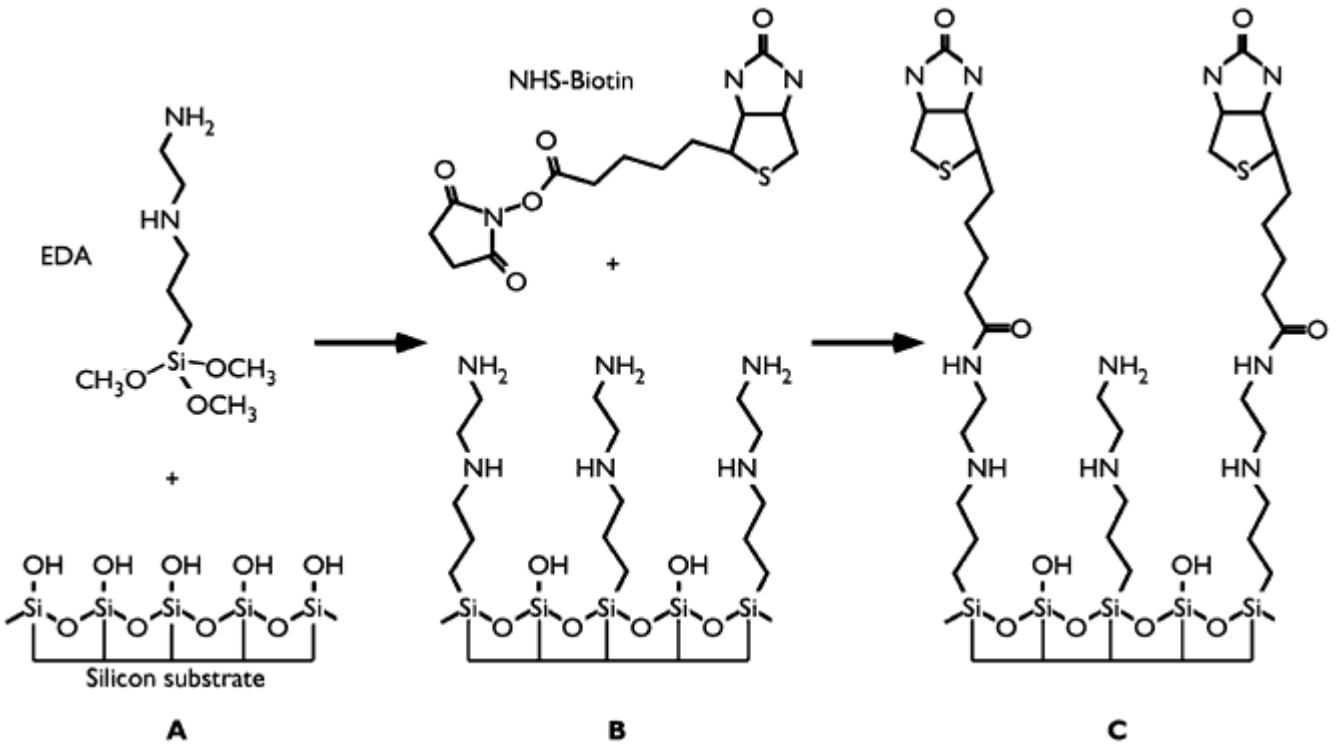
NHS-Biotin
EDA
Silicon substrate
A
B
C

Biotin-Streptavidin

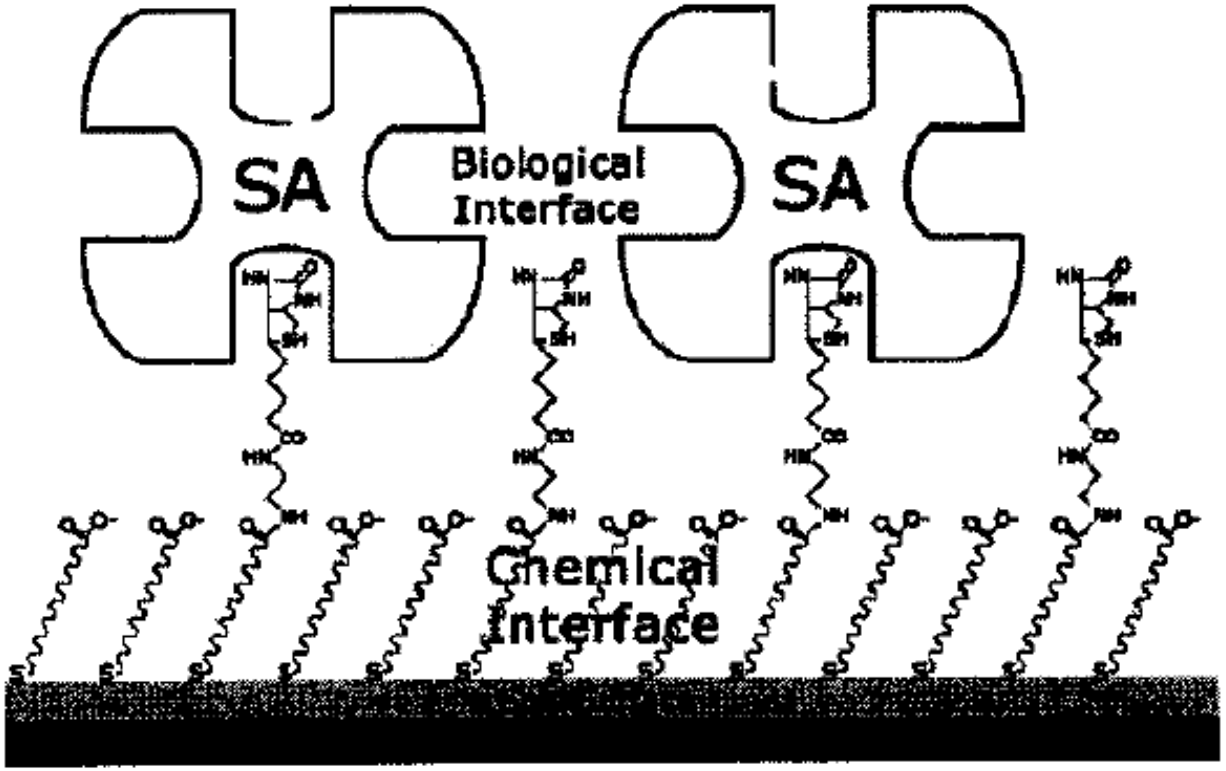

Figure 2.3 Schematic respresentation of a steptavidin sensor surface assembled on a reaction-controlled biotinylated SAM [28].

GeneChip

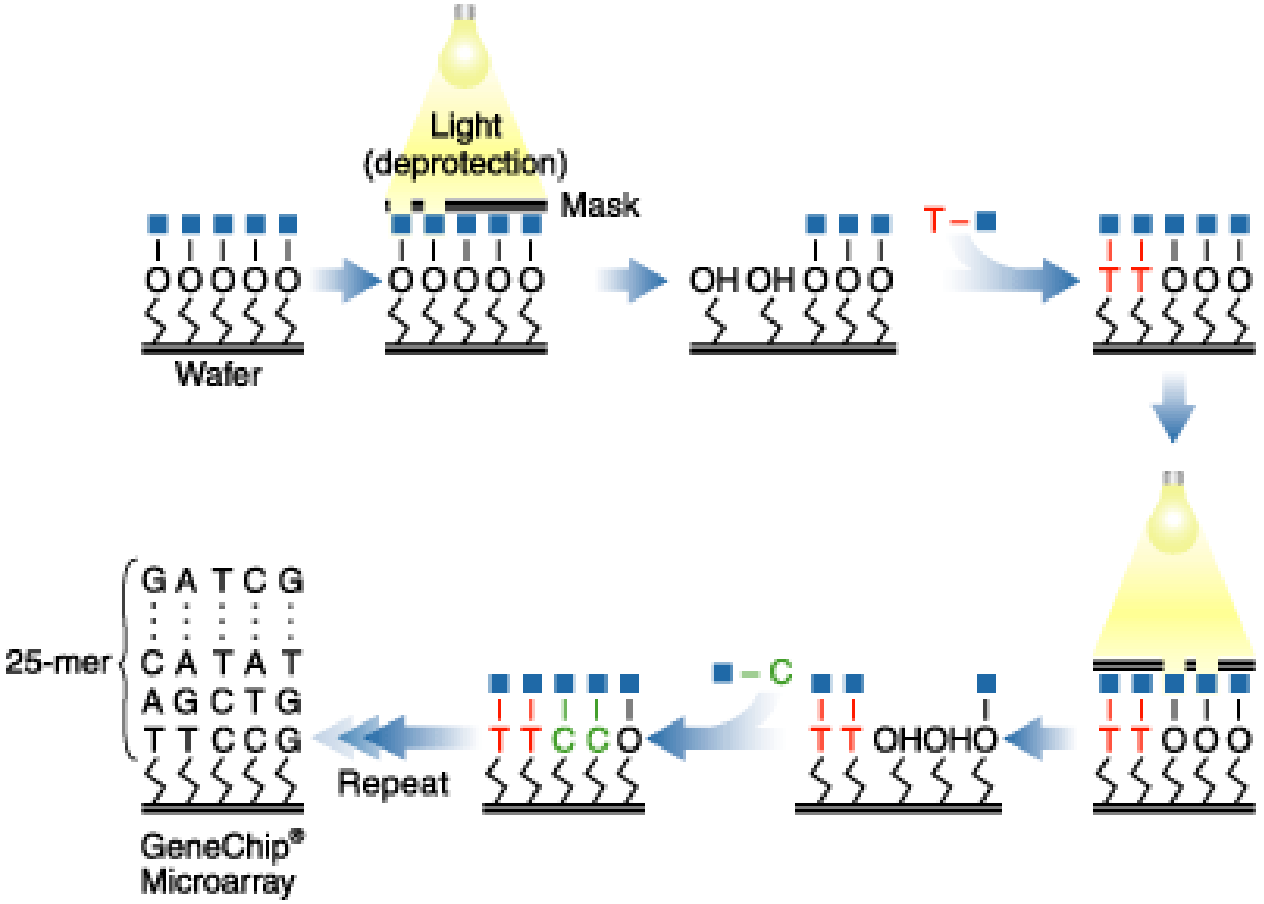
Light
(deprotection)
Mask
Wafer
T
C
Repeat
25-mer
G A T C G
C A T A T
A G C T G
T T C C G
GeneChip®
Microarray

Scheme

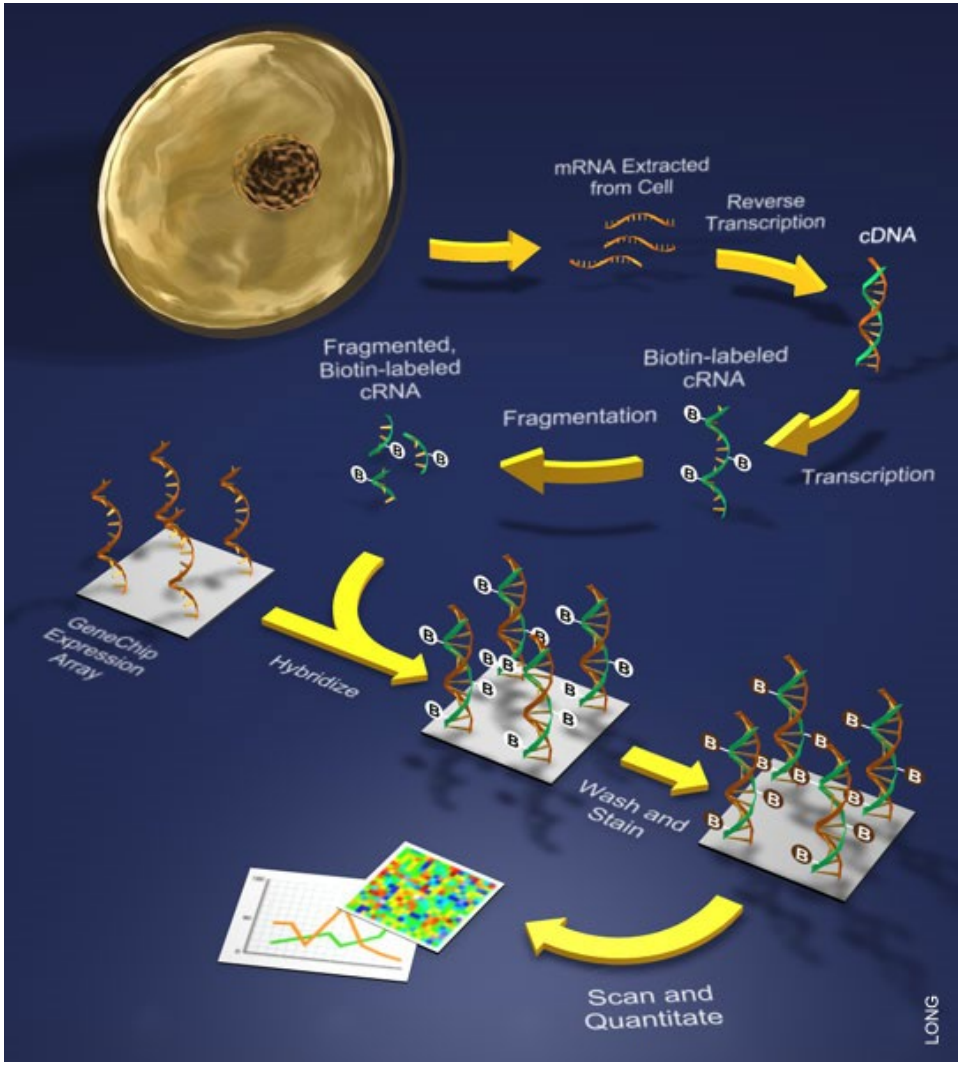
mRNA Extracted from Cell
Reverse Transcription
cDNA
Fragmented, Biotin-labeled cRNA
Biotin-labeled cRNA
Fragmentation
Transcription
GeneChip Expression Array
Hybridize
Wash and Stain
Scan and Quantitate
LONG

cDNA Microarray

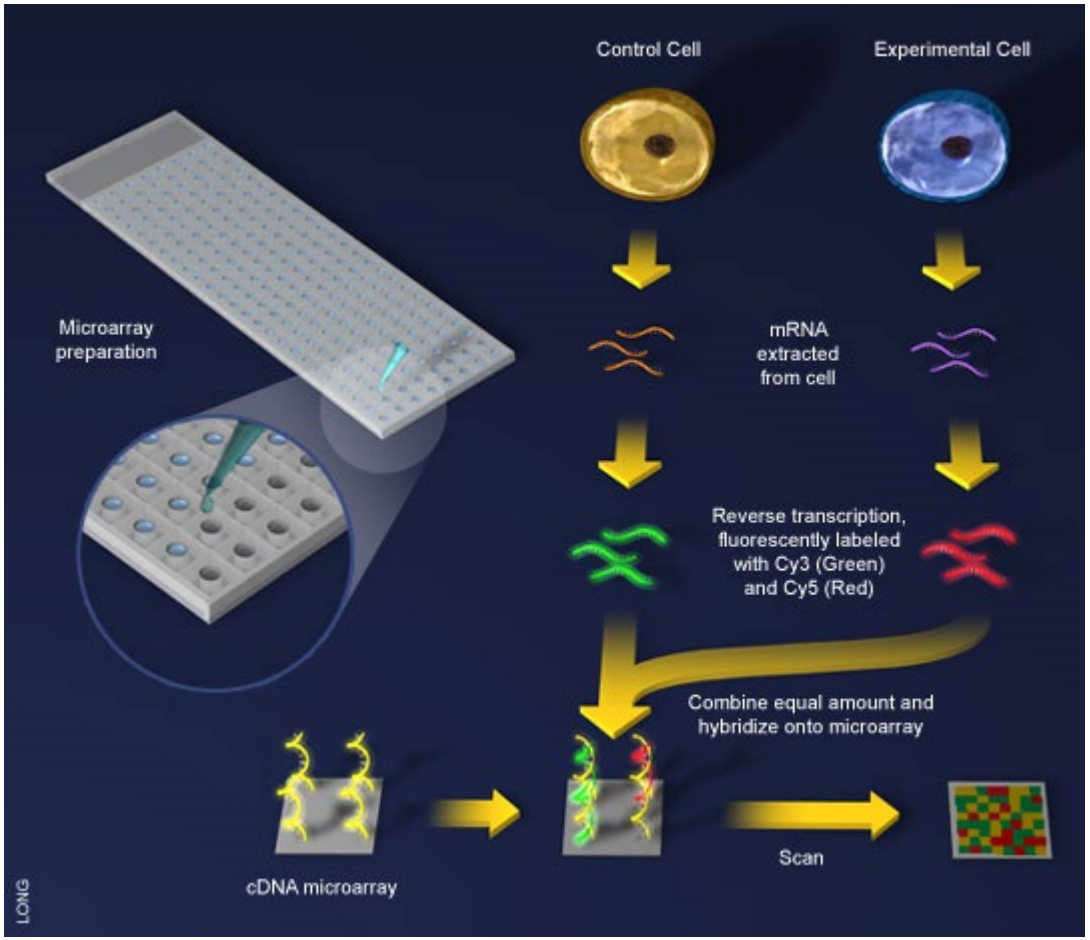

Protein Array

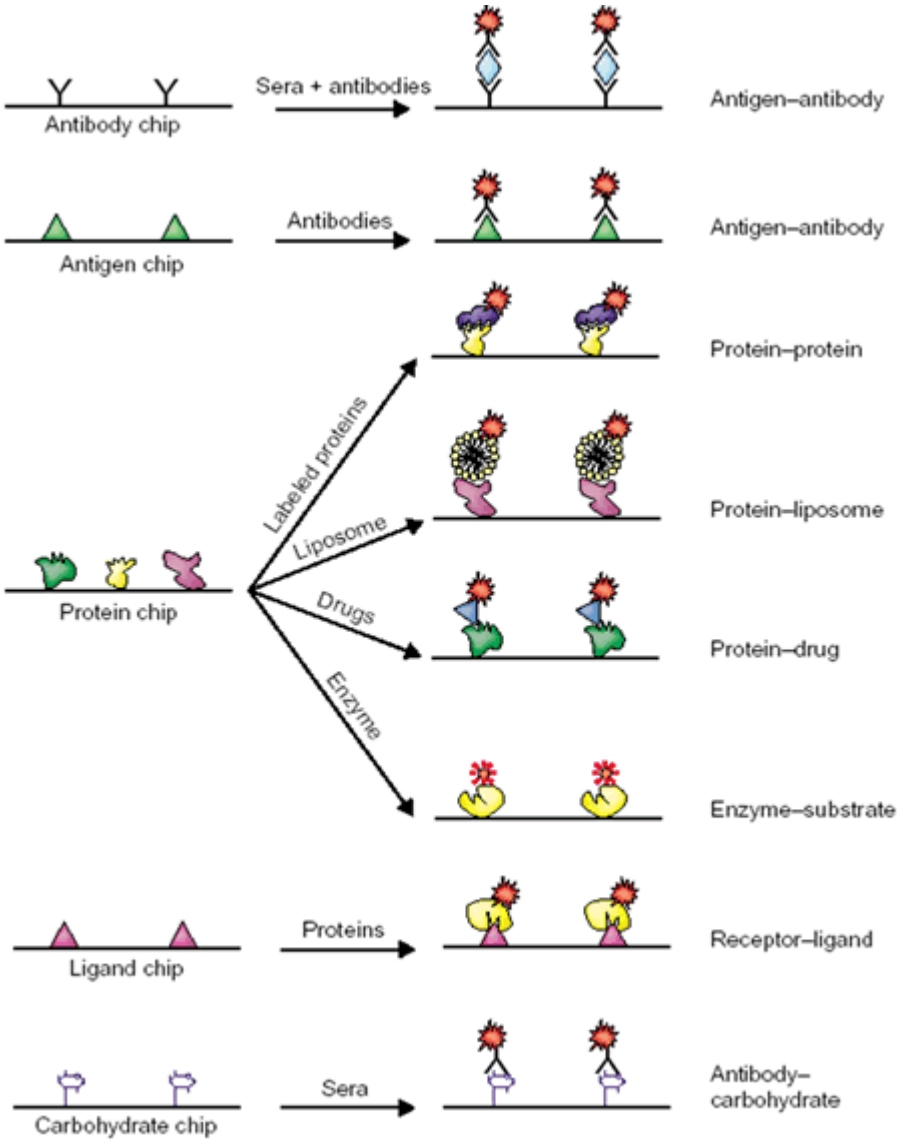

Current Opinion in Chemical Biology

BSA Blocking

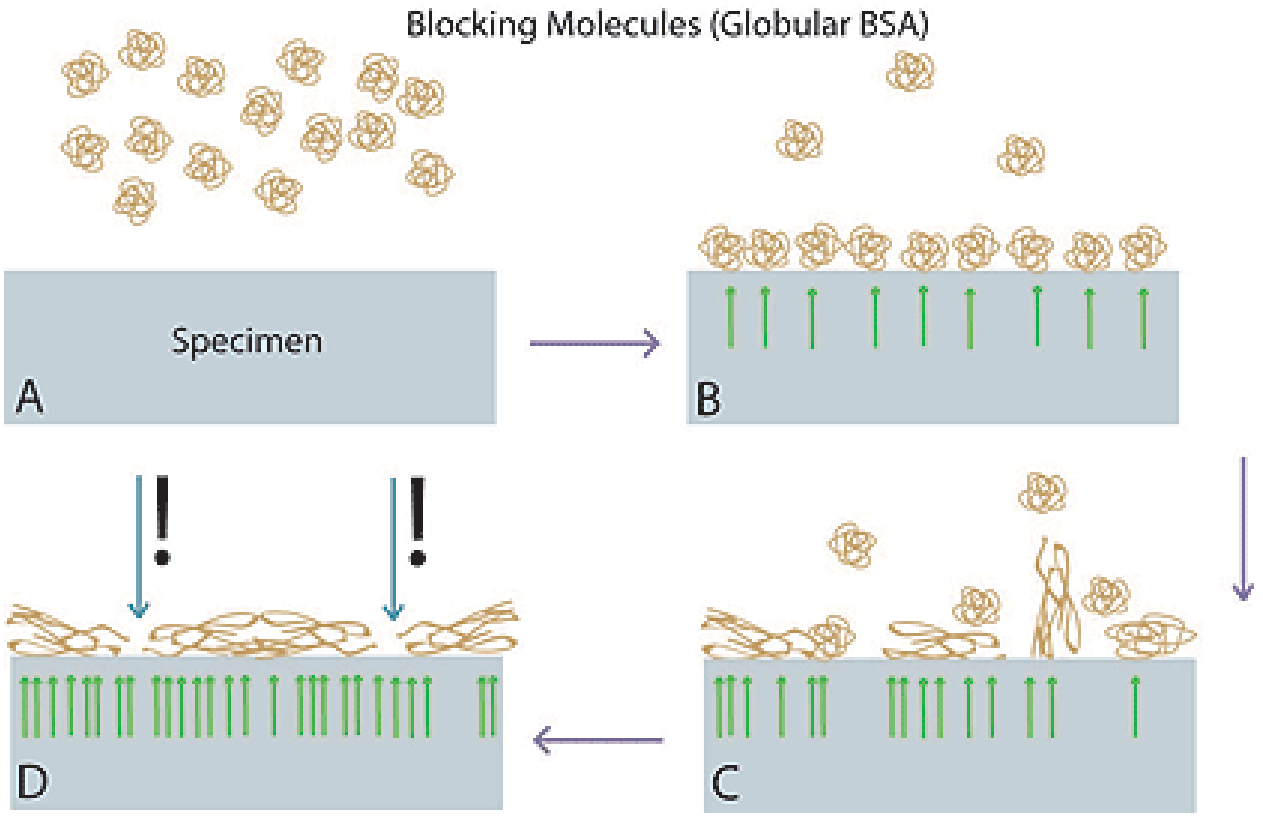

Cell Array

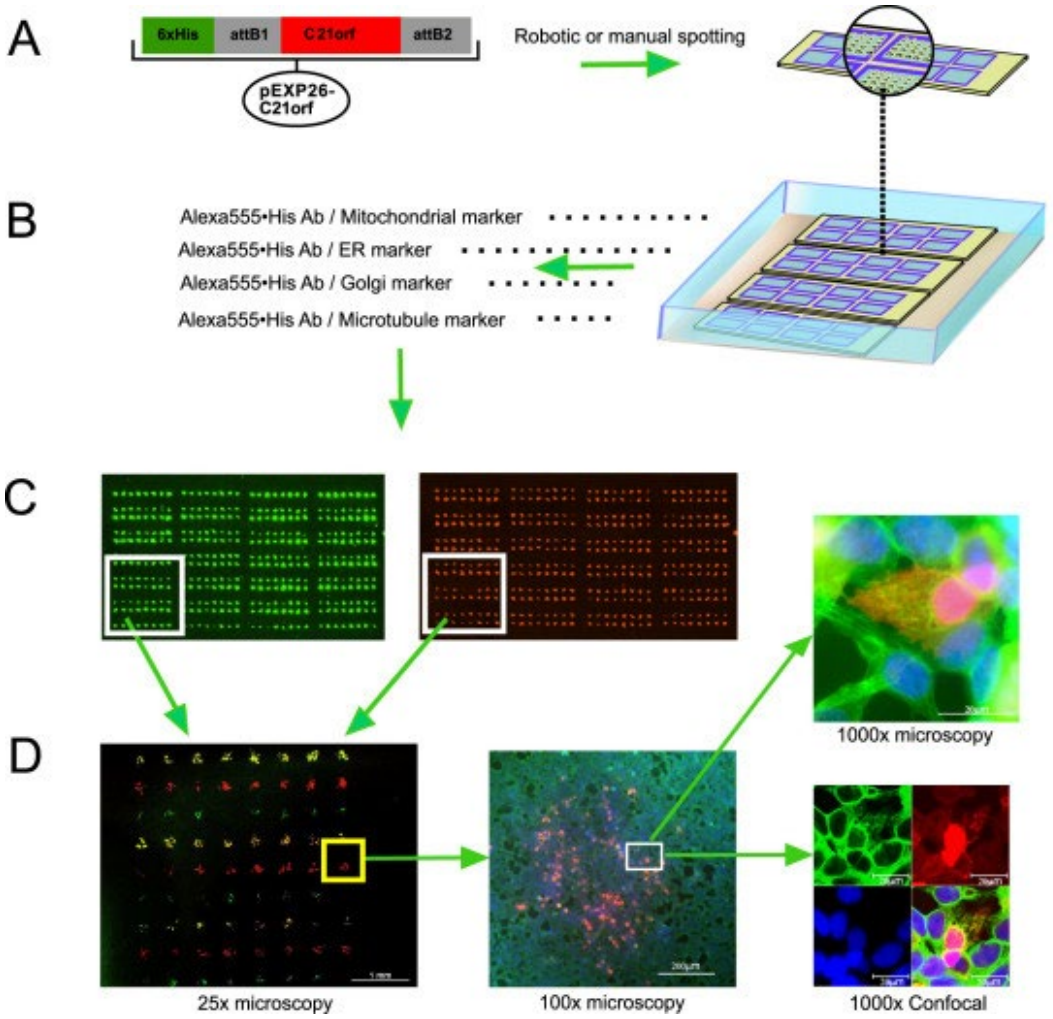
A
6xHis
attB1
C21orf
attB2
pEXP26-C21orf
Robotic or manual spotting
B
Alexa555•His Ab / Mitochondrial marker
Alexa555•His Ab / ER marker
Alexa555•His Ab / Golgi marker
Alexa555•His Ab / Microtubule marker
C
D
25x microscopy
100x microscopy
1000x microscopy
1000x Confocal

hCG immunoassay

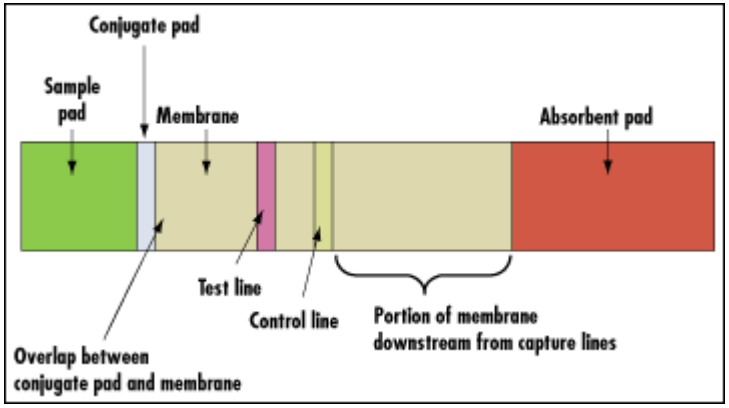

human chorionic gonadotropin (hCG)

Nucleotide Sensor

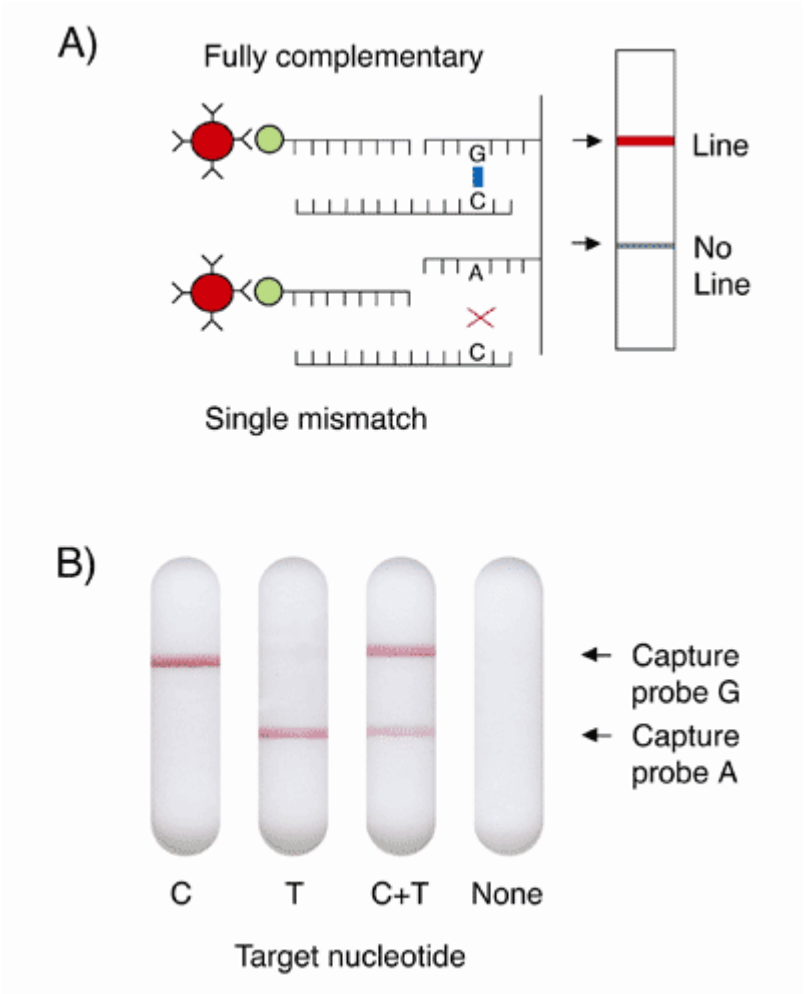

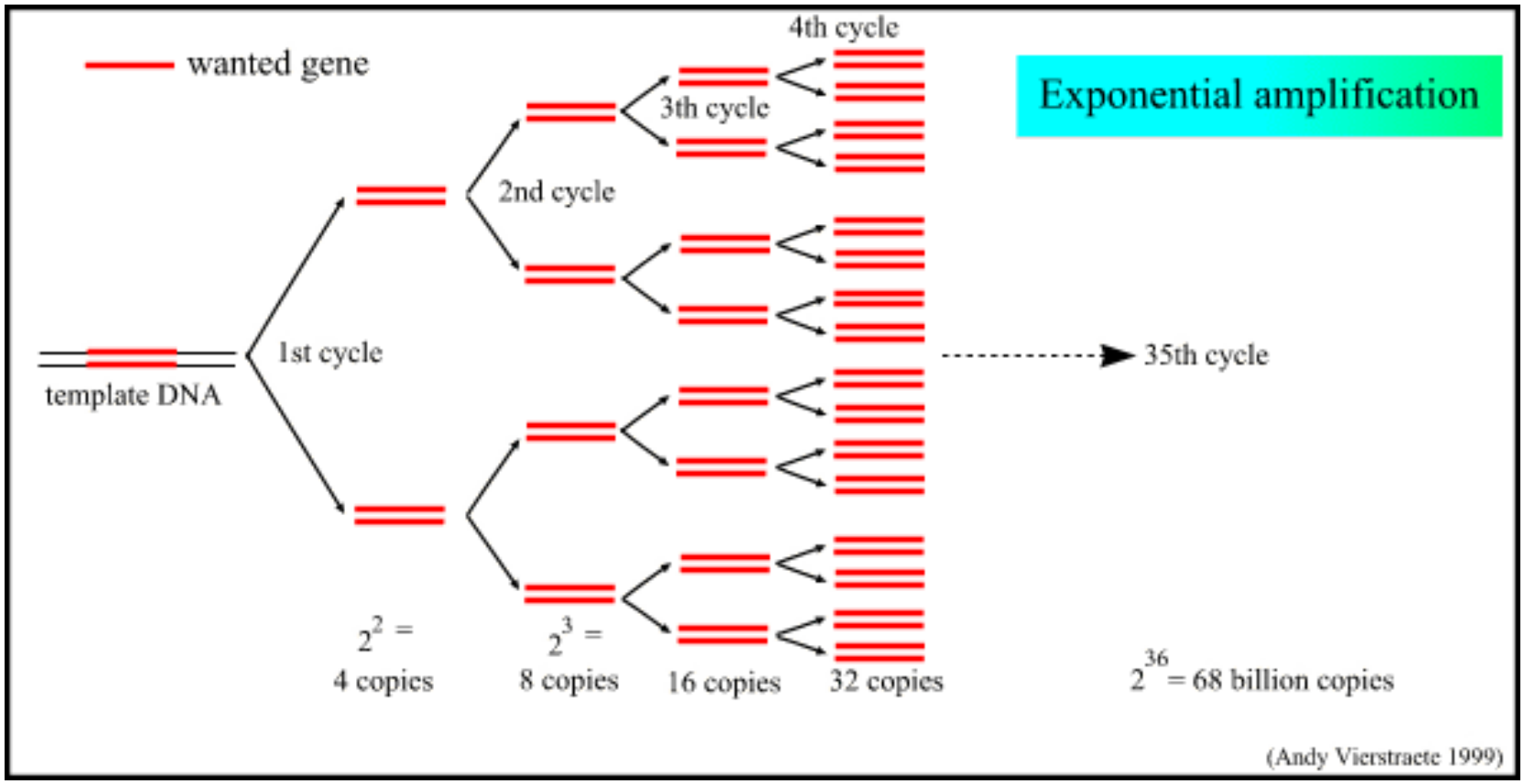
wanted gene
Exponential amplification
4th cycle
3th cycle
2nd cycle
1st cycle
template DNA
35th cycle
2^2 =
4 copies
2^3 =
8 copies
16 copies
32 copies
2^{36} = 68 billion copies
(Andy Vierstraete 1999)

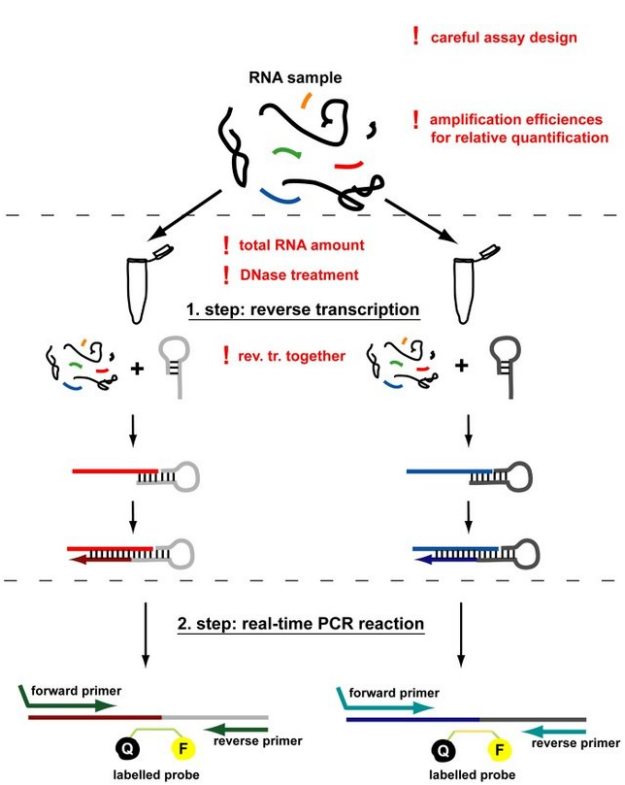
! careful assay design
RNA sample
! amplification efficiences for relative quantification
! total RNA amount
! DNase treatment
1. step: reverse transcription
! rev. tr. together
2. step: real-time PCR reaction
forward primer
reverse primer
Q
F
labelled probe
forward primer
reverse primer
Q
F
labelled probe

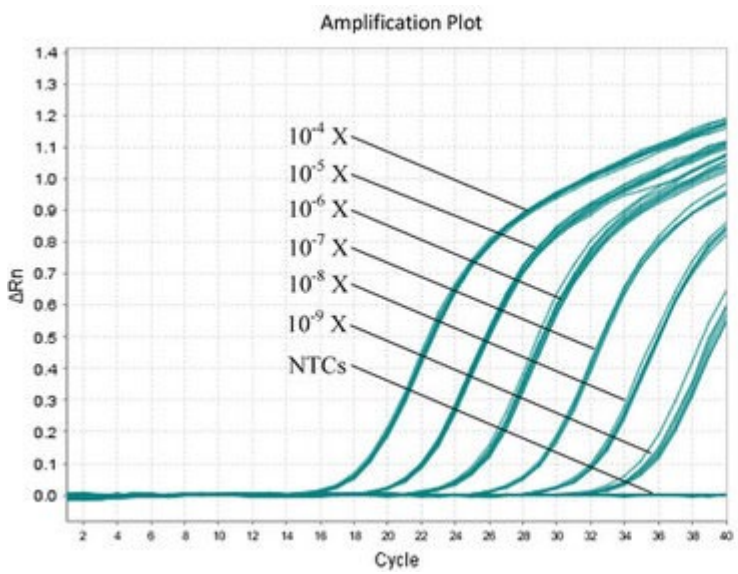
Amplification Plot
ΔRn
Cycle
10-4 X
10-5 X
10-6 X
10-7 X
10-8 X
10-9 X
NTCs

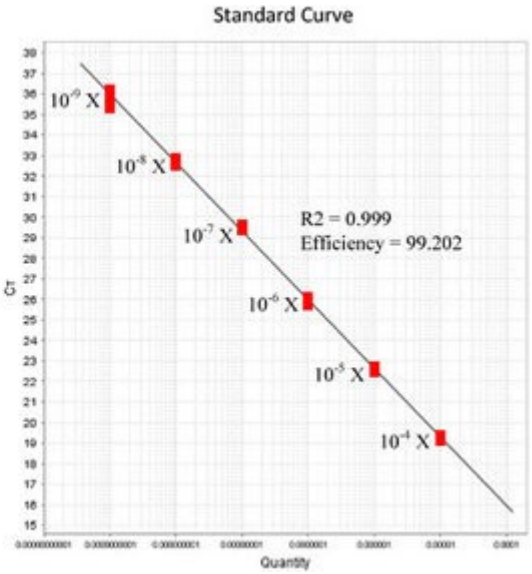
Standard Curve
Ct
Quantity
10-9 X
10-8 X
10-7 X
10-6 X
10-5 X
10-4 X
R2 = 0.999
Efficiency = 99.202

PROTOCOL OF SARS-COV-2 DETECTION USING REAL-TIME RT-PCR

Target gene → RdRp gene (Corman *et al.* 2020)

PCR amplification regions → nCoV_IP2/12621-12727 and nCoV_IP4/14010-14116 (Institut Pasteur, Paris)

Primer sets and probes → designed based on the first sequences of SARS-CoV-2 available on the GISAID database

RNA extraction → NucleoSpin® RNA Virus or viral RNA mini kit (QIAGEN)

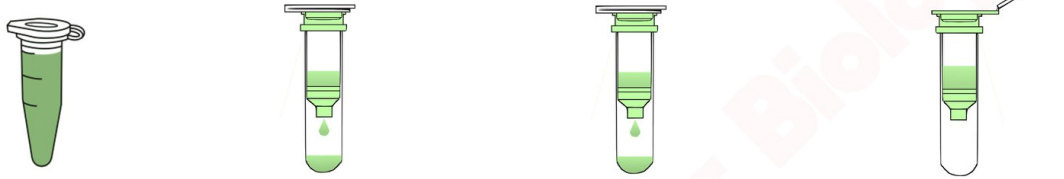

Sample lysis

5 min incubation of sample in Lysis Buffer containing Proteinase K

Binding of viral RNA

Ethanol addition and transfer of lysate to Column

Washing

1st Wash Buffer (high salt concentration)
2nd Wash Buffer (low salt concentration)

Elution of viral RNA

Elution in 20-50 µl RNase-free water or Elution Buffer

Real-time Multiplex RT-PCR (Institut Pasteur, Paris)

Multiplex Mix (nCoV_IP2&IP4)

Sample RNA	5 µl
H20	1.3 µl
Reaction mix 2X	12.50 µl
MgSO4 (50mM)	0.40 µl
Forward Primer1 (10µM)	1.00 µl
Reverse Primer1 (10µM)	1.00 µl
Forward Primer2 (10µM)	1.00 µl
Reverse Primer2 (10µM)	1.00 µl
Probe 1 (10µM)	0.4 µl
Probe 2 (10µM)	0.4 µl
SuperscriptIII RT/Platinum Taq Mix	1.00 µl

Amplification Cycles (Lightcycler System)

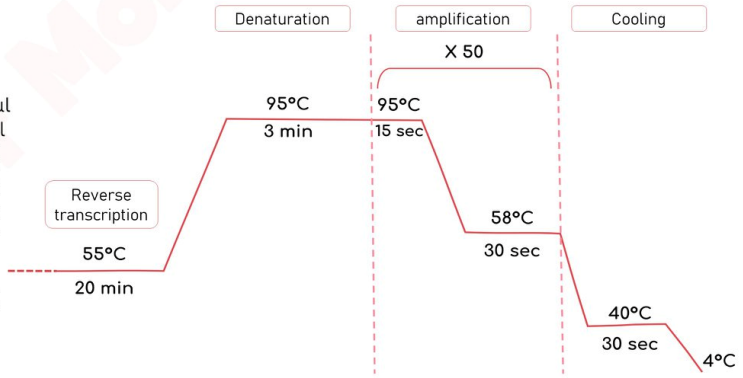

POSITIVE CONTROL

Positive control for real-time RT-PCR is the in vitro transcribed RNA derived from strain BetaCoV_Wuhan_WIV04_2019. The transcript contains the **amplification regions** of the RdRp and E gene as positive strand.

M. MERZOUG

References

1. Institut Pasteur, Paris, « Protocol: Real-time RT-PCR assays for the detection of SARS-CoV-2 », OMS, 2 mars 2020.
2. Corman VM, Landt O, Kaiser M, et al. Detection of 2019 novel coronavirus (2019-nCoV) by real-time RT-PCR. Euro Surveill 2020;25.

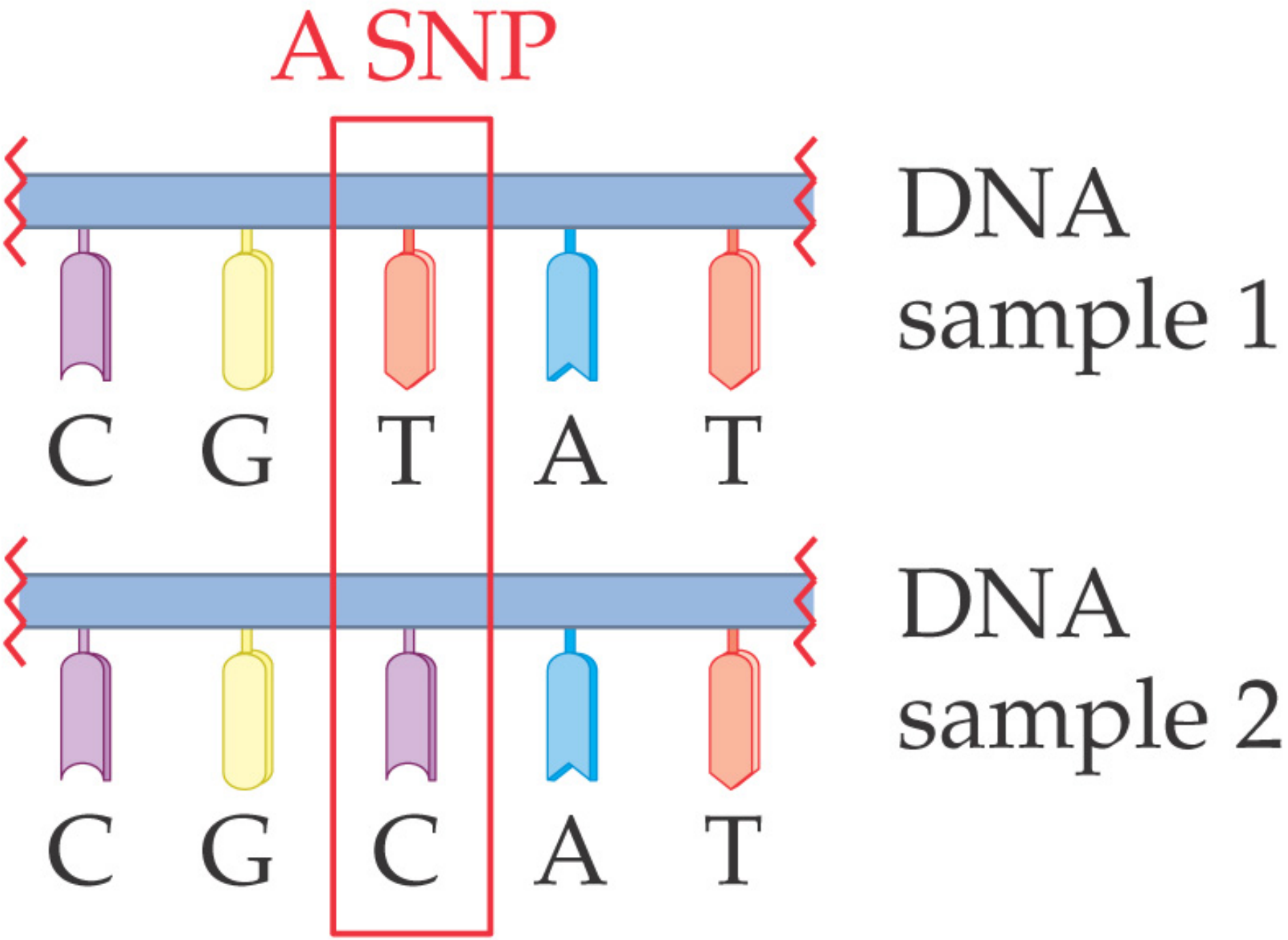
A SNP
C G T A T
C G C A T
DNA sample 1
DNA sample 2

DNA Sequencing

Next Generation Sequencing 1: Overview - Eric Chow

https://www.youtube.com/watch?v=mI0Fo9kaWqo

DNA Sequencing

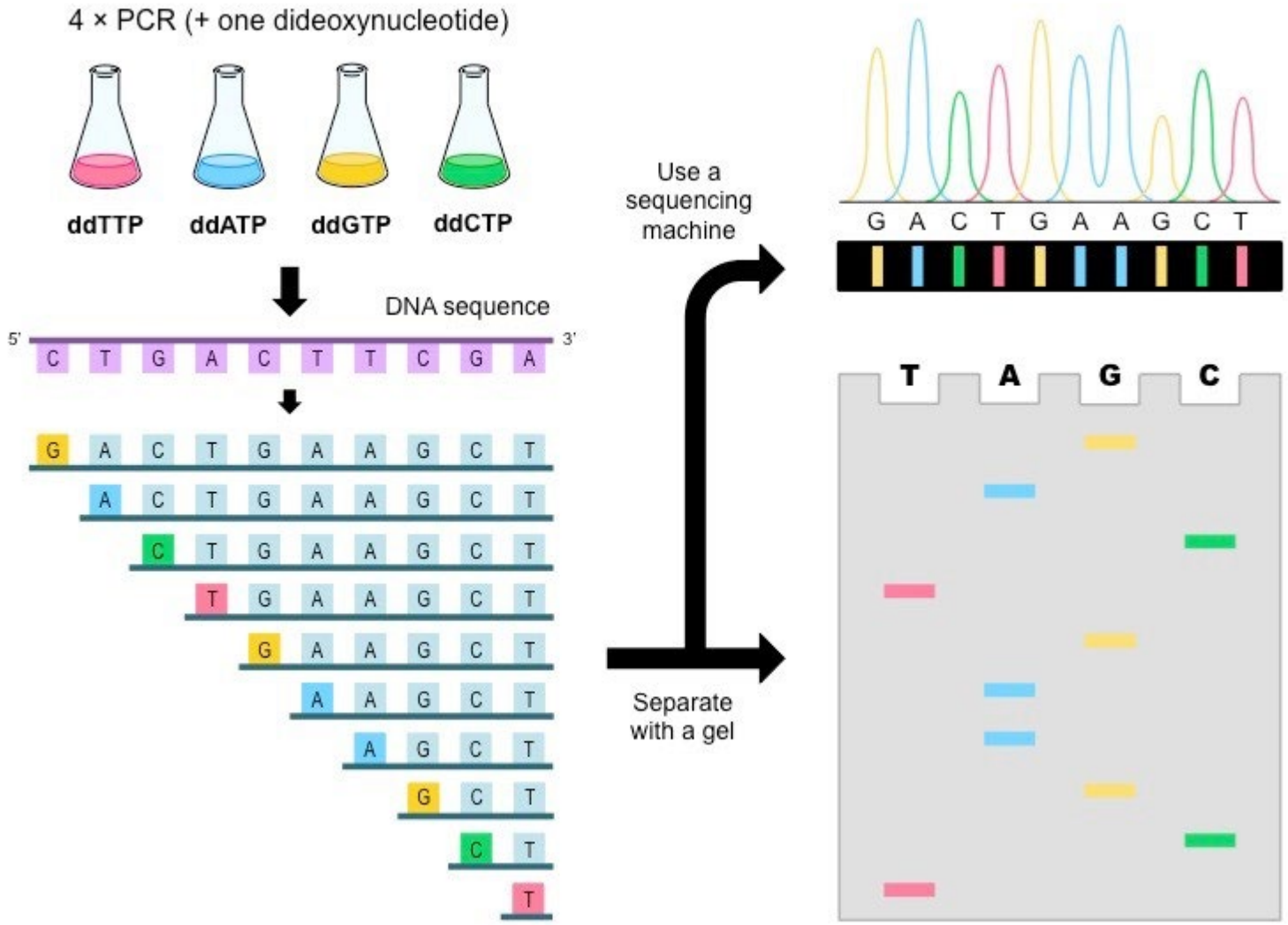

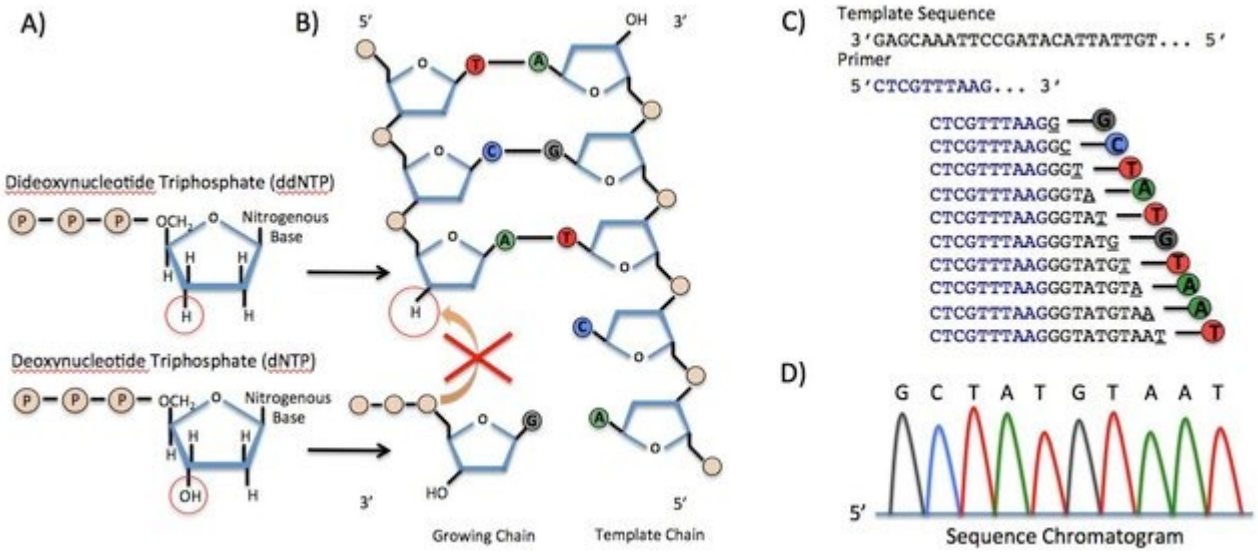
A)
B)
C)
D)
Dideoxynucleotide Triphosphate (ddNTP)
Deoxynucleotide Triphosphate (dNTP)
Nitrogenous Base
5′
3′
OH
HO
Growing Chain
Template Chain
Template Sequence
3′GAGCAAATTCCGATACATTATTGT... 5′
Primer
5′CTCGTTTAAG... 3′
CTCGTTTAAGG
CTCGTTTAAGGC
CTCGTTTAAGGGT
CTCGTTTAAGGGTA
CTCGTTTAAGGGTAT
CTCGTTTAAGGGTATG
CTCGTTTAAGGGTATGT
CTCGTTTAAGGGTATGTA
CTCGTTTAAGGGTATGTAA
CTCGTTTAAGGGTATGTAAT
G C T A T G T A A T
5′
Sequence Chromatogram

DNA Sequencing

https://www.youtube.com/watch?v=vK-HlMaitnE

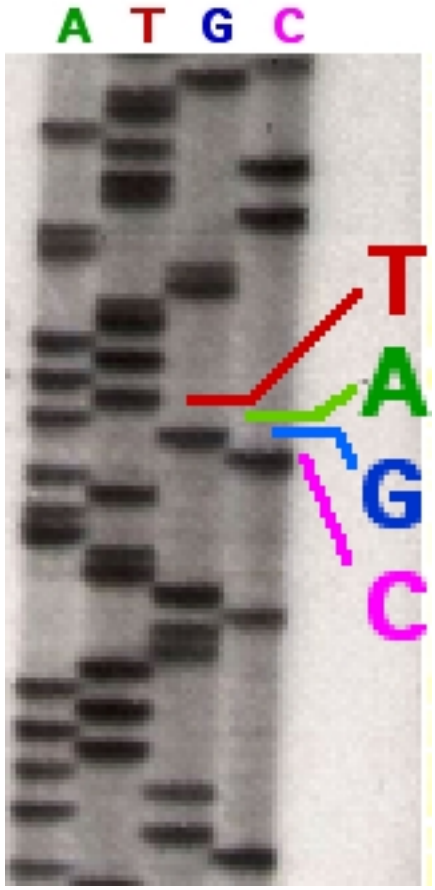

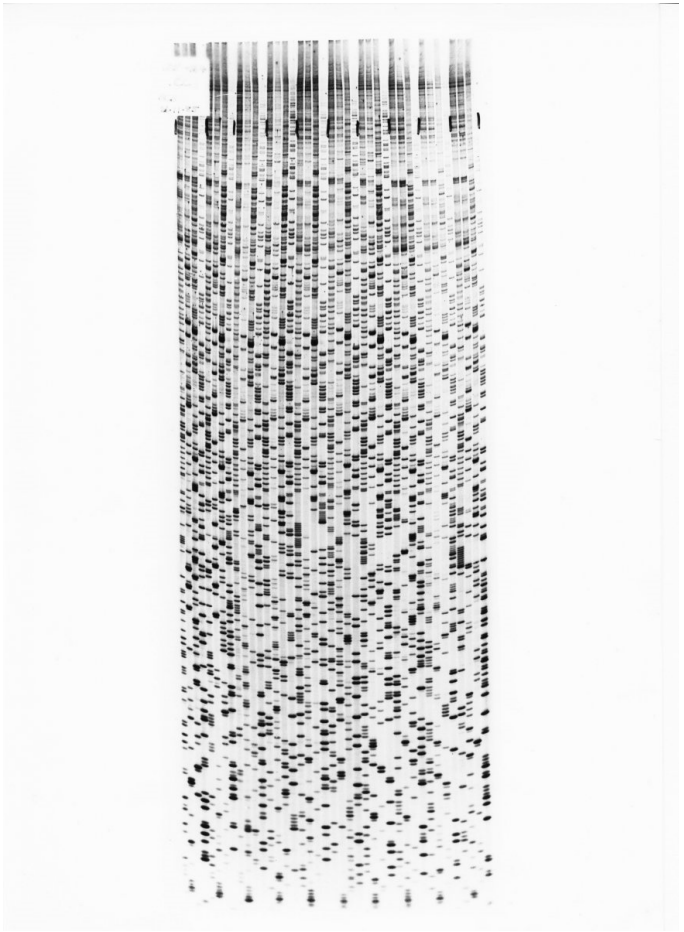

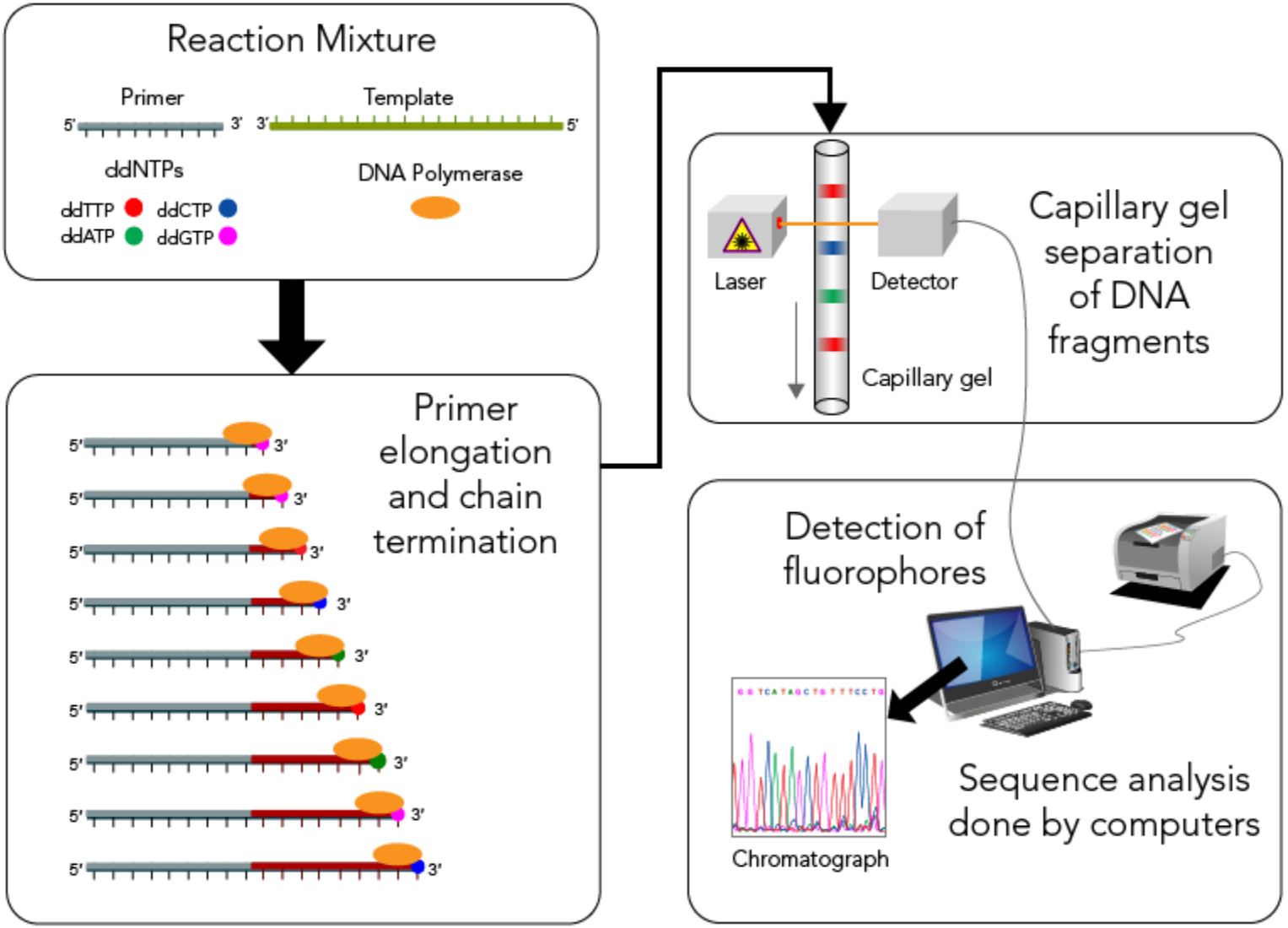
Reaction Mixture
Primer
Template
5'
3'
3'
5'
ddNTPs
DNA Polymerase
ddTTP
ddCTP
ddATP
ddGTP
Primer elongation and chain termination
Capillary gel separation of DNA fragments
Laser
Detector
Capillary gel
Detection of fluorophores
Chromatograph
Sequence analysis done by computers

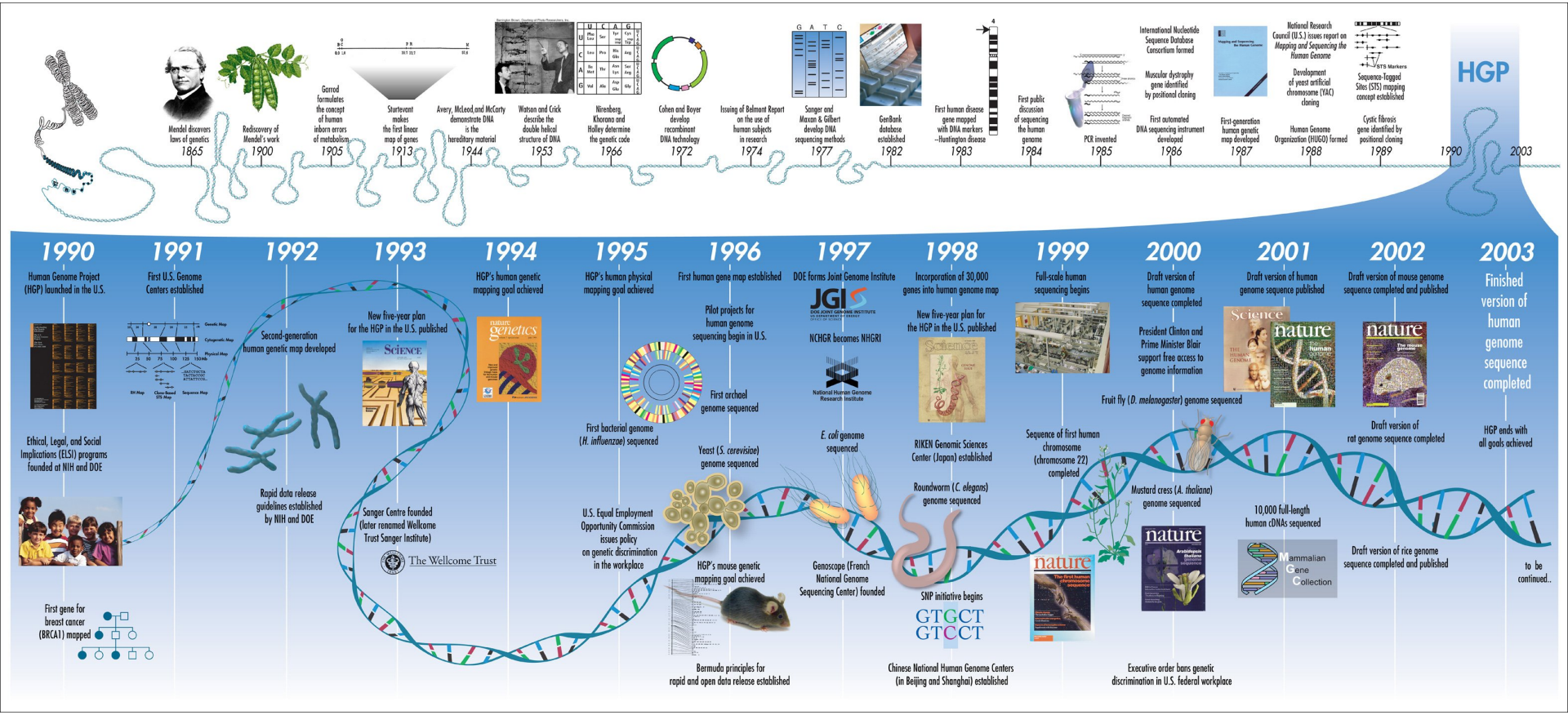
HGP
1865 Mendel discovers laws of genetics
1900 Rediscovery of Mendel's work
1905 Garrod formulates the concept of human inborn errors of metabolism
1913 Sturtevant makes the first linear map of genes
1944 Avery, McLeod, and McCarty demonstrate DNA is the hereditary material
1953 Watson and Crick describe the double helical structure of DNA
1966 Nirenberg, Khorana and Holley determine the genetic code
1972 Cohen and Boyer develop recombinant DNA technology
1974 Issuing of Belmont Report on the use of human subjects in research
1977 Sanger and Maxam & Gilbert develop DNA sequencing methods
1982 GenBank database established
1983 First human disease gene mapped with DNA markers –Huntington disease
1984 First public discussion of sequencing the human genome
1985 PCR invented
1986 International Nucleotide Sequence Database Consortium formed
Muscular dystrophy gene identified by positional cloning
First automated DNA sequencing instrument developed
1987 First-generation human genetic map developed
1988 National Research Council (U.S.) issues report on Mapping and Sequencing the Human Genome
Development of yeast artificial chromosome (YAC) cloning
Human Genome Organization (HUGO) formed
1989 STS Markers
Sequence-Tagged Sites (STS) mapping concept established
Cystic fibrosis gene identified by positional cloning
1990
2003
1990
Human Genome Project (HGP) launched in the U.S.
Ethical, Legal, and Social Implications (ELSI) programs founded at NIH and DOE
First gene for breast cancer (BRCA1) mapped
1991
First U.S. Genome Centers established
1992
Second-generation human genetic map developed
Rapid data release guidelines established by NIH and DOE
1993
New five-year plan for the HGP in the U.S. published
Sanger Centre founded (later renamed Wellcome Trust Sanger Institute)
The Wellcome Trust
1994
HGP's human genetic mapping goal achieved
1995
HGP's human physical mapping goal achieved
First bacterial genome (H. influenzae) sequenced
U.S. Equal Employment Opportunity Commission issues policy on genetic discrimination in the workplace
1996
First human gene map established
Pilot projects for human genome sequencing begin in U.S.
First archael genome sequenced
Yeast (S. cerevisiae) genome sequenced
HGP's mouse genetic mapping goal achieved
Bermuda principles for rapid and open data release established
1997
DOE forms Joint Genome Institute
JGI
NCHGR becomes NHGRI
National Human Genome Research Institute
E. coli genome sequenced
Genoscope (French National Genome Sequencing Center) founded
1998
Incorporation of 30,000 genes into human genome map
New five-year plan for the HGP in the U.S. published
RIKEN Genomic Sciences Center (Japan) established
Roundworm (C. elegans) genome sequenced
SNP initiative begins
GTGCT
GTCCT
Chinese National Human Genome Centers (in Beijing and Shanghai) established
1999
Full-scale human sequencing begins
Sequence of first human chromosome (chromosome 22) completed
2000
Draft version of human genome sequence completed
President Clinton and Prime Minister Blair support free access to genome information
Fruit fly (D. melanogaster) genome sequenced
Mustard cress (A. thaliana) genome sequenced
Executive order bans genetic discrimination in U.S. federal workplace
2001
Draft version of human genome sequence published
10,000 full-length human cDNAs sequenced
Mammalian Gene Collection
2002
Draft version of mouse genome sequence completed and published
Draft version of rat genome sequence completed
Draft version of rice genome sequence completed and published
2003
Finished version of human genome sequence completed
HGP ends with all goals achieved
to be continued..

NGS Illumina

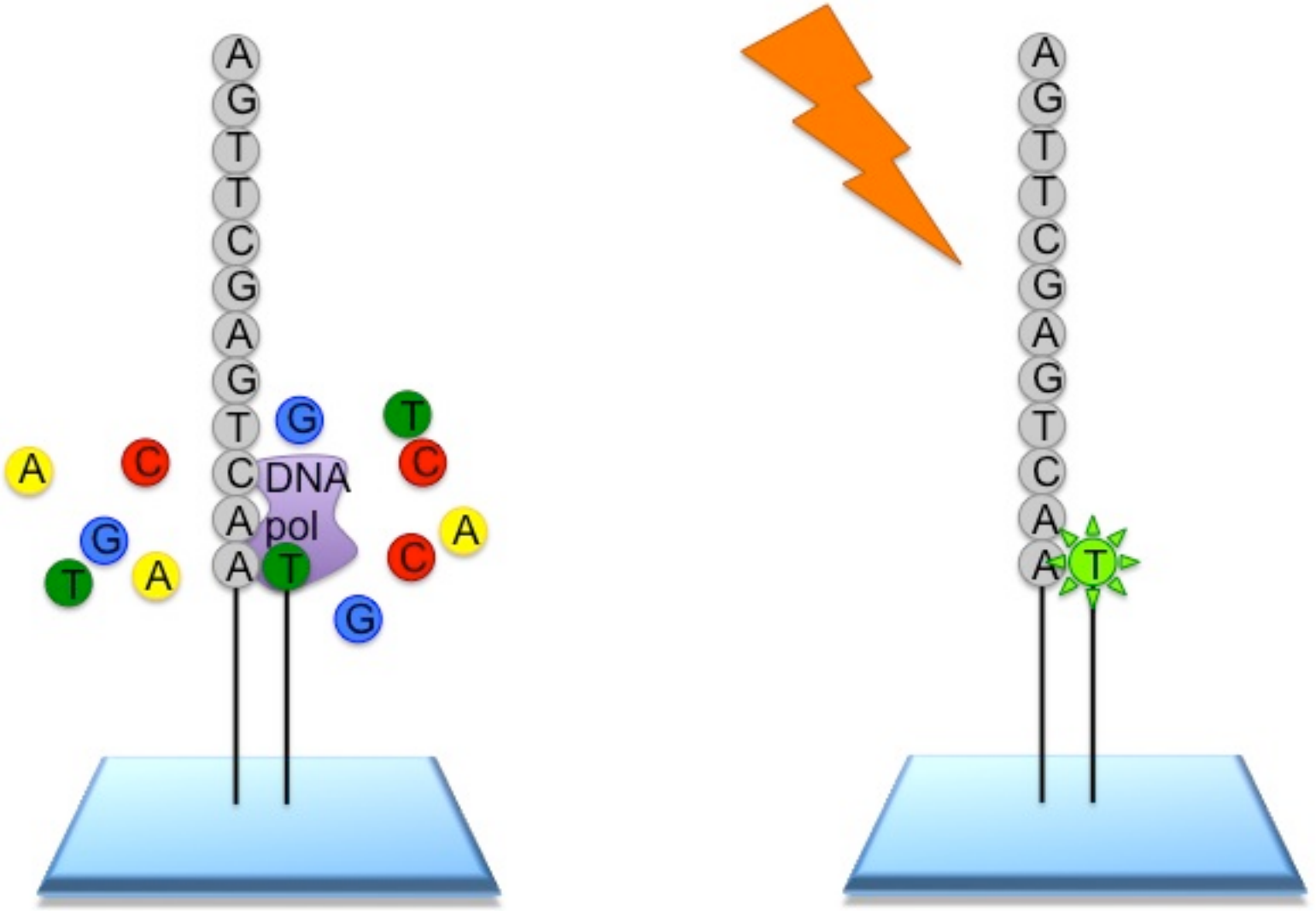

Sequence by Synthesis

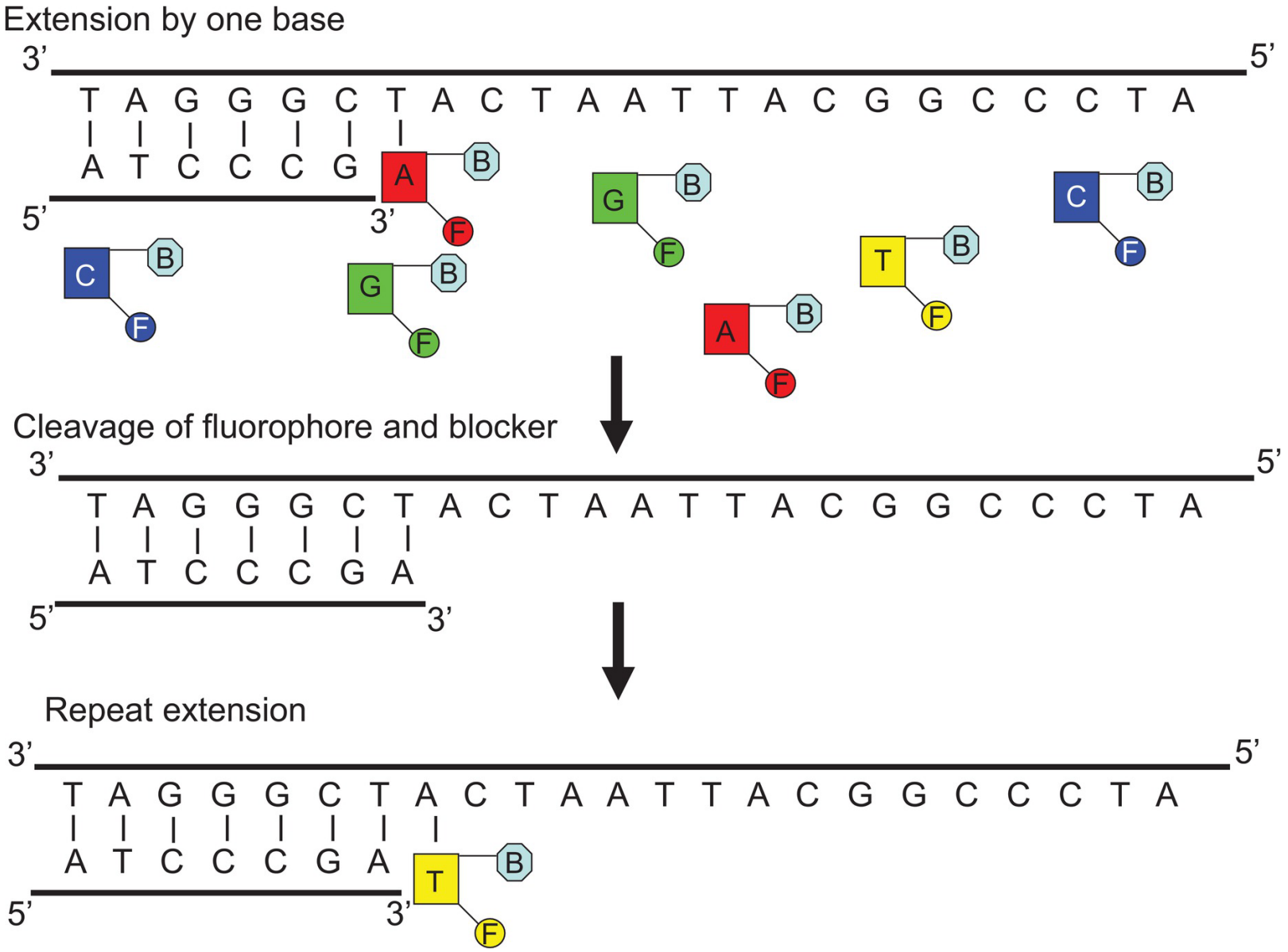

NGS Illumina

https://www.youtube.com/watch?v=CZeN-IgjYCo

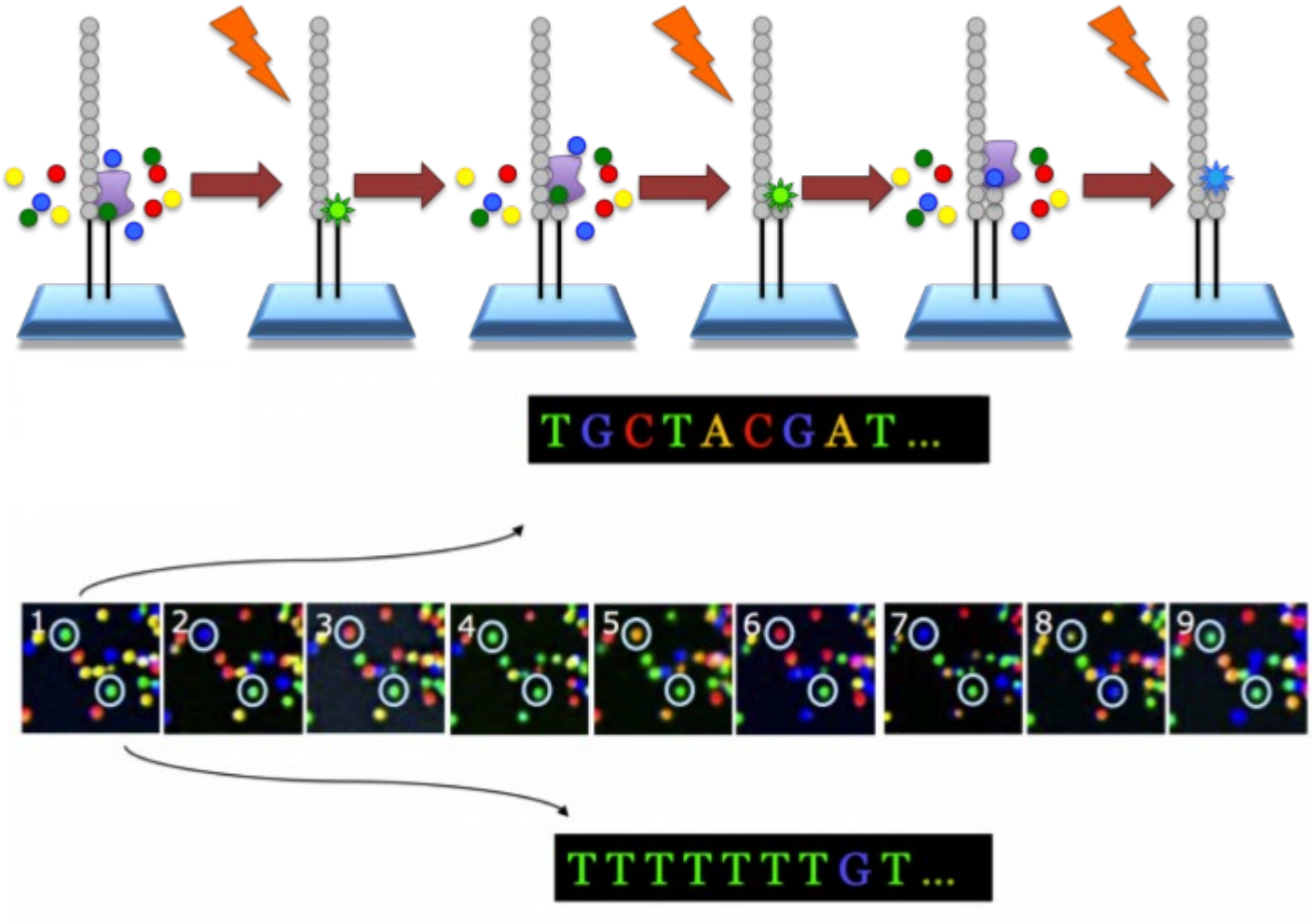

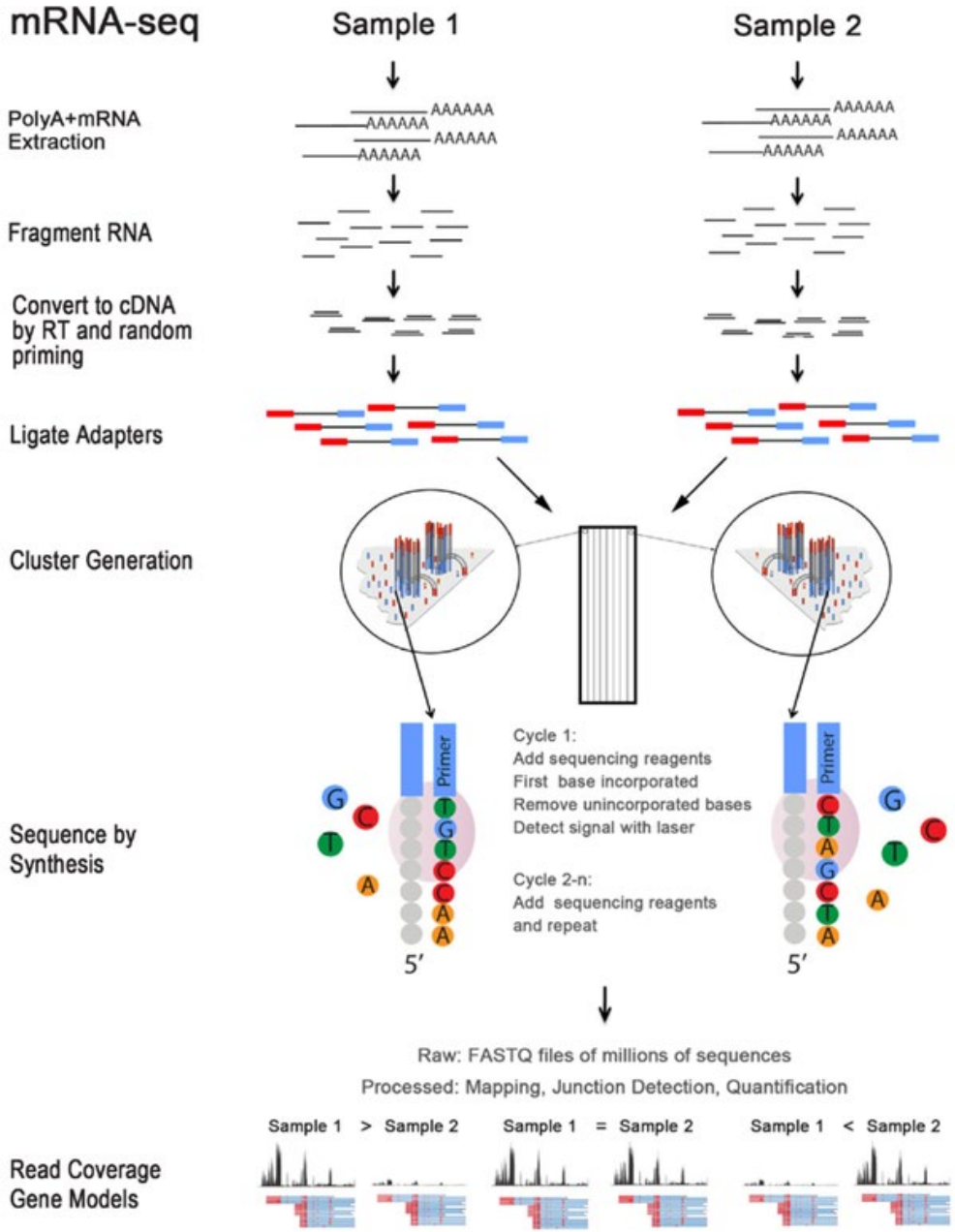
mRNA-seq
Sample 1
Sample 2
PolyA+mRNA Extraction
AAAAAA
Fragment RNA
Convert to cDNA by RT and random priming
Ligate Adapters
Cluster Generation
Sequence by Synthesis
Primer
Cycle 1:
Add sequencing reagents
First base incorporated
Remove unincorporated bases
Detect signal with laser
Cycle 2-n:
Add sequencing reagents and repeat
5′
Raw: FASTQ files of millions of sequences
Processed: Mapping, Junction Detection, Quantification
Read Coverage Gene Models
Sample 1 > Sample 2
Sample 1 = Sample 2
Sample 1 < Sample 2

The four main advantages of NGS over classical Sanger sequencing are:

speed
cost
sample size
accuracy

NGS is significantly cheaper, quicker, needs significantly less DNA and is more accurate and reliable than Sanger sequencing.

NGS is quicker than Sanger sequencing in two ways. Firstly, the chemical reaction may be combined with the signal detection in some versions of NGS, whereas in Sanger sequencing these are two separate processes. Secondly and more significantly, only one read (maximum ~1kb) can be taken at a time in Sanger sequencing, whereas NGS is massively parallel, allowing 300Gb of DNA to be read on a single run on a single chip.
The first human genome sequence cost in the region of £300M. Using modern Sanger sequencing methods, aided by data from the known sequence, a full human genome would still cost £6M. Sequencing a human genome with Illumina today would cost only £6,000.

Third Generation Sequencing

PacBio SMRT seq

DNA passes thru polymerase in an illuminated volume

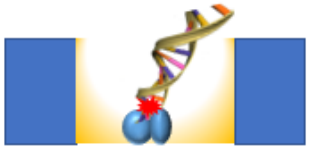

Raw output is fluorescent signal of the nucleotide incorporation, specific to each nucleotide

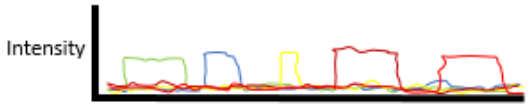

A,C,T,G have known pulse durations, which are used to infer methylated nucleotides

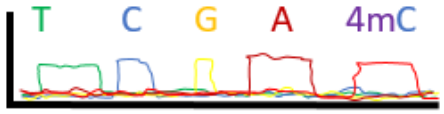

Oxford Nanopore

DNA passes thru nanopore

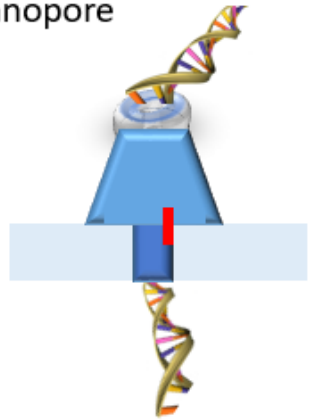

Raw output is electrical signal caused by nucleotide blocking ion flow in nanopore

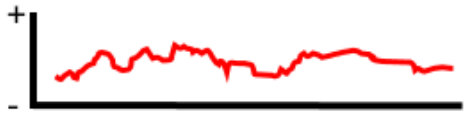

Each nucleotide has a specific electric “signature”

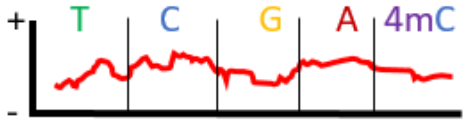

Zero Mode Waveguide

https://www.youtube.com/watch?v=NHCJ8PtYCFc

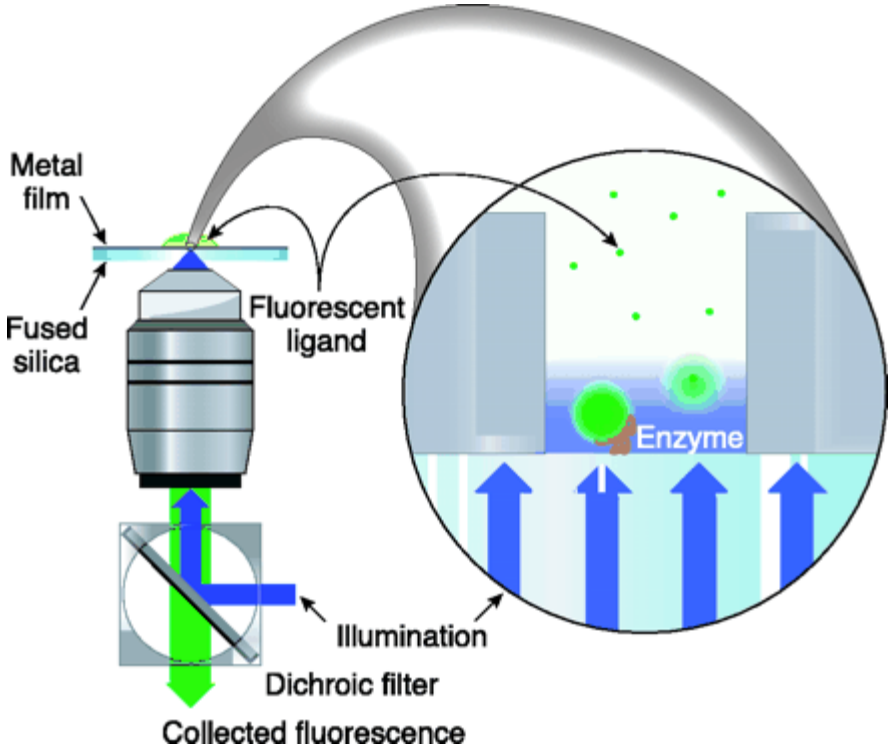

SCIENCE VOL 299 31 JANUARY 2003

Zero Mode Waveguide

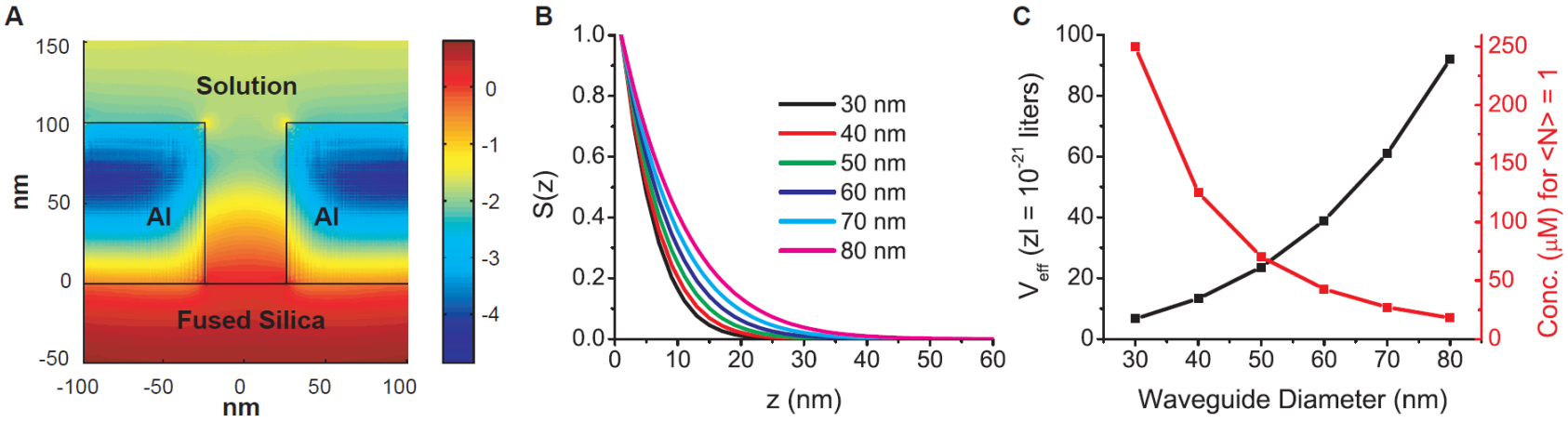

50 x 50 x 10 nm^3 = 2.5 x 10^4 x 10^{-21} cc = 2.5 x 10^{-20} L= 25 zeptoliter

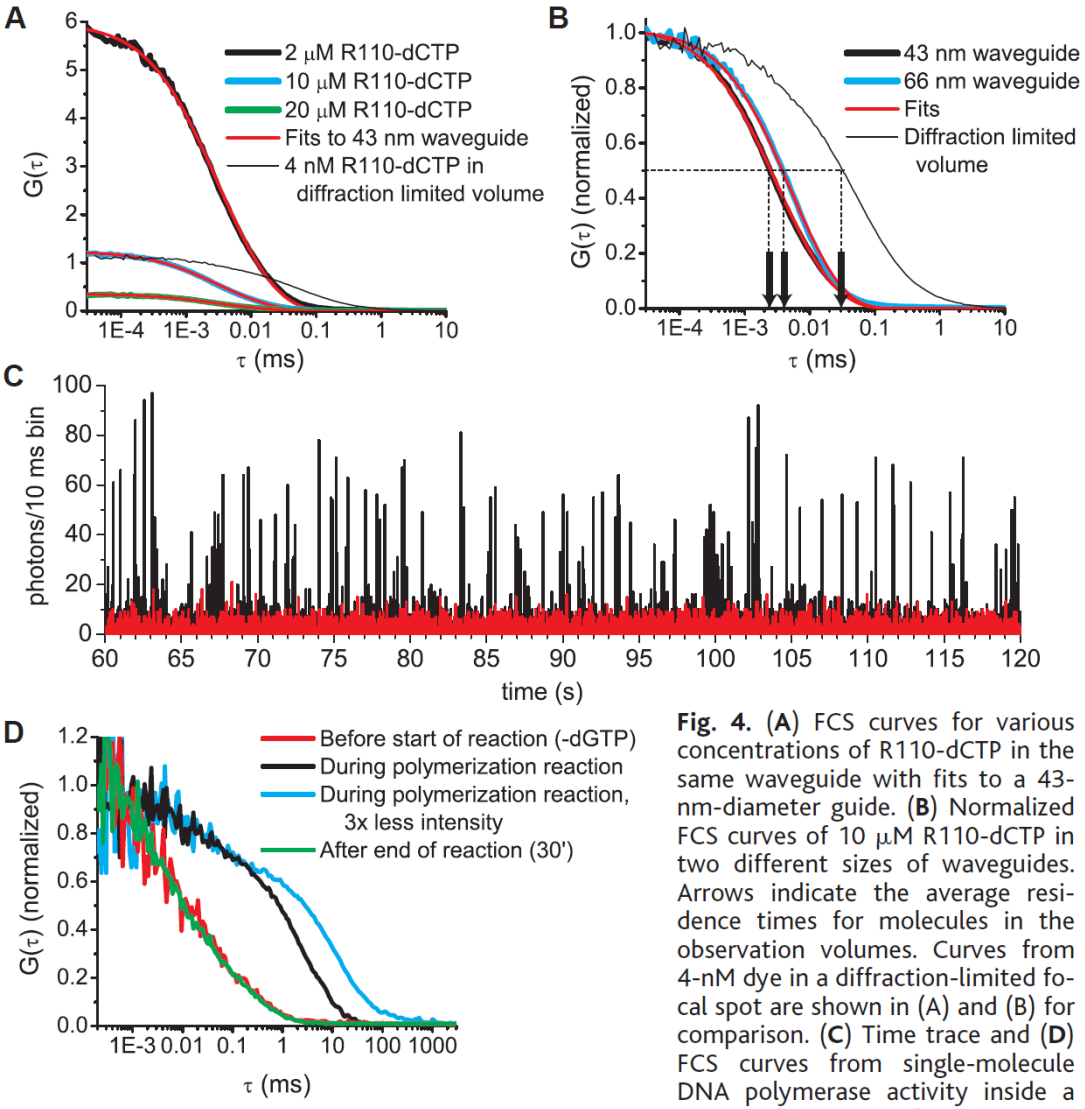

Fig. 4. (**A**) FCS curves for various concentrations of R110-dCTP in the same waveguide with fits to a 43-nm-diameter guide. (**B**) Normalized FCS curves of 10 μM R110-dCTP in two different sizes of waveguides. Arrows indicate the average residence times for molecules in the observation volumes. Curves from 4-nM dye in a diffraction-limited focal spot are shown in (A) and (B) for comparison. (**C**) Time trace and (**D**) FCS curves from single-molecule DNA polymerase activity inside a zero-mode waveguide. Incorporation events and subsequent photobleaching of coumarin-dCTP appear as distinct fluorescence bursts in the black time trace (10-ms time bins). This results in a long-time shoulder in the corresponding FCS curves during polymerization (black and blue curves) in (D). Decreasing the intensity results in slower photobleaching as seen by the longer residence time in the blue curve. The red curves in (C) and (D) are the corresponding negative controls (absence of one native nucleotide) in the same waveguide before initiation of the reaction. The green curve in (D) is the control after the reaction has stopped.

Real-Time DNA Sequencing from Single Polymerase Molecules

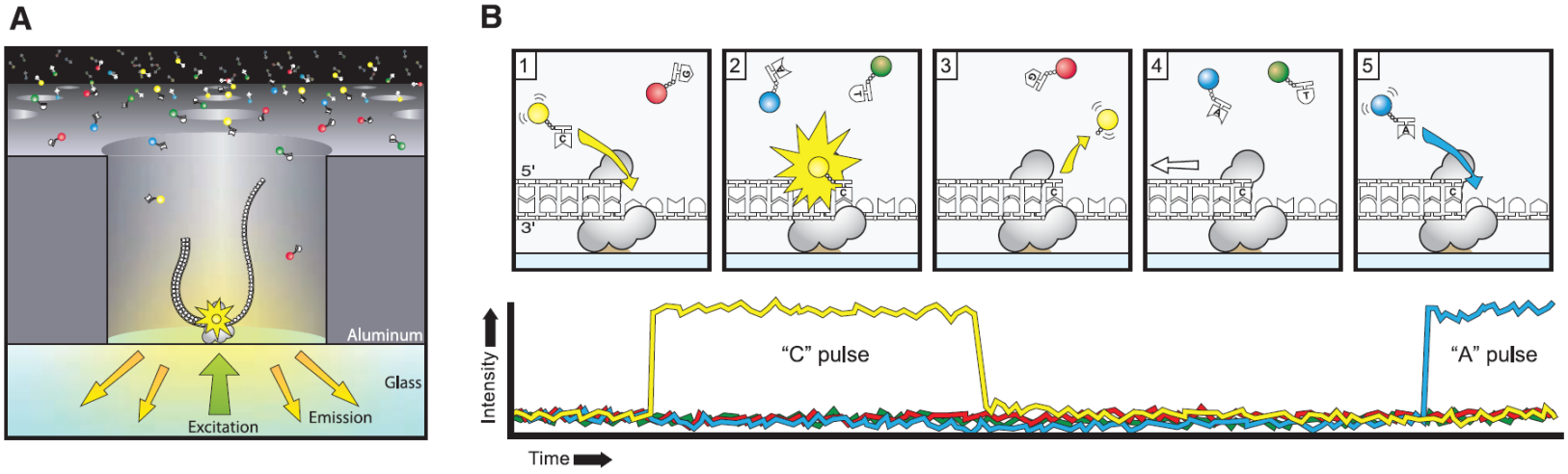

SCIENCE VOL 323 2 JANUARY 2009

Nanopore Sequencing

https://www.youtube.com/watch?v=RcP85JHLmnI

https://www.youtube.com/watch?v=qzusVw4Dp8w

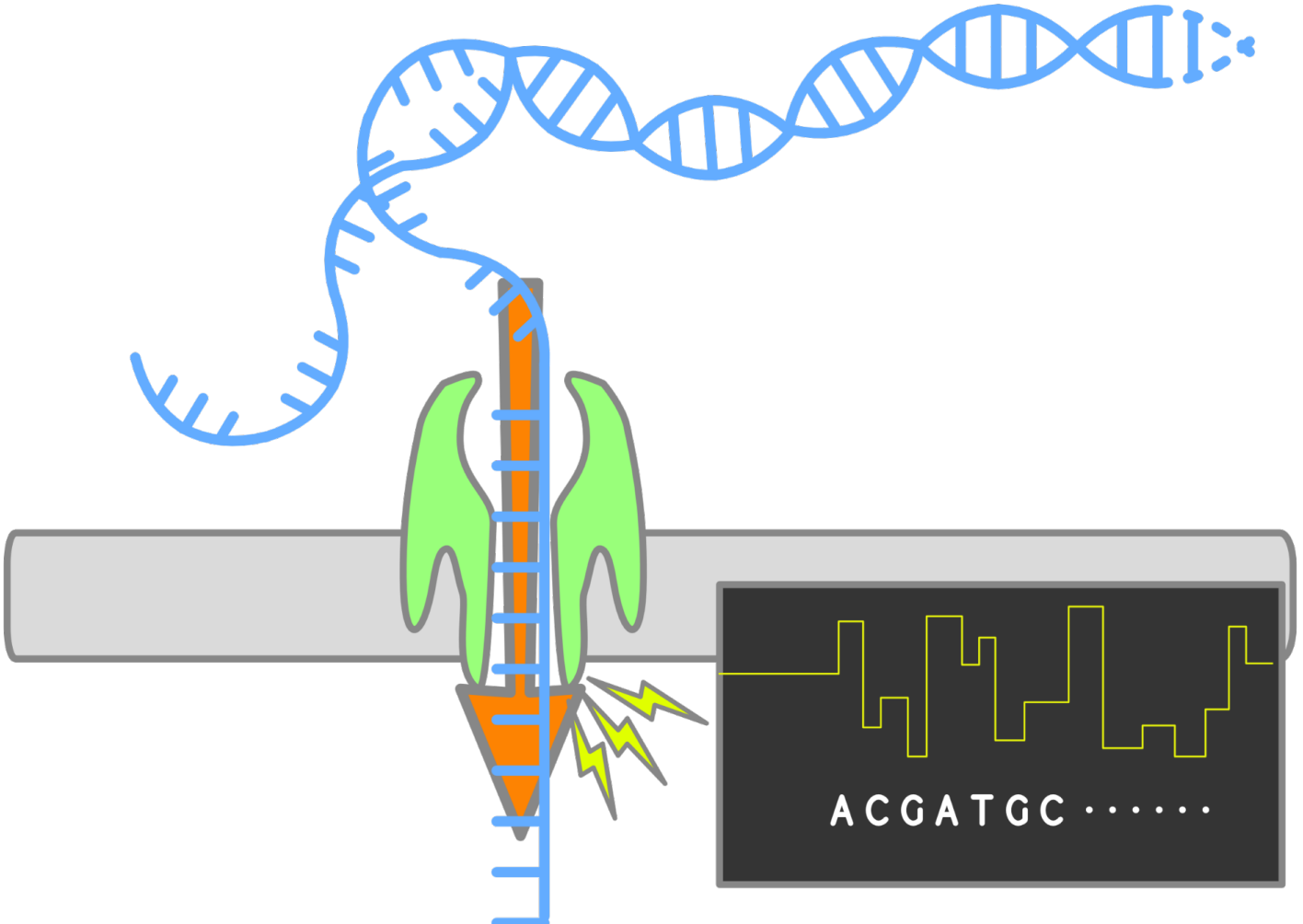

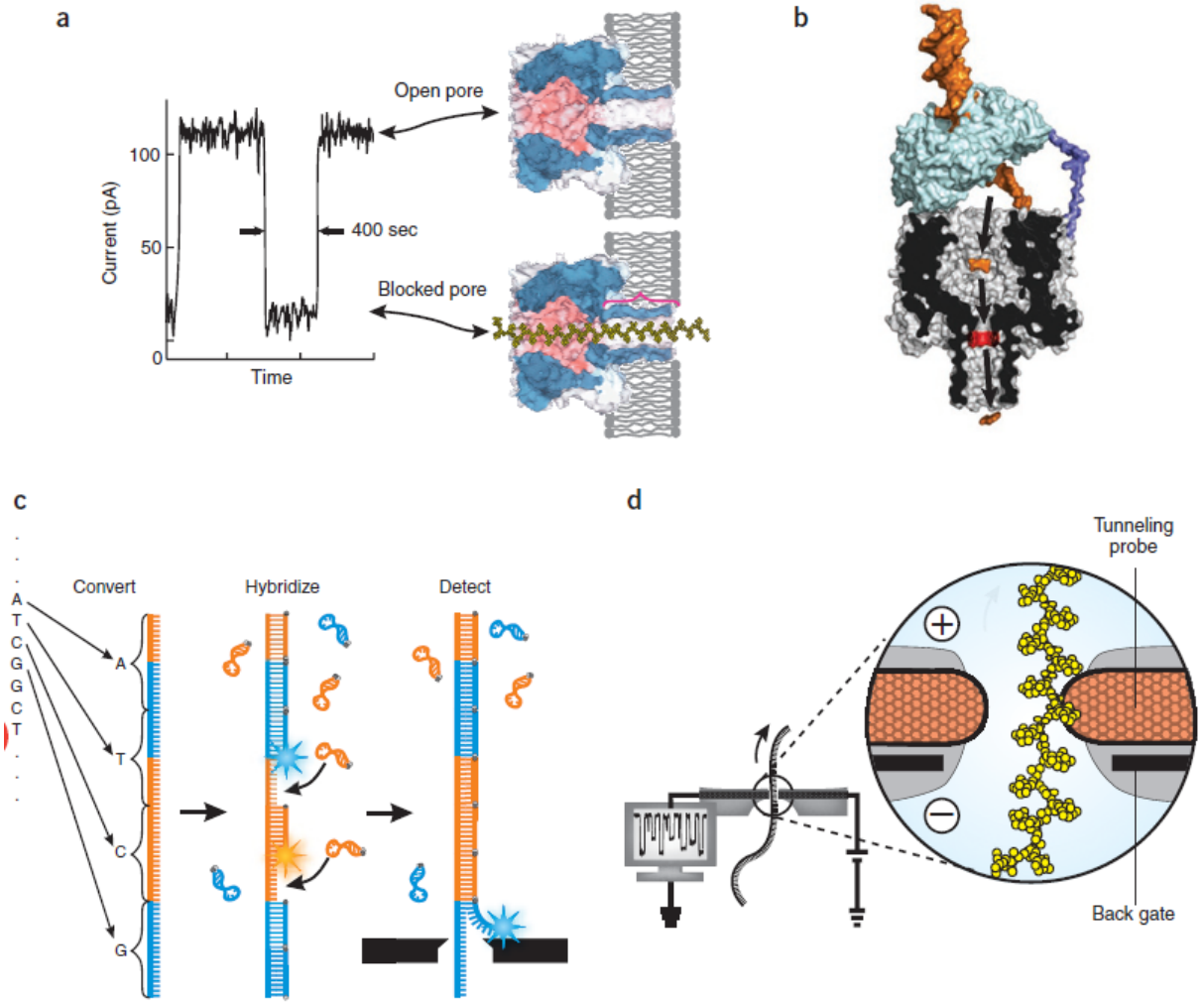
a
Open pore
100
50
0
Current (pA)
400 sec
Blocked pore
Time
b
c
Convert
Hybridize
Detect
A
T
C
G
G
C
T
A
T
C
G
d
Tunneling probe
Back gate

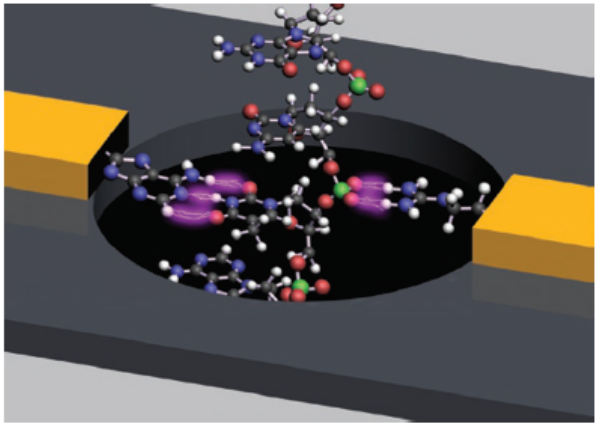

Figure 2 A nanopore reader with chemically functionalized probes. As a strand of DNA emerges from a nanopore, a 'phosphate grabber' on one functionalized electrode and a 'base reader' on the other electrode form hydrogen bonds (light blue ovals) to complete a transverse electrical circuit through each nucleotide as it is translocated through the nanopore.

Digital PCR

Droplet digital PCR

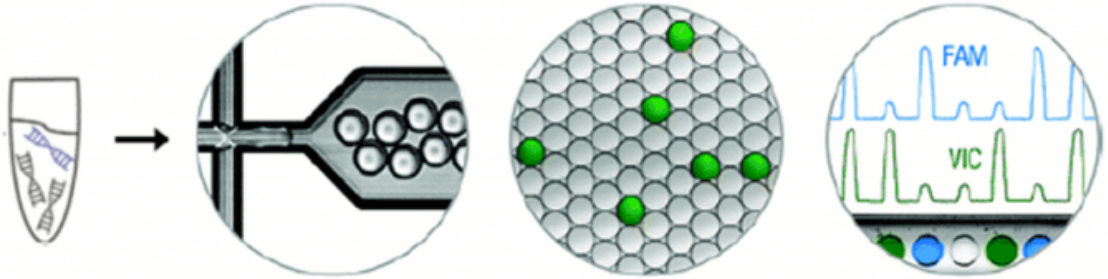

Bio-Rad QX100

1. MAKE	2. CYCLE	3. READ	
Sample is partitioned into 20,000 droplets	Run PCR cycles in all droplets simultaneously	Measure fluorescence intensity in each droplet	Calculate concentration from number of positive droplets

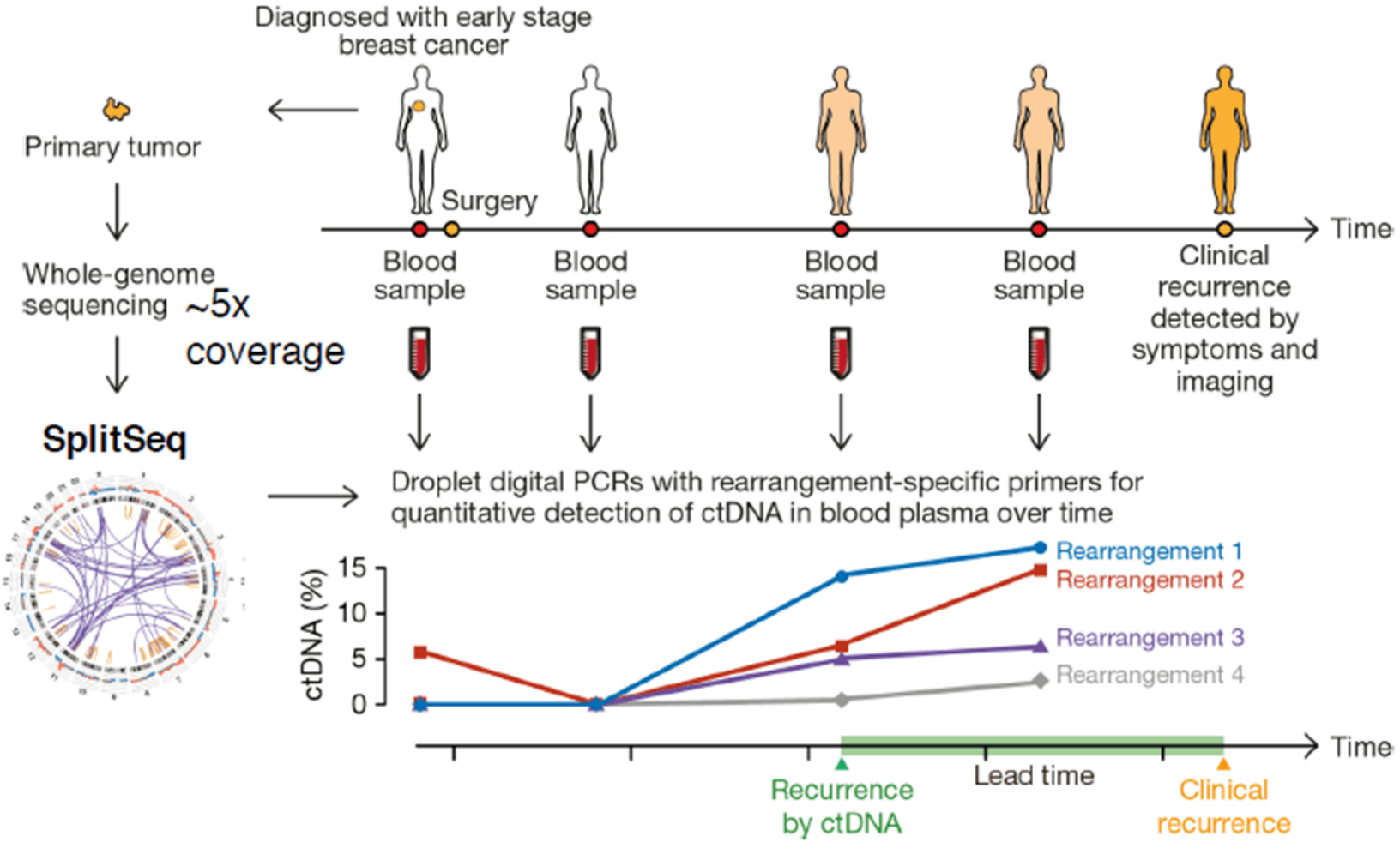
Diagnosed with early stage breast cancer
Primary tumor
Surgery
Time
Whole-genome sequencing
~5x coverage
Blood sample
Blood sample
Blood sample
Blood sample
Clinical recurrence detected by symptoms and imaging
SplitSeq
Droplet digital PCRs with rearrangement-specific primers for quantitative detection of ctDNA in blood plasma over time
ctDNA (%)
15
10
5
0
Rearrangement 1
Rearrangement 2
Rearrangement 3
Rearrangement 4
Time
Lead time
Recurrence by ctDNA
Clinical recurrence

Recombinant DNA

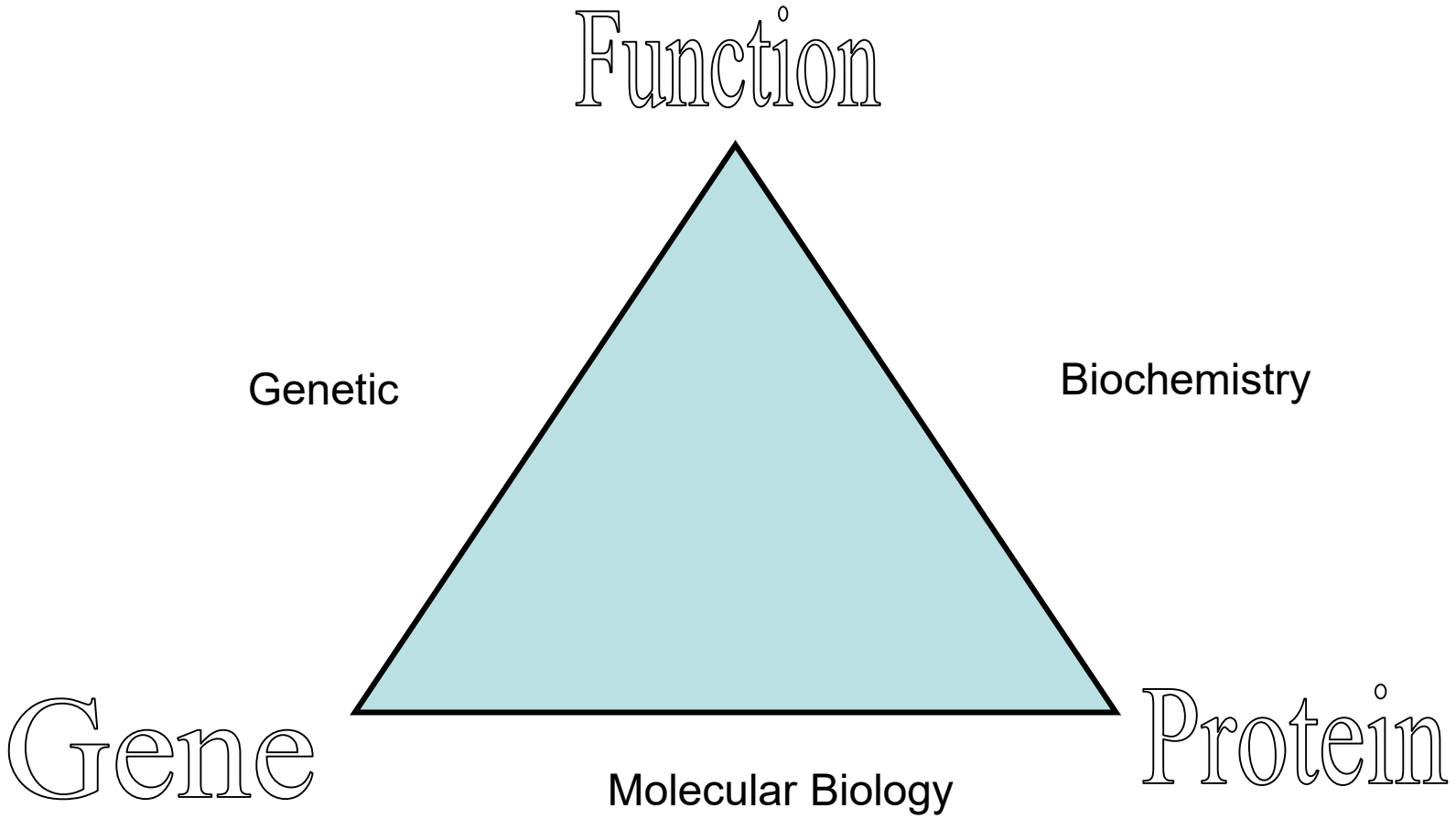

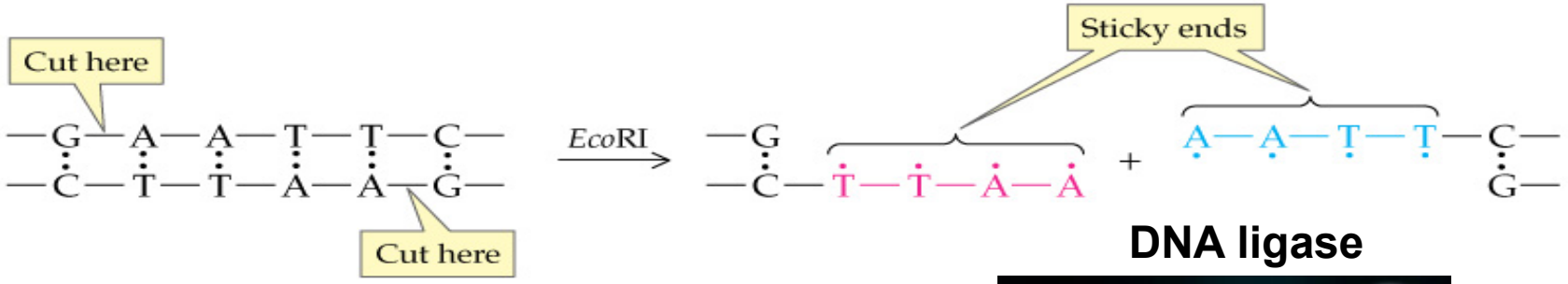

Restriction Enzyme

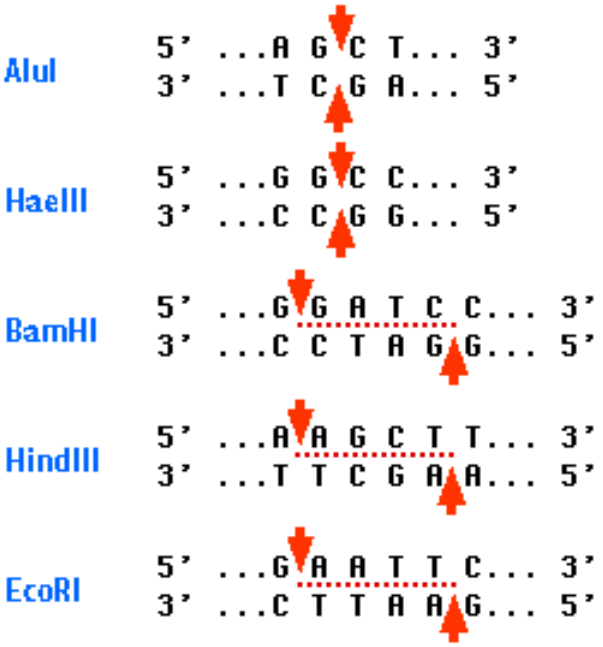

AluI and **HaeIII** produce blunt ends

BamHI **HindIII** and **EcoRI** produce "sticky" ends

DNA ligase

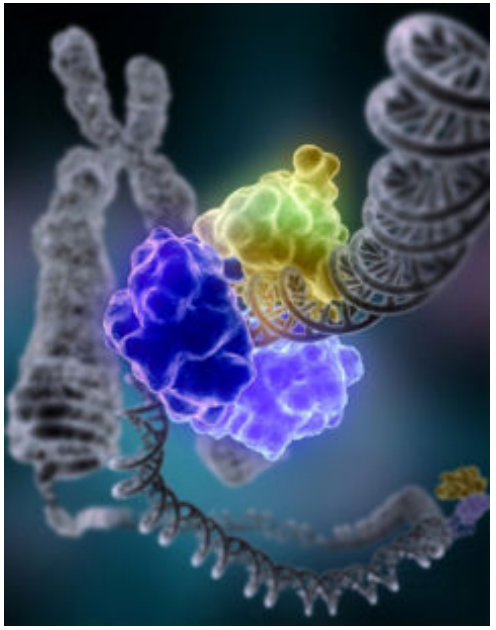

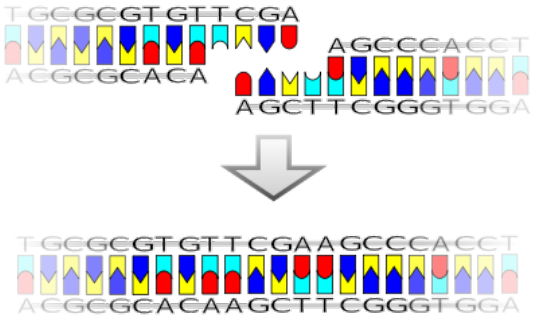

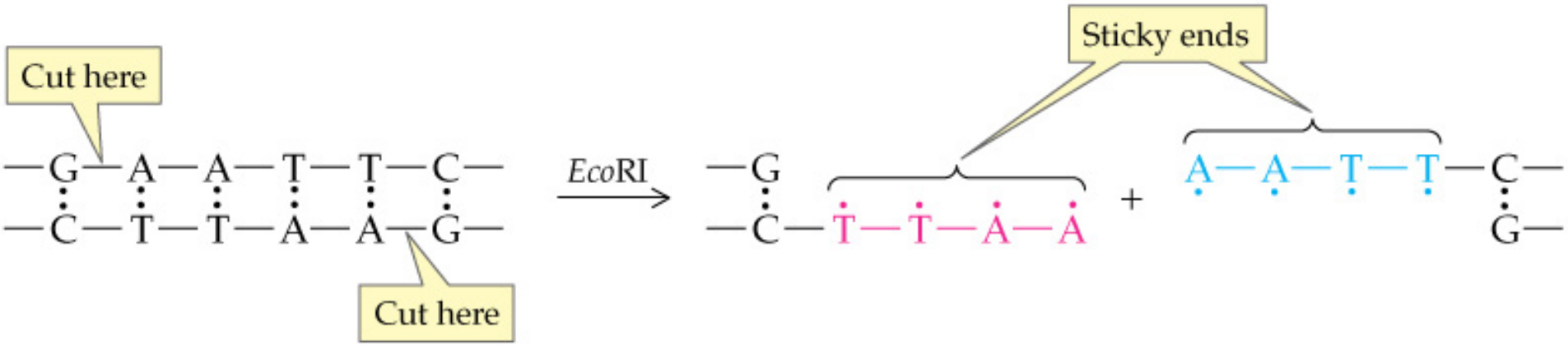
Cut here
G A A T T C
C T T A A G
Cut here
EcoRI
Sticky ends
G
C T T A A
+
A A T T C
G

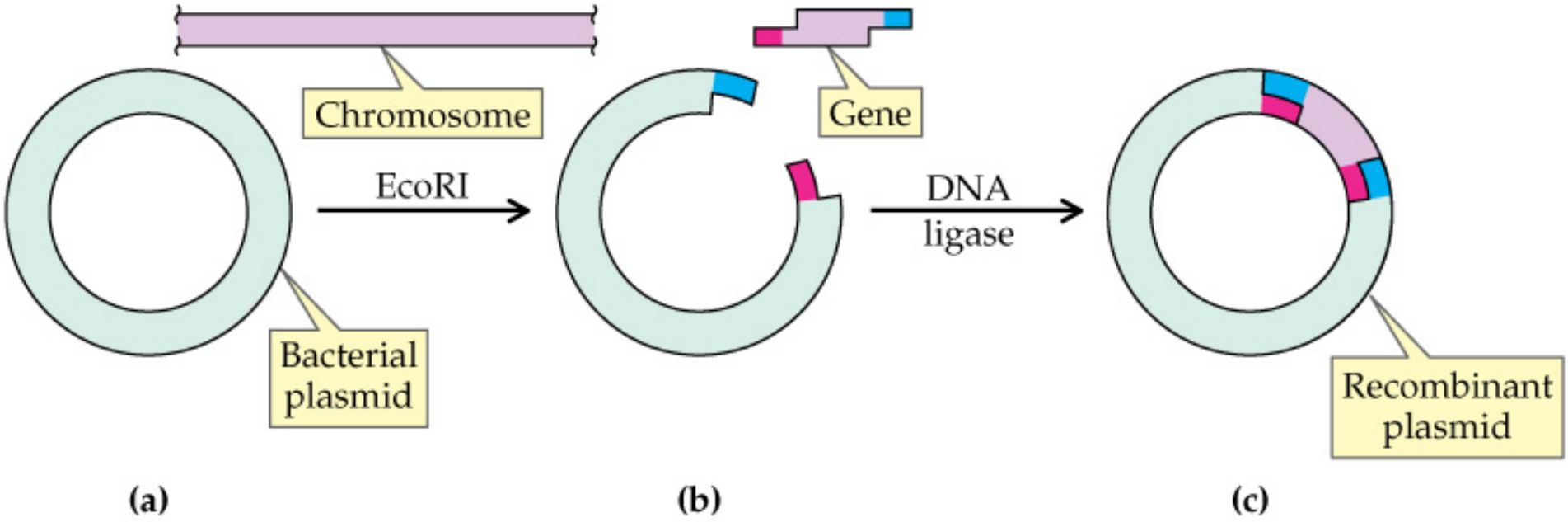
Chromosome
Gene
EcoRI
DNA
ligase
Bacterial
plasmid
Recombinant
plasmid
(a)
(b)
(c)

β-Galactosidase

The enzyme that splits lactose into glucose and galactose. Coded by a gene (lacZ) in the lac operon of Escherichia coli.

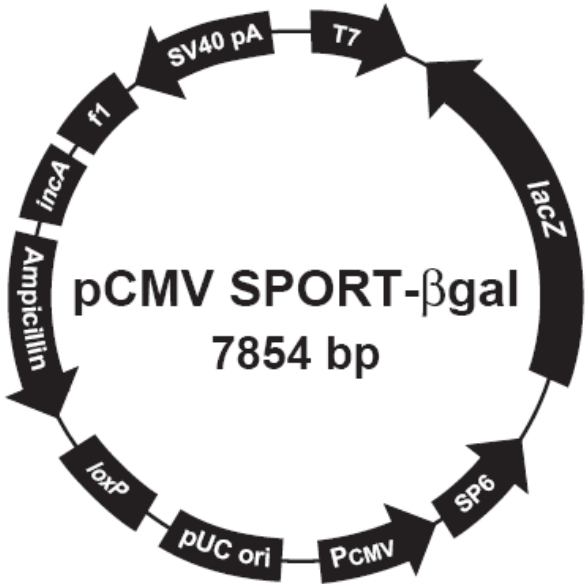

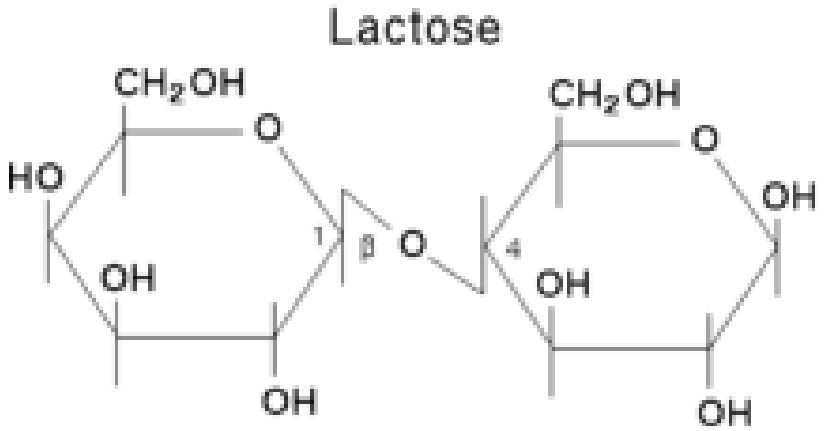

PUC is a family of plasmids that have an ampicillin resistance gene and more importantly a *lacZ* gene. A functional lacZ gene will produce the protein β - galactosidase. Bacterial colonies in which β - galactosidase is produced, will form blue colonies in the presence of the substrate 5 - bromo - 4 - chloro - 3 - indolyl - b - D - galactoside or as it is more commonly referred to, X-gal.

CRISPR CAS9

CRISPRs (**clustered regularly interspaced short palindromic repeats**) are segments of prokaryotic DNA containin g short repetitions of base sequences. Each repetition is followed by short segments of "spacer DNA" from previous exposures to a bacterial virus or

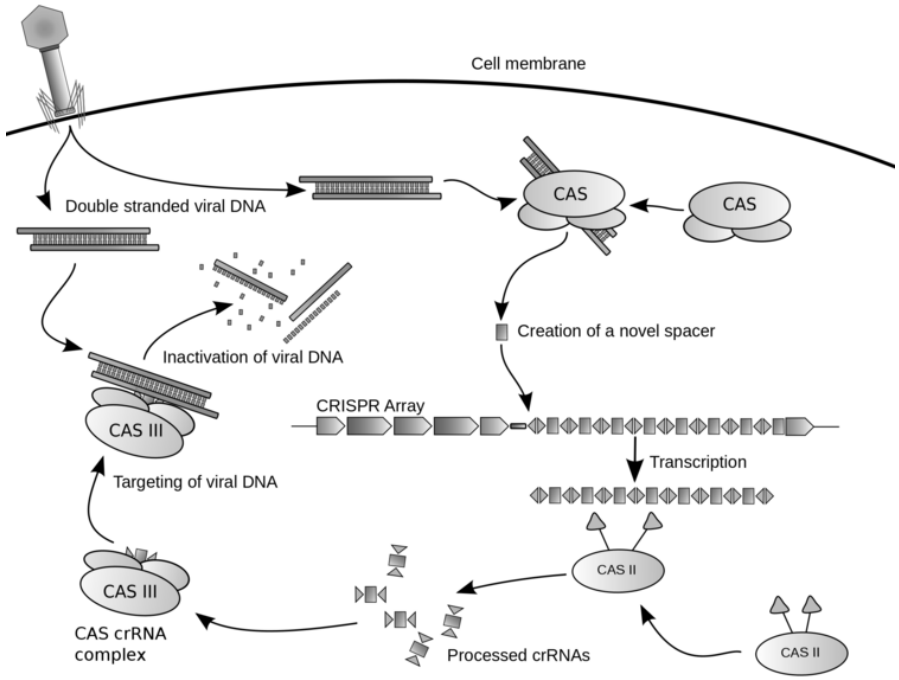

Movie

- https://youtu.be/2pp17E4E-O8

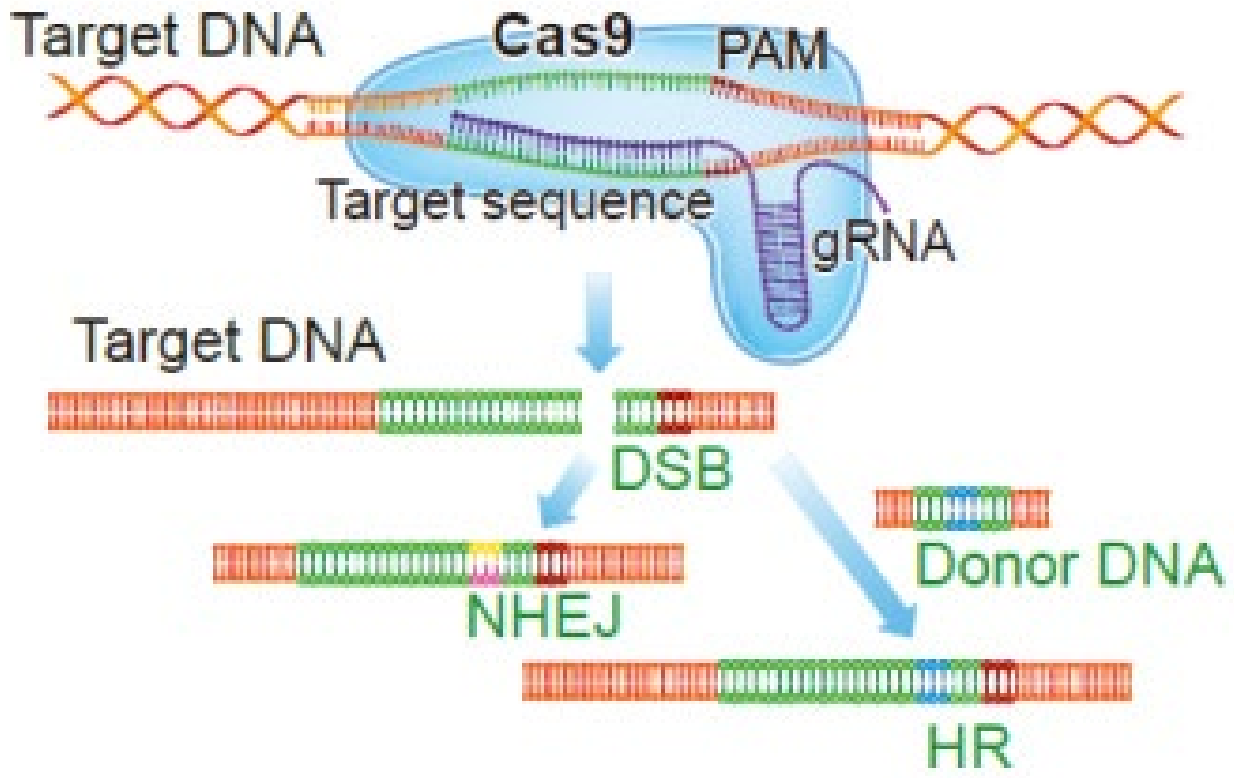
Target DNA
Cas9
PAM
Target sequence
gRNA
Target DNA
DSB
NHEJ
Donor DNA
HR

Optogenetics

https://www.youtube.com/watch?v=I64X7vHSHOE

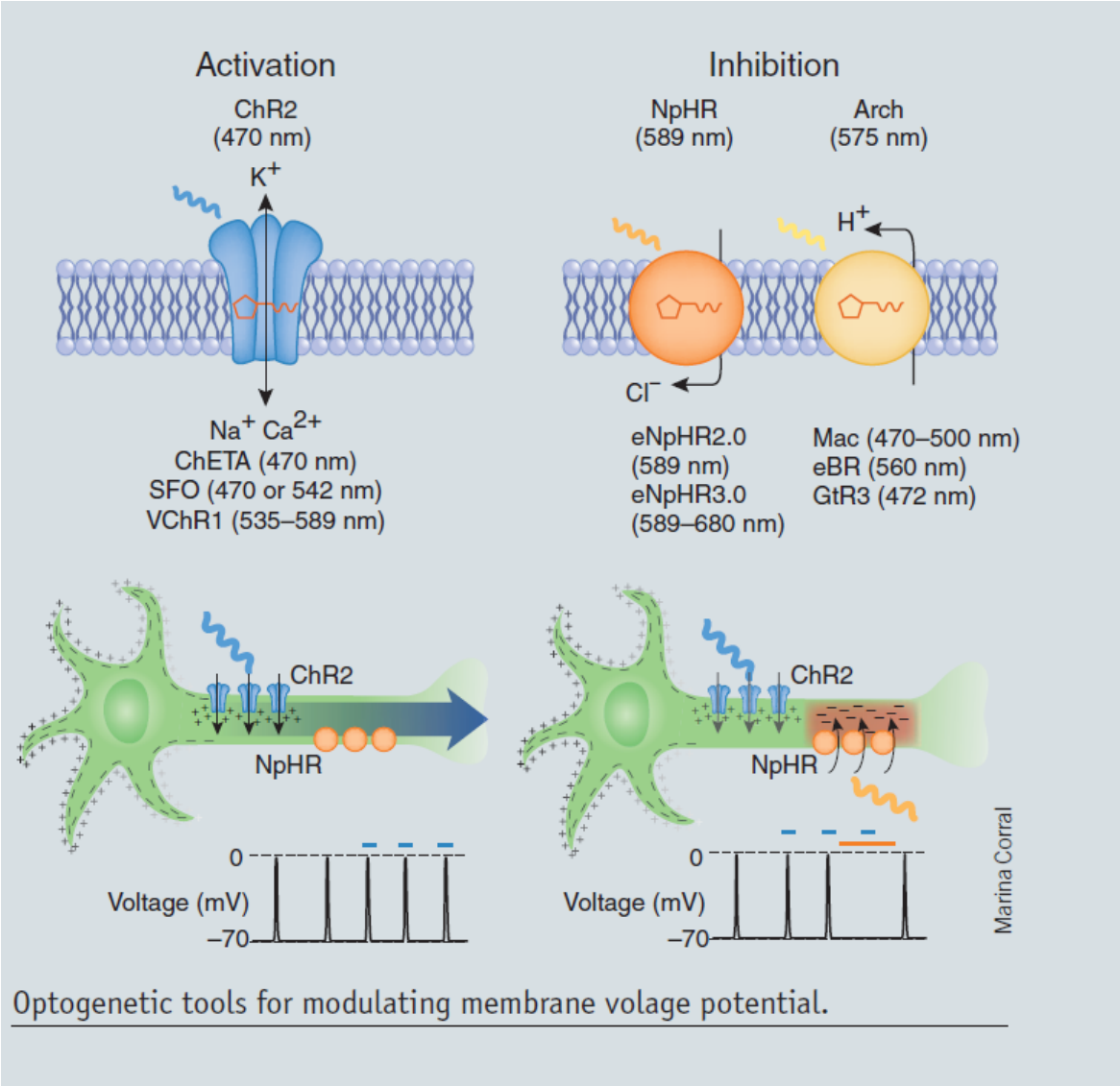

Optogenetic tools for modulating membrane volage potential.